

# **Synthetic investigation of Mn(I) and Re(I) N-Heterocyclic carbene complexes**

by

**Belinda van der Westhuizen**

Submitted in partial fulfilment of the degree

**Magister Scientiae**

In the Faculty of Natural- and Agricultural Sciences

University of Pretoria

Pretoria

Supervisors:

Dr. M. Landman

Dr. D. I. Bezuidenhout

November 2010

## Declaration

I declare that the dissertation, which I hereby submit for the degree Magister Scientiae at the University of Pretoria, is my own work and has not previously been submitted by me for a degree at this or any other tertiary institution.

The X-ray structure determinations were performed by David Liles at the University of Pretoria.

---

Signature

---

Date

# Acknowledgements

I would like to express my sincere gratitude to the following people and institutions:

Drs. Marilé Landman and Daniela Bezuidenhout for their guidance, support and motivation to successfully finish this study;

Prof Martin Albrecht for the opportunity to visit his lab at the University College of Dublin, Ireland, as well as the friends I made in Ireland who gave me the motivation for the last stretch;

Mr Eric Palmer for recording of the NMR spectra;

Mr Dave Liles for the X-ray crystallography;

My colleagues Nina van Jaarsveld, Mia Ackermann, Elize Smit, Shandre Buitendach and Prof Simon Lotz for their encouragement and camaraderie;

My family for their understanding and support even through the late night hours:

Adel van der Westhuizen

Antoinette Southey

Ben van der Westhuizen

Jacques van Zyl

Marie van der Westhuizen

Mariëtte van der Westhuizen

Riaan van Zyl

My dancing teacher, Lewis Tolley, with whom I could dance my heart out;



All my friends for their patience and support especially Aurelie Tournie who kept me in 'the zone';

My community for their constant prayers, understanding and invaluable presence and guidance in my life.

All my love,

Belinda

# Table of Contents

## Summary

## List of complexes

## List of abbreviations

## Chapter 1: Introduction

1.1 Overview	1
1.2 Fischer and Schrock type carbenes	3
1.3 <i>N</i> -Heterocyclic carbene complexes	7
1.4 Aim	14

## Chapter 2: Diaminocarbenes

2.1 Background	16
2.2 Structure and general properties	17
2.3 Methods towards the synthesis of imidazol-2-ylidenes	19
2.4 Applications	21
2.5 Side reactions	22
2.6 Synthesis, results and discussion	25

## **Chapter 3: Monometal NHC complexes and experimental results**

3.1 Background	31
3.2 Focus of this study	36
3.3 Synthesis, results and discussion	38
3.4 Conclusion	63

## **Chapter 4: Dimetal NHC complexes and experimental results**

4.1 Background	65
4.2 Approaches towards the NHC target molecules	67
4.3 Focus of this study	71
4.4 Synthesis, results and discussion	72
4.5 Conclusion	107

## **Chapter 5: Structural and Theoretical study**

5.1 Molecular modelling	108
5.2 Computational details and validation of the theoretical method	111
5.3 Structural analysis	113
5.4 Vibrational analysis	120
5.5 Molecular orbital analysis	125
5.6 Conclusion	126

## **Chapter 6: Concluding remarks and Future work**

6.1 Conclusion	127
6.2 Future work	127

## **Chapter 7: Experimental: Standard Operational Procedure and Specifications**

7.1 Standard Operational Procedure	131
7.2 Specifications	131

### **Appendix CD: Crystallographic data**

# Summary

**Synthetic investigation of Mn(I) and Re(I) N-heterocyclic carbene complexes**

by

**Belinda van der Westhuizen**

Supervisor: Dr. M. Landman

Co-supervisor: Dr. D. I. Bezuidenhout

Submitted in partial fulfilment of the requirements for the degree Magister Scientiae,  
Department of Chemistry, University of Pretoria

The study involves synthetic approaches towards the preparation of novel NHC complexes of low valent rhenium and manganese transition metals. Diverse methods of synthesis were studied.

The direct approach, in which the ylidene obtained from deprotonation of 1,3-bis(2,4,6-trimethylphenyl)imidazolium chloride was added to the metal substrate, proved to be unsuccessful as isolation of the free carbene should rather be performed in an argon filled glove box under extreme inert conditions.

By way of further investigation the ylidene was prepared by *in situ* methods and then quenched with the metal substrate. Different bases for deprotonation purposes and reaction conditions were explored.

All routes employed were investigated and compared using group VII transition metal substrates  $\text{Re}(\text{CO})_5\text{Br}$ ,  $\text{Mn}(\text{CO})_5\text{Br}$ ,  $\text{Re}_2(\text{CO})_{10}$  and  $\text{Mn}_2(\text{CO})_{10}$ .



Isolation and purification of these products proved to be very challenging due to the insolubility in some organic solvents with consequent problematic spectroscopic analyses of the complexes. The tendency of the products to undergo various side reactions is observed in all reactions. Specifically, hydrolysis of the imidazolium ligand, followed by vinyl formation, yielded the mesitylformamide compound (**3**).

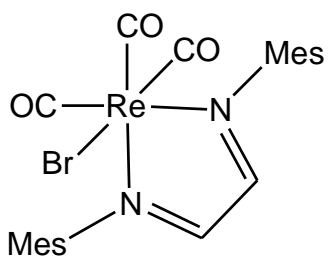
The results obtained for some of the monometal substrates indicated that the target complexes were formed but could not be isolated. However, the synthesis route employing deprotonation by *n*BuLi as base and  $[\text{Mn}_2(\text{CO})_{10}]$  as dimetal substrate lead to the isolation of the target dinuclear complex  $[\text{Mn}_2(\text{CO})_9\text{IMes}]$  (**9**).

Other novel complexes obtained during the course of this study include the biscarbene tetrarhenium complex  $[\text{Re}_2(\text{CO})_9\text{C}(\text{OEt})\text{C}_4\text{H}_2\text{OC}(\text{OEt})\text{Re}_2(\text{CO})_9]$  (**12**) and various side reaction products. In many cases, metal-metal bond cleavage and carbonyl insertion was observed, as is evident in the complex  $\text{IMesH}[\text{ReO}_4]$  (**6**) and ketene product (**13**).

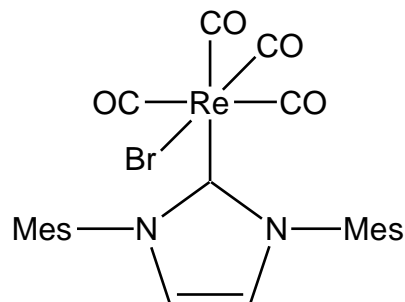
Structural and theoretical studies were performed to investigate the bond character between the carbene ligand and the metal.

## List of Compounds

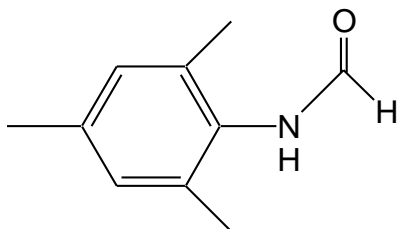
1:



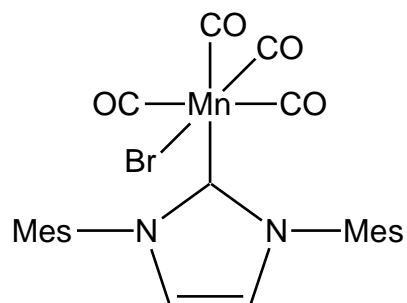
2:



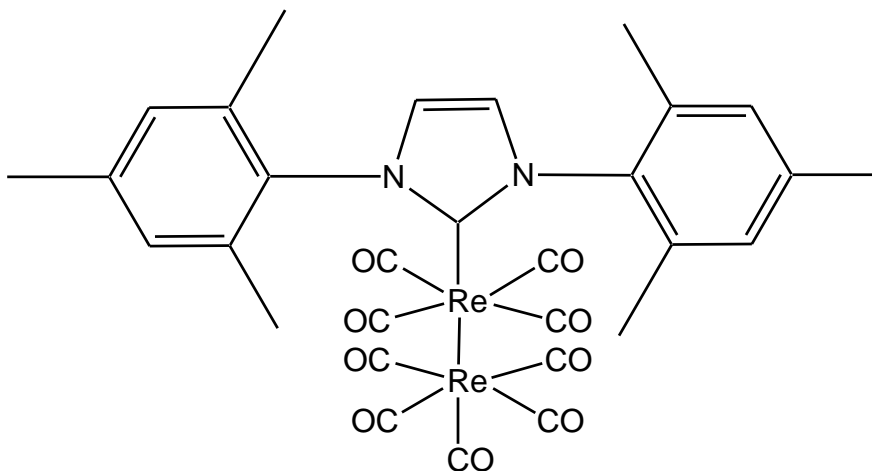
3:



4:

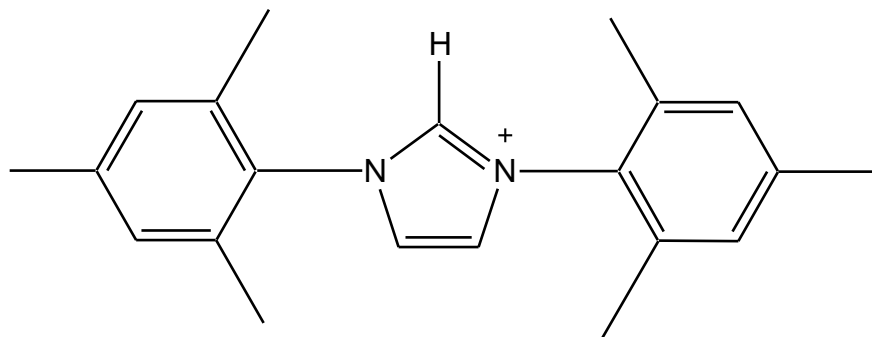
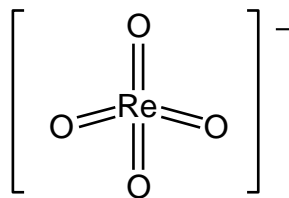


5:

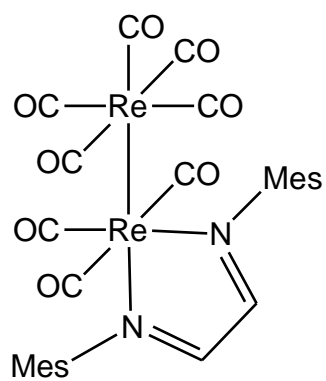




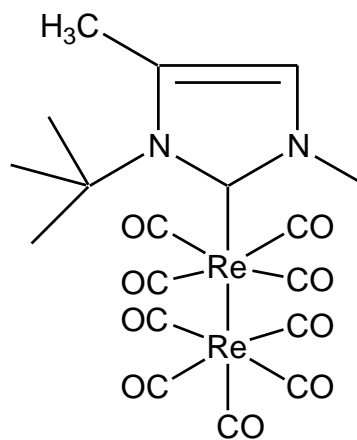
6:



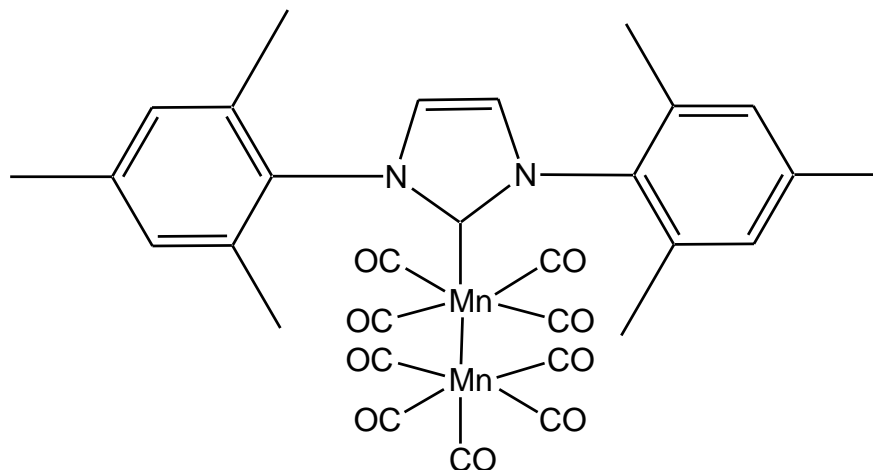
7:



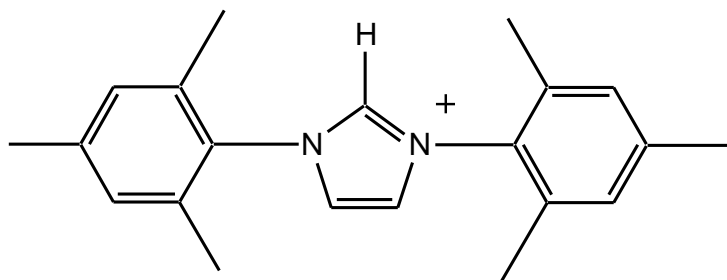
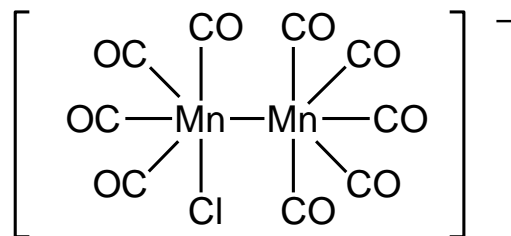
8:



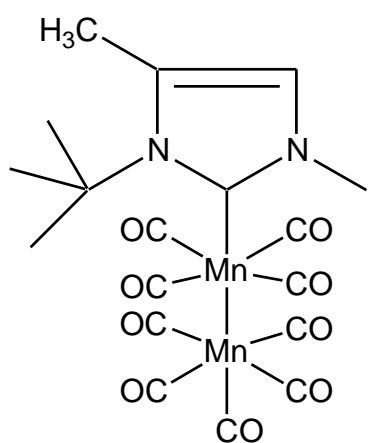
9:



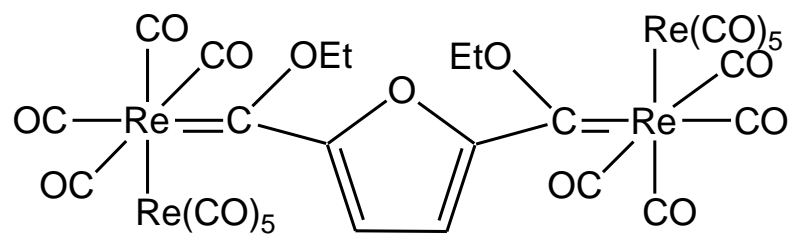
10:



11:

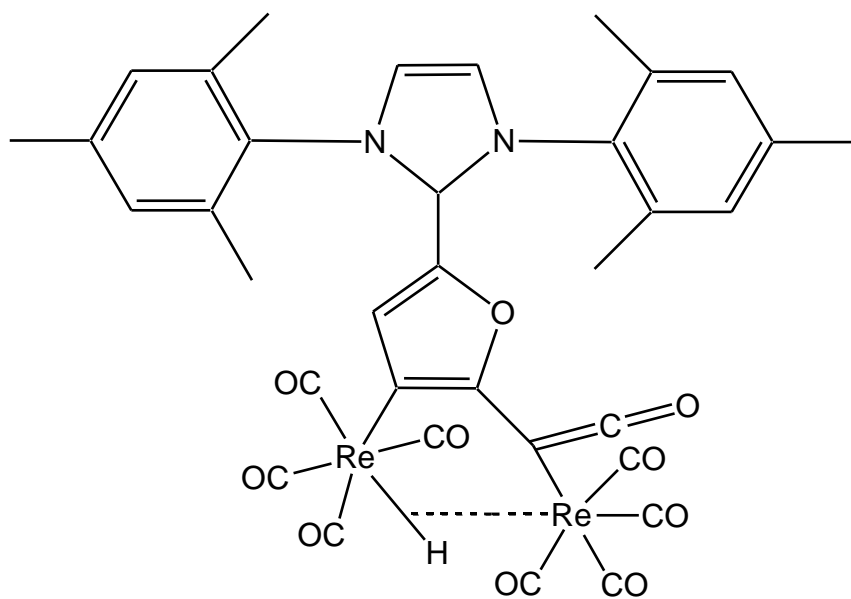


12:





13:



## List of Abbreviations

Å	:	Angstrom
Bu	:	butyl
Cp*	:	pentamethylcyclopentadienyl
dcm	:	dichloromethane
dvtms	:	divinyl tetramethylsiloxane
Et	:	ethyl
Fu	:	furan
Ha	:	Hartrees
Hex	:	hexane
HOMO	:	Highest Occupied Molecular Orbital
IMes	:	1,3-bis(2,4,6-trimethylphenyl)imidazol-2-ylidene
IMesHCl	:	1,3-bis(2,4,6-trimethylphenyl)imidazolium chloride
Imine	:	Glyoxal-bis(2,4,6-trimethylphenyl) imine
IR	:	Infrared
Mes	:	Mesityl
LDA	:	Lithium diisopropylamide
LiTMP	:	Lithium tetramethylpiperidide
LUMO	:	Lowest Unoccupied Molecular Orbital
Me	:	methyl
MS	:	Mass Spectrometry
n.o.	:	not observed
nBuLi	:	n-butyl lithium
NHC	:	<i>N</i> -heterocyclic carbene

NMR	:	Nuclear Magnetic Resonance
Ph	:	Phenyl
RMSD	:	Root Mean Square Deviation
RT	:	room temperature
SM	:	starting material
<sup>t</sup> BuOK	:	potassium tertiary butoxide
Th	:	thiophene
thf	:	tetrahydrofuran
Tlc	:	thin layer chromatography
TM	:	transition metal
UV	:	ultraviolet
$\delta$	:	chemical shift
$\lambda$	:	wavelength
$\nu$	:	wavenumber

## Chapter 1: Introduction

### 1.1 Overview

A carbene is classified as a compound with a divalent carbon atom which is neutral and reactive<sup>1</sup>. When two covalent bonds are formed with this carbene carbon centre, two of the four valence electrons are left. The two electron configurations found for carbenes are either singlet or triplet state (Figure 1.1). If the compound contains  $\pi$ -donating substituents, for example nitrogen atoms, the preferred state would be singlet. The singlet state can be both nucleophilic and electrophilic because of the lone pair and empty p-orbital on the carbene carbon. Examples of a singlet and triplet state carbene can be seen in Figures 1.3 and 1.5 respectively.

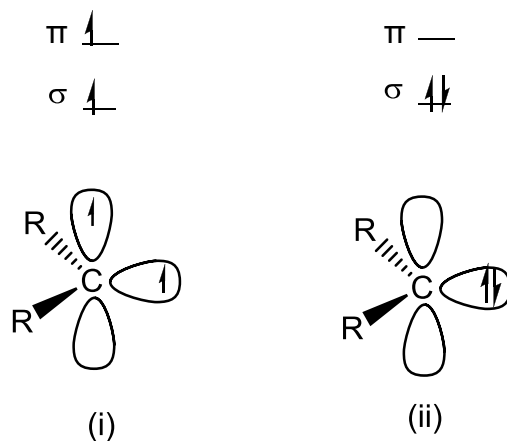


**Figure 1.1:** (i) Triplet and (ii) singlet carbenes

(1) (a) Canal, J. P.; Abernethy, C. D.; Clyburne, J. A. C. *J. Chem. Ed.* **2008**, 85, 416; (b) de Frémont, P.; Marion, N.; Nolan, S. P. *Coord. Chem. Rev.* **2009**, 253, 862.



Flemming divided the substituent and  $\pi$ -system interaction into three classes<sup>2e</sup>. Compounds of the form  $[\text{ML}_n\text{C}(\text{R})_2]$  have substituents (R) which can be  $\pi$ -electron donors (e.g.  $-\text{NR}_2$ ,  $-\text{OR}$ ,  $-\text{SR}$ , halogens),  $\pi$ -electron acceptors (e.g.  $-\text{COR}$ ,  $-\text{SOR}$ ,  $-\text{SO}_2\text{R}$ ,  $-\text{NO}$ ,  $-\text{NO}_2$ ) and conjugated substituents (e.g. alkenes, alkynes, aryl groups)<sup>2</sup>. The type of R substituent influences the ground state of the carbene. The carbene centre interacting with  $\pi$ -electron donor substituents can be deduced to have singlet ground states and those interacting with  $\pi$ -electron acceptors and conjugated substituents, triplet ground states<sup>2</sup>.

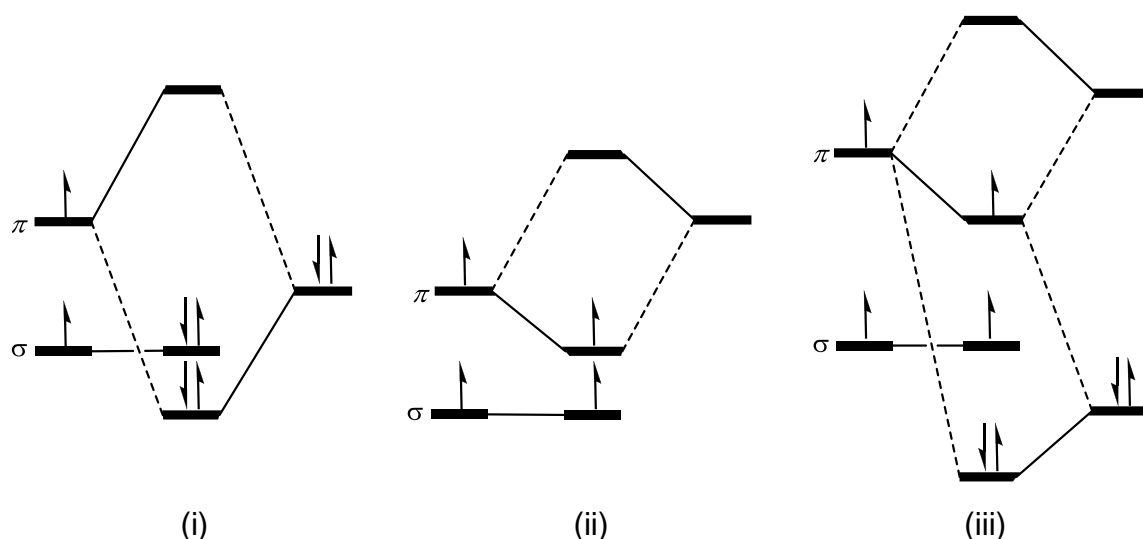


**Figure 1.2:** Carbene interaction with (i)  $\pi$ -electron donors, (ii)  $\pi$ -electron acceptors and (iii) conjugated substituents<sup>2</sup>

(2) (a) Regitz, M., Ed.; *Carbene(oides), Carbyne*; Houben-Weyl, Thieme: Stuttgart, **1989**; (b) Wentrup, C. *Reactive Molecules*; Wiley: New York, **1984**; (c) Moss, R. A., Jones, M., Jr., Eds.; *Carbenes*; Wiley: New York, **1973**, *I*, **1975**, *II*; (d) Kirmse, W. *Carbene Chemistry*, 2<sup>nd</sup> ed.; Academic Press: New York, **1971**; (e) Fleming, I. *Frontier Orbitals and Organic Chemical Reactions*; Wiley: New York, **1976**; (f) Rauk, A. *Orbitals Interaction Theory of Organic Chemistry*; Wiley: New York, **1994**; (g) Sander, W.; Bucher, G.; Wielacher, S. *Chem. Rev.* **1993**, *93*, 1583; (h) Trozzolo, A. M. *Acc. Chem. Res.* **1968**, *1*, 329; (i) Moss, R. A.; Jones, M., Jr., Eds; *Carbenes*, Wiley: New York, **1975**, *I*, 185.

## 1.2 Fischer and Schrock type carbenes

Complexes which contain a carbene carbon atom attached to the metal are referred to as organometallic carbene complexes. By using transition metals (TMs), stabilisation of carbenes can occur in two ways, resulting in two different types of carbene complexes: Schrock carbene and Fischer carbene complexes<sup>1</sup>.

In Schrock carbene complexes  $\sigma$ - and  $\pi$ - bonds between the metal and carbene carbon are formed by sharing electrons (Figure 1.3). This type of complex has a nucleophilic carbene carbon and is usually formed with early TMs in high oxidation states. Mostly ligands with weaker  $\pi$ -accepting character are bound to these metals and in general a triplet carbene ground state is found.

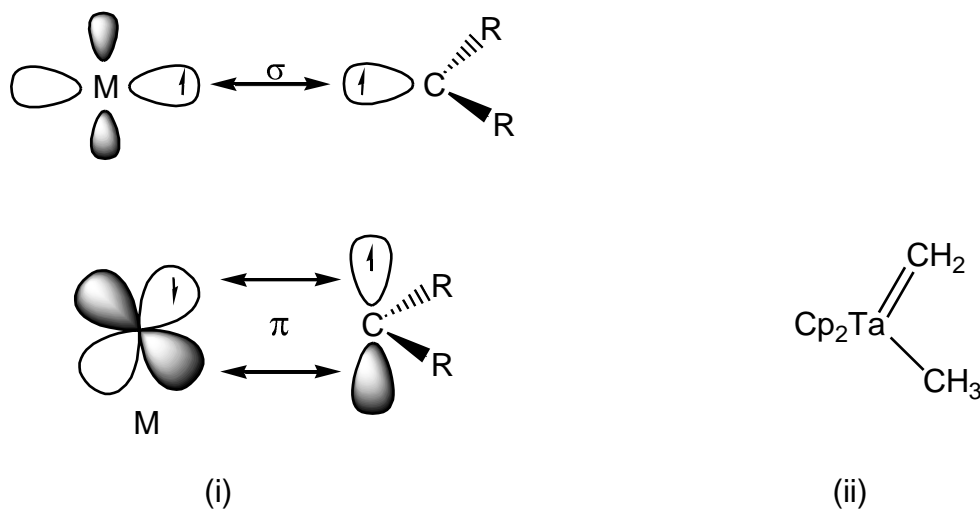


**Figure 1.3:** (i) Stabilization of the carbene carbon atom in Schrock carbene complexes<sup>1</sup> and (ii) an example of such a compound<sup>3</sup>

(3) Schrock, R. R. *Acc. Chem. Res.* **1979**, *12*, 98.

Schrock carbene complexes have, amongst others, application in olefin metathesis<sup>4</sup>, also called *trans*-alkylidenation. Robert H. Grubbs, Richard R. Schrock and Yves Chauvin did ground-breaking work on olefin metathesis. This includes preparation of molybdenum, tungsten<sup>5</sup> and ruthenium<sup>6</sup> carbene complexes for application in olefin metathesis as well as the proposed mechanism<sup>7</sup> for the reaction. It involves the rearrangement of alkene fragments by cleaving the carbon-carbon double bonds in olefins<sup>8</sup> (Figure 1.4). The 2005 Nobel Prize for Chemistry was awarded to these three scientists.

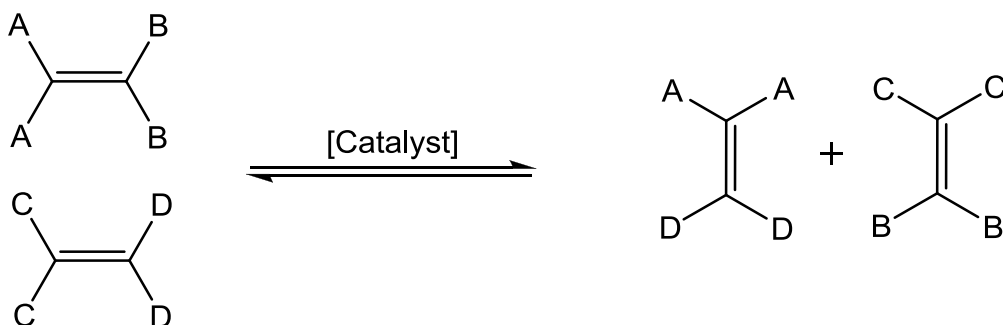


**Figure 1.4:** General scope of olefin metathesis

(4) (a) Murdzek, J. S.; Schrock, R. R. *Organometallics* **1987**, *6*, 1373; (b) Schrock, R. R.; Krouse, S. A.; Knoll, K.; Feldman, J.; Murdzek, J. S.; Young, D. C. *J. Mol. Catal.* **1988**, *46*, 243; (c) Furstner, A. *Angew. Chem., Int. Ed. Engl.* **2000**, *39*, 3012.

(5) (a) Schrock, R. R. *Acc. Chem. Res.* **1986**, *19*, 342; (b) Schrock, R. R. *Angew. Chem., Int. Ed. Engl.* **2006**, *45*, 3748.

(6) (a) Nguyen, S. T.; Johnson, L. K.; Grubbs, R. H.; Ziller, J. W. *J. Am. Chem. Soc.* **1992**, *114*, 3974; (b) Grubbs, R. H. *Angew. Chem., Int. Ed. Engl.* **2006**, *45*, 3760.

(7) Hérisson, J. L.; Chauvin, Y. *Macromol. Chem.* **1971**, *141* 161.

(8) Astruc, D. *New J. Chem.* **2005**, *29*(1), 42.

The  $\sigma$ -bond in Fischer carbene complexes is formed by donation of the carbon lone pair into the empty orbital of the metal and the  $\pi$ -bond is formed by donation of the electron lone pair from the metal orbital into the empty p-orbital of the carbon atom (Figure 1.5). Fischer carbene complexes are usually formed with later TMs in lower oxidation states. The ligands are characterised as stronger  $\pi$ -acceptors and the carbene carbon as electrophilic. The ground state of this type of carbene is generally singlet.

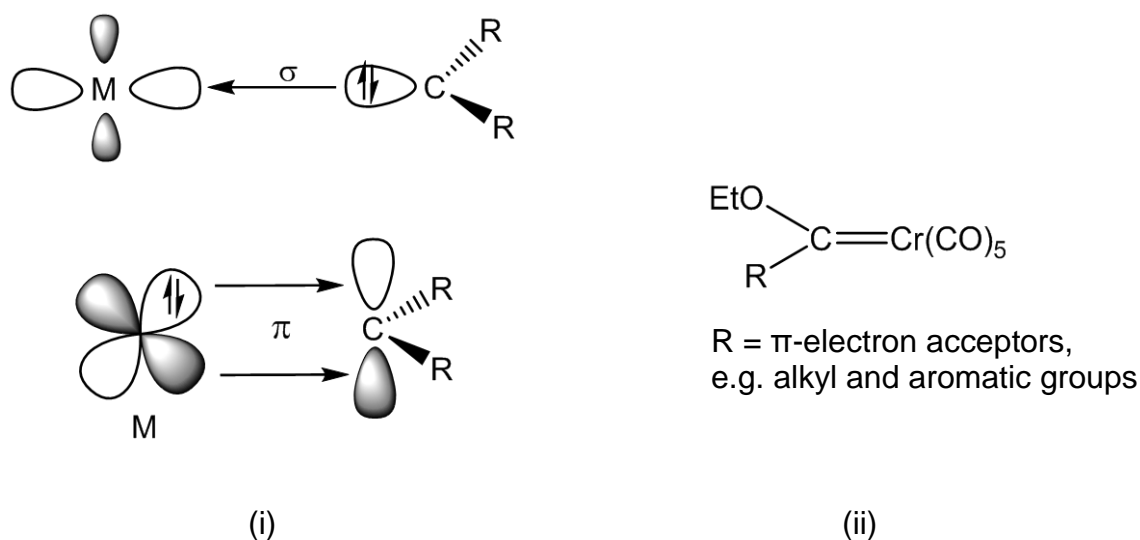


**Figure 1.5:** (i) Stabilization of the carbene carbon atom in Fischer carbene complexes<sup>1</sup> and (ii) an example of this type of complex<sup>9</sup>

Several applications of Fischer carbenes in organic synthesis include sigmatropic rearrangement and Michael additions to  $\alpha$ ,  $\beta$ -unsaturated carbene complexes<sup>10</sup>.

(9) Fischer, E. O.; Maasböl, A. *Angew. Chem. Int. Ed. Engl.* **1964**, 3, 645.

(10) Wulff, W. D. *Compr. Org. Syn.* **1998**, 1065.

Another important application is the reaction of Fischer carbene complexes with alkenes, known as the Dötz or benzannulation reaction. An example is the reaction of a chromium pentacarbonyl complex containing a vinylic or an alkoxy group with an alkyne (Figure 1.6). This C-C coupling reaction affords a substituted phenol  $\pi$ -coordinated to  $\text{Cr}(\text{CO})_3$  after the release of carbon monoxide<sup>11</sup>.

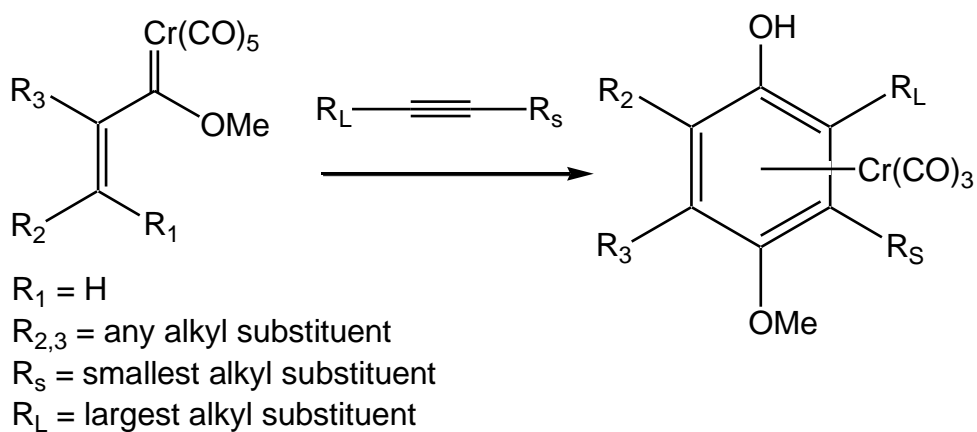


**Figure 1.6:** A general reaction scheme for the Dötz reaction

(11) (a) Dötz, K. H. *Angew. Chem., Int. Ed. Engl.* **1975**, *14*, 644; (b) Dötz, K. H.; Dietz, R.; von Imhof, A.; Lorenz, H.; Huttner, G. *Chem. Ber.* **1976**, *109*, 2033; (c) Timko, J. M.; Yamashita, A. *Org. Synth.* **1998**, *9*, 1; (d) Dötz, K. H. *Pure Appl. Chem.* **1983**, *55*, 1689.

### 1.3 *N*-Heterocyclic carbene complexes

Another type of carbene, called *N*-heterocyclic carbene (NHC), has a carbene carbon atom in the singlet state which is covalently bonded to two nitrogen atoms<sup>1</sup>. The carbene ligand coordinates to the metal (Figure 1.7)<sup>12</sup> to form an *N*-heterocyclic carbene complex.

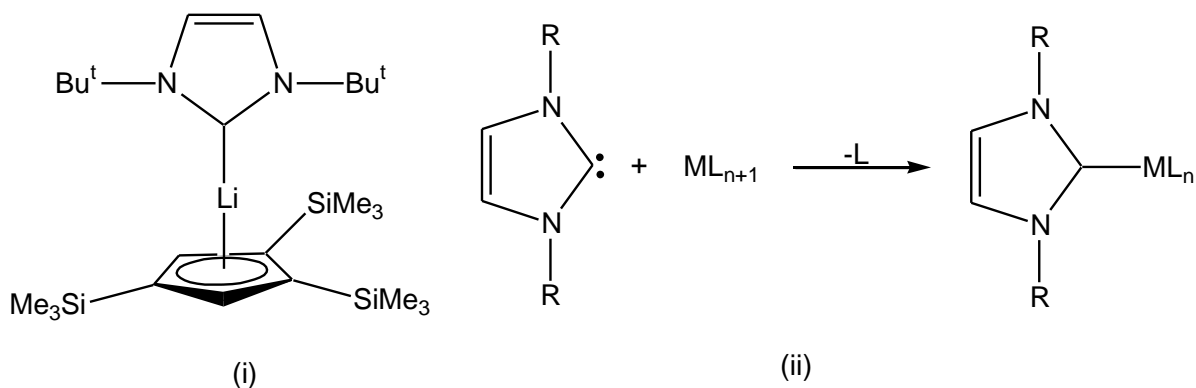


**Figure 1.7:** (i) An example<sup>13</sup> of an NHC complex and (ii) a preparatory method of synthesising these complexes

At first glance this type of complexes may seem to be a subgroup of the Fischer carbene complexes but differences are significant enough for it to be introduced as a separate type of carbene complex. These differences include the character of the M-C bond, rotation around the M-C bond and backbonding from the metal (see later: Chapter 3).

(12) Herrmann, W. A.; Köcher, C. *Angew. Chem., Int. Ed. Engl.* **1997**, 36, 2162.

(13) Arduengo, A. J.; Tamm, M.; Calabrese, J. C.; Davidson, F.; Marshall, W. J. *Chemistry Letters* **1999**, 1021.

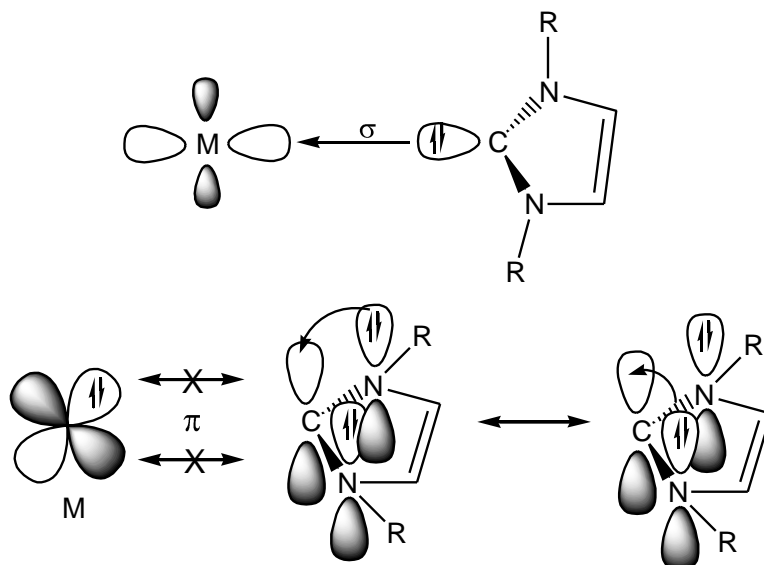


**Figure 1.8:** Stabilization of carbenes in NHC complexes<sup>1</sup>

Both steric and electronic factors contribute to the stability of these carbenes<sup>14</sup>. Electronic stabilisation (Figure 1.8) occurs via the donation of  $\pi$ -electrons into the p-orbital of the carbene carbon by the N-atom. Kinetic stabilisation is achieved by introducing bulky substituents on the N-atoms of the imidazole ring. This not only slows the decomposition process of the compound, but the presence of these highly steric groups around the reactive metal centre limits reaction with external reagents.

The free carbenes appear to mimic phosphorus ligands<sup>15</sup>. The tertiary phosphine ligands of catalysts containing TMs can now be replaced by NHCs<sup>16</sup> which lead to the development of the first generation Grubbs catalyst into what is now called

(14) Arduengo III, A. J.; Dias, H. V. R.; Harlow, R. L.; Kline, M. *J. Am. Chem. Soc.* **1992**, *114*, 5530.

(15) (a) Herrmann, W. A. *Angew. Chem., Int. Ed. Engl.* **2002**, *41*, 1290 and references therein; (b) Herrmann, W. A.; Mihalios, D.; Kiprof, K.; Belmdjahed, F. *Chem. Ber.* **1992**, *125*, 1795; (c) Chianese, A. R.; Li, X.; Janzen, M. C.; Faller, J. W.; Crabtree, R. H. *Organometallics* **2003**, *22*, 1663.

(16) Herrmann, W. A.; Baskakov, D.; Herdtweck, E.; Hoffmann, S. D.; Bunlaksananusorn, T.; Rampf, F.; Rodefeld, L. *Organometallics* **2006**, *25*, 2449.

the second generation Grubbs catalyst<sup>17</sup> (Figure 1.9). The Grubbs catalyst is a carbene complex containing the transition metal ruthenium (Ru) and five ligands. The 1<sup>st</sup> generation Grubbs catalyst contains two chloro-, two phosphine- and one carbene ligand. The same ligands are present in the 2<sup>nd</sup> generation Grubbs catalyst except one phosphine-ligand is replaced by an *N*-heterocyclic carbene ligand. This means that instead of one carbene ligand, two carbenes are now coordinated to the ruthenium.

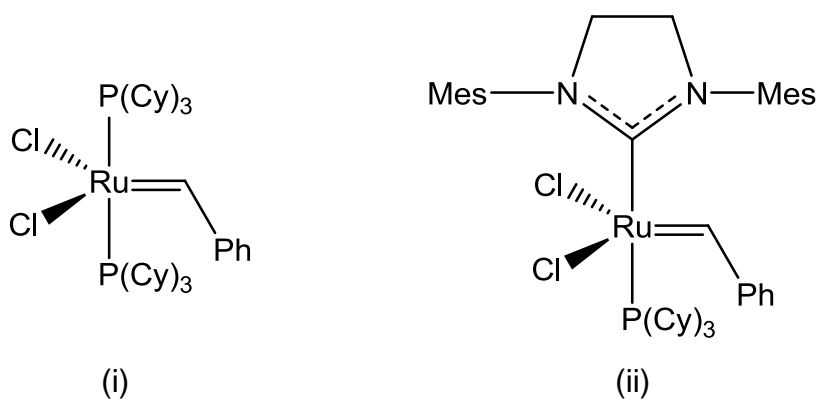


**Figure 1.9:** The (i) first and (ii) second generation Grubbs catalyst

The second generation Grubbs catalysts have the same uses in organic synthesis as the first generation, such as Suzuki coupling, aryl aminations, and metathesis reactions<sup>18</sup> (Figure 1.10) but a higher activity was observed<sup>15(a), 19</sup> due to the additional steric bulk of the complex which protects the reaction centre from external reactions.

(17) Delaude, L.; Szypa, M.; Demonceau, A.; Noels, A. F. *Adv. Synth. Catal.* **2002**, *344*, 6.

(18) Grubbs, R.H.; Tumas, W. *Science* **1989**, *243*, 907.

(19) (a) Kantchev, E. A. B.; O'Brien, C. J.; Organ, M. G. *Angew. Chem., Int. Ed. Engl.* **2007**, *46*, 2768; (b) Díez-González, S.; Nolan, S. P. *Coord. Chem. Rev.* **2007**, *251*, 874.



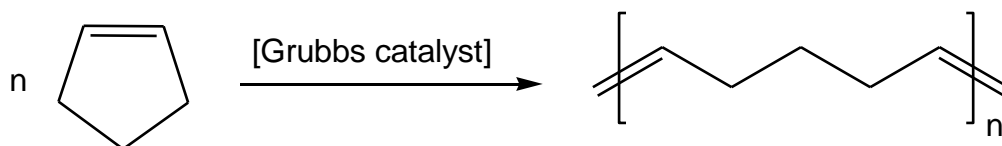


**Figure 1.10:** A ring opening metathesis polymerisation reaction utilising the Grubbs catalyst

Another application of NHC complexes is found in the Heck coupling reaction (Figure 1.11).

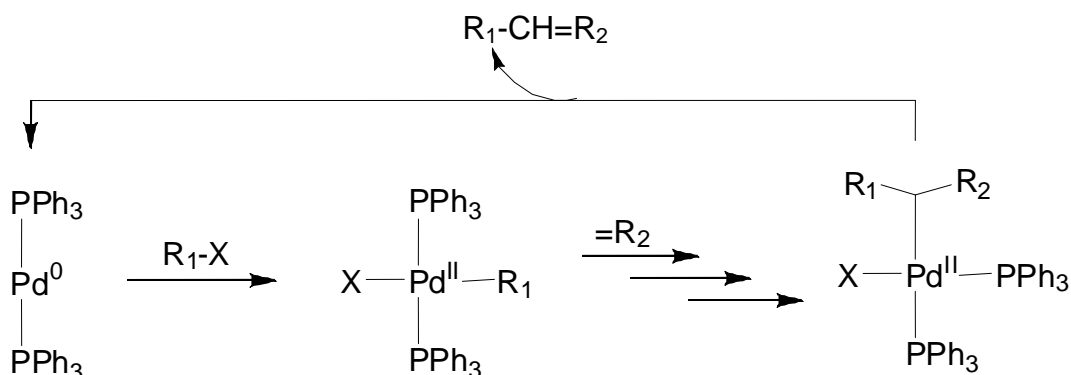


**Figure 1.11:** Palladium phosphine catalyst as employed in the Heck reaction

This reaction is catalysed by a  $\text{Pd}^0$  catalyst<sup>20</sup>. Initially it is activated from  $[\text{Pd}^{\text{II}}(\text{OAc})_2]$  to  $[\text{Pd}^0(\text{PPh}_3)_2]$  after which it enters the catalytic cycle, reacting with  $\text{R}_1\text{-X}$ , an aryl halide, by inserting itself into the aryl-halide bond. In the next step an alkene ( $\text{R}_2$ ) is incorporated and coupled with the aryl compound. The catalyst is then transformed into the *cis*-isomer and after reductive elimination it is regenerated, with the  $\text{PPh}_3$  ligands *trans* to each other. This configuration is the most stable form of the  $[\text{Pd}^0(\text{PPh}_3)_2]$  complex considering the large bulk of the

(20) (a) Heck, R. F.; Nolley, Jr., J. P. *J. Org. Chem.* **1972**, *37*, 2320; (b) Mizoroki, T.; Mori, K.; Ozaki, A. *Bull. Chem. Soc. Jap.* **1971**, *44*, 581

$\text{PPh}_3$  ligand. The configurational changes between the *cis*- and *trans*-isomers increase the reaction time, which can be avoided by the use of the platinum NHC catalyst which is already in the *cis*-conformation. The *cis*-NHC complex is more stable compared to the *trans* conformation of the  $[\text{Pd}^0(\text{NHC})_2]$  complex due to the free rotation that is allowed around the Pd-C bond and the negligible  $\pi$ -back bonding from the metal to the carbene carbon atom. (For more detail see reference).

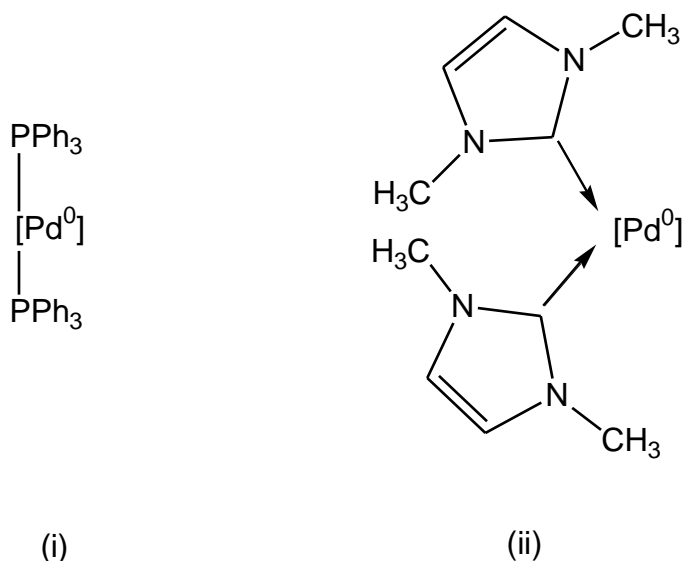


**Figure 1.12:** Heck coupling catalysts showing different configurations employed

Occasionally, severe reaction conditions are needed in the Heck reaction, for example high temperatures are necessary for chloroarene activation and  $\text{Pd}(\text{PPh}_3)_2$  is very unstable under these conditions.

Other limitations experienced with the phosphine ligands include phosphine degradation by P-C bond cleavage<sup>21</sup> and the requirement of a great excess ligand<sup>22</sup>.

(21) Garrou, P. E. *Chem. Rev.* **1985**, *85*, 171.

(22) (a) Falbe, J., Ed.; *New Synthesis with Carbon Monoxide*; Springer, Berlin, **1980**; (b) Herrmann, W. A.; Kohlpaintner, C. W. *Angew. Chem.* **1993**, *105*, 1588; *Angew. Chem. Int. Ed. Engl.* **1993**, *32*, 1524.

Some of these disadvantages can be overcome by utilizing NHC instead of phosphine ligands. Furthermore, the ability to modify these carbenes makes it an even more attractive substitute.

NHCs are not only useful because of their steric bulk, protection and increased kinetic stabilization, but can also be used in the non-complexed form (without a metal attached to the NHC) as an organocatalyst (see later: Chapter 2).

*N*-heterocyclic carbenes form complexes with a wide variety of metals in the form  $ML_n$  (monometal substrates) and  $M_2L_n$  (dimetal substrates). These include main group element, rare earth metals<sup>10</sup> as well as transition metals<sup>23</sup> (Figure 1.13).

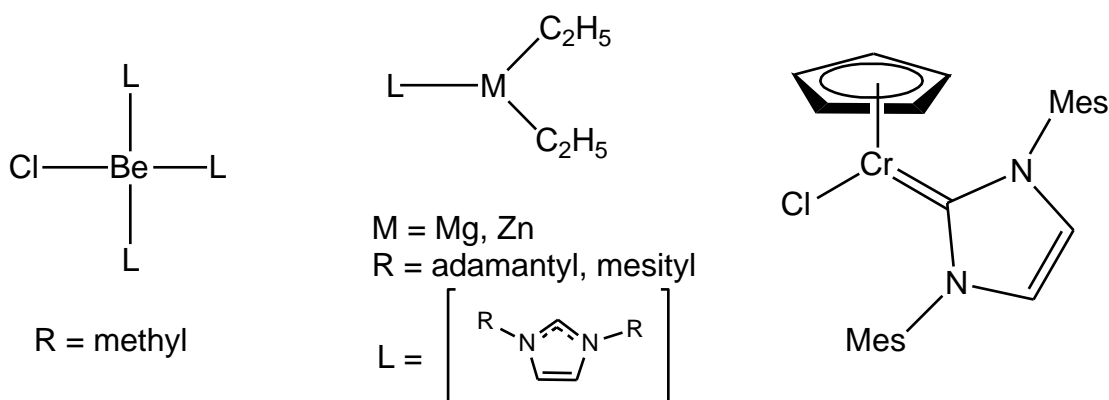


**Figure 1.13:** Examples of NHC complexes containing different metals

Research in this relatively new field expanded rapidly in a short period of time mainly because these carbene ligands:

- are phosphine mimics leading to catalyst engineering and fine tuning<sup>24</sup>
- have lower toxicity than their phosphine analogues<sup>25</sup>

(23) Voges, M. H.; Rømming, C.; Tilset, M. *Organometallics* **1999**, *18*, 529

(24) (a) Weskamp, T.; Böhm, V. P. W.; Herrmann, W. A. *J. Organomet. Chem.* **2000**, *600*, 12; (b) Jafapour, L.; Nolan, S. P. *Adv. Organomet. Chem.* **2001**, *46*, 181.

- form stronger bonds to the metal centre than the phosphines<sup>26</sup>
- display great structural versatility by varying substituents on the nitrogen atoms: chirality, functionalisation, immobilisation, water solubility and chelate effects<sup>27</sup>
- complexed to a variety of metals, and even without the coordinated metal, can be used as catalysts<sup>28</sup>

---

(25) (a) Waltman, A. W.; Grubbs, R. H. *Organometallics* **2004**, *23*, 3105; (b) Dharmasena, U. L.; Foucault, H. M.; Dos Santos, E. N.; Fogg, D. E.; Nolan, S. P. *Organometallics*. **2005**, *24*, 1056; (c) Hu, X.; Castro-Rodriguez, I.; Olsen, K.; Meyer, K. *Organomet.* **2004**, *23*, 755; (d) Dorta, R.; Stevens, E. D.; Hoff, C. D.; Nolan, S. P. *J. Am. Chem. Soc.* **2003**, *125*, 10490; (e) Nakai, H.; Hu, X.; Zakharov, L. N.; Rheingold, A. L.; Meyer, K. *Inorg. Chem.* **2004**, *43*, 855; (f) Castarlenas, R.; Esteruelas, N. A.; Onate, E. *Organometallics* **2005**, *24*, 4343; (g) Buchgraber, P.; Toupet, L.; Guerchais, V. *Organometallics* **2003**, *22*, 5144; (h) Caddick, S.; Cloke, F. G. N.; Hitchcock, P. B.; Lewis, A. K. D. *Angew. Chem., Int. Ed. Engl.* **2004**, *43*, 5824; (i) Danopoulos, A. A.; Hankin, D. M.; Wilkinson, G.; Cafferkey, S. M.; Sweet, T. K. N.; Hursthouse, M. B. *Polyhedron* **1997**, *16*, 3879; (j) Voges, M. H.; Rømming, C.; Tilset, M. *Organometallics* **1999**, *18*, 529.

(26) PhD theses filed under the supervision of W. A. Herrmann (all Technische Universität München): (a) Mihalios, D. PhD thesis, **1992**; (b) Roesky, P. W. PhD thesis, **1994**; (c) Elison, M. PhD thesis, **1995**; (d) Fischer, J. PhD thesis, **1996**; (e) Artus, G. R. J. PhD thesis, **1996**; (f) Reisinger, C. P. PhD thesis, **1997**; (g) Köcher, C. PhD thesis, **1997**; (h) Steinbeck, M. PhD thesis, **1997**; (i) Booßen, L. J. PhD thesis, **1997**; (j) Runte, O. PhD thesis, **2000**; (k) Weskamp, T. PhD thesis, **1999**; (l) Schwarz, J. PhD thesis, **2000**; (m) Böhm, V. P. W. PhD thesis, **2000**; (n) Köhl, F. J. PhD thesis, **2000**; (o) Prinz, M. PhD thesis, **2001**.

(27) (a) Herrmann, W. A.; Weskamp, T.; Böhm, V. P. W. *Adv. Organomet. Chem.* **2002**, *48*, 1; (b) Bourissou, D.; Guerret, O.; Gabbaï, F. P.; Bertrand, G. *Chem. Rev.* **2000**, *100*, 39.

(28) Breslow, R. *J. Am. Chem. Soc.* **1958**, *80*, 3719.

## 1.4 Aim

Although there is a representative amount of NHC complexes with Group VII transition metals in high oxidation states (Re(V, VI, VII) and Tc(V)), not many are known of complexes with these transition metals in low oxidation states. It was decided to investigate the possibility of synthesising NHC complexes with Group VII transition metals (Re(I) and Mn(I)).

Crystallographically characterised representatives of Re(V) and Tc(V) *N*-heterocyclic carbene complexes were published in 2003<sup>29</sup> (Figure 1.14), but are too limited in scope to understand the chemistry of *N*-heterocyclic complexes with Group VII transition metals.

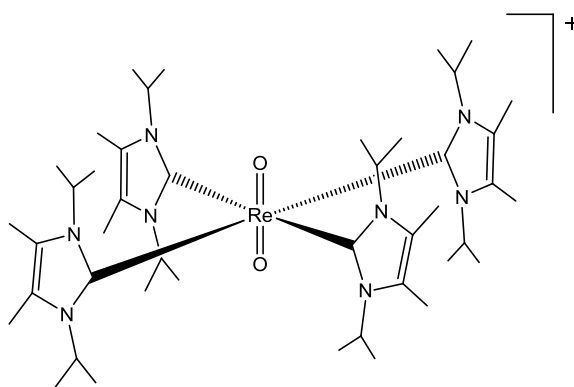


**Figure 1.14:** Structural characterisation of this Re(V) complex and its Tc analogue has been done

This study focuses on approaches toward the synthesis of NHC complexes of Re(I) and Mn(I). The ligand chosen in synthesising these complexes is the ylidene formed from deprotonation of 1,3-bis(2,4,6-trimethylphenyl)imidazolium chloride. This ylidene can be isolated as a free carbene. Since there are no literature reports of direct NHC-group VII transition metal coupling, it was deemed the best route to follow as an initial investigation. The route of *in situ*

(29) (a) Braband, H.; Zahn, T. I.; Abram, U. *Inorg. Chem.* **2003**, *42*, 6160; (b) Royo, B.; Herdtweck, E.; Romão, C. C. *Eur. J. Inorg. Chem.* **2004**, *16*, 3305.

deprotonation followed by quenching of the formed ylidene with the metal substrate was also explored by using different bases and reaction conditions. These routes were investigated and compared by using group VII transition metal substrates  $[\text{Re}(\text{CO})_5\text{Br}]$ ,  $[\text{Mn}(\text{CO})_5\text{Br}]$ ,  $[\text{Re}_2(\text{CO})_{10}]$  and  $[\text{Mn}_2(\text{CO})_{10}]$ .

## Chapter 2: Diaminocarbenes

### 2.1 Background

Since the late 1960s extensive studies have been done on *N*-heterocyclic carbenes (NHCs)<sup>1</sup>. After Arduengo's breakthrough in 1991 when he isolated a free NHC, interest in the synthesis of imidazole-2-ylidenes grew rapidly as it was found that these ligands are excellent alternatives to phosphine ligands in the field of organometallic catalysis<sup>2</sup>, for example the Heck coupling reaction (Chapter 1).

Öfele and Wanzlick synthesised the first NHC complexes in 1968<sup>1</sup> and 1971<sup>3</sup> respectively (Figure 2.1, (i) and (ii)). The first free carbenes were not isolated until 1988 when Bertrand isolated the phosphinocarbene<sup>4</sup> (Figure 2.1 (iii)). Arduengo prepared the first imidazol-2-ylidene (1,3-diadamantylimidazol-2-ylidene) in 1991<sup>5</sup> (Figure 2.1 (iv)). In fact, the first stable triplet carbene was only isolated in 1995 by Tomoika<sup>6</sup> (Figure 2.1 (v)), but is not a diaminocarbene.

---

(1) Öfele, K. J. *Organomet. Chem.* **1968**, *12*, 42

(2) Herrmann, W. A.; Elison, M.; Fischer, J.; Köcher, C.; Artus, G. R. J. *Angew. Chem., Int. Ed. Engl.* **1995**, *34*, 2371.

(3) (a) Wanzlick, H. W.; Schönherr, H. J. *Angew., Chem. Int. Ed. Engl.* **1968**, *7*, 141; (b) Luger, P.; Ruban, G. *Acta Crystallogr. Sect. B* **1971**, *27*, 2276.

(4) Igau, A.; Grutzmacher, H.; Baccero, A.; Bertrand, G. *J. Am. Chem. Soc.* **1988**, *110*, 6463.

(5) Arduengo III, A. J.; Harlow, R. L.; Kline, M. *J. Am. Chem. Soc.* **1991**, *113*, 361.

(6) Tomoika, H.; Watanabe, T.; Hirai, K.; Furukawa, K.; Takui, T.; Itoh, K. *J. Am. Chem. Soc.* **1995**, *117*, 6476.

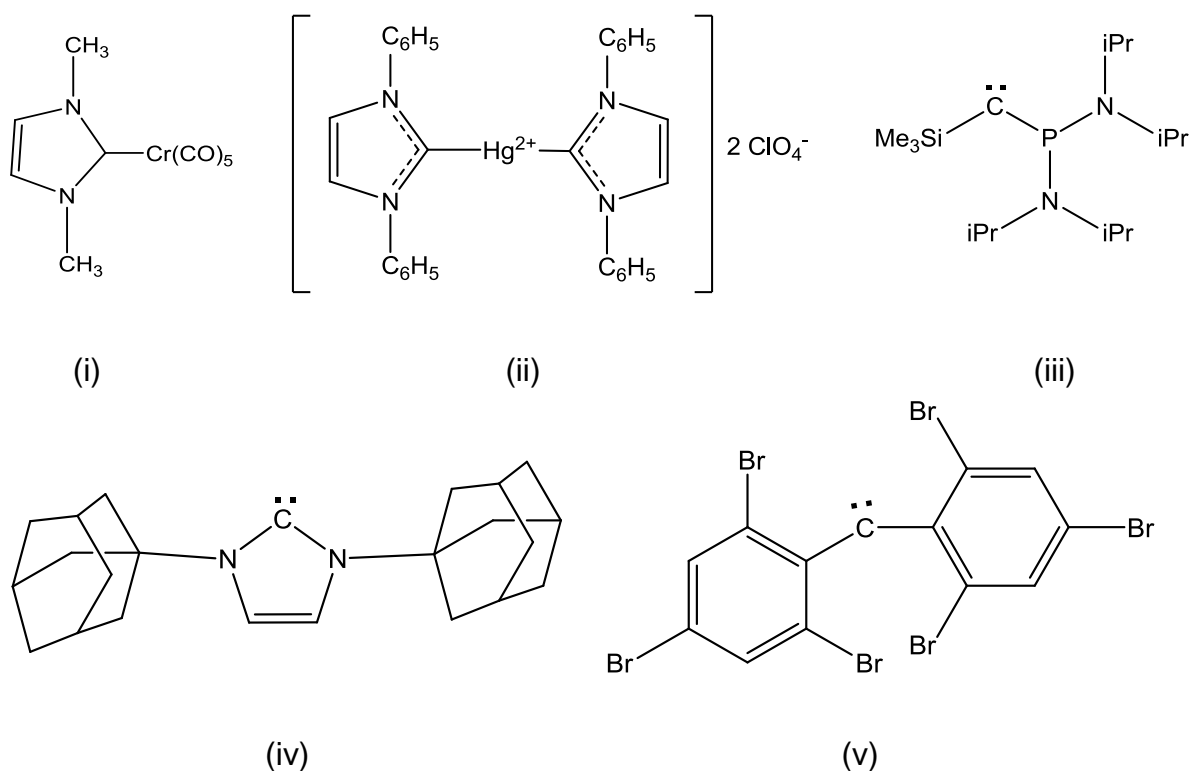


Figure 2.1: Early free NHCs and NHC complexes

## 2.2 Structure and general properties

In the early 1990's the importance of the  $\pi$ -donation from the two nitrogen lone pairs into the empty p-orbital of the carbene carbon was underestimated by Arduengo<sup>7</sup> and Cioslowski<sup>8</sup>. Heinemann *et al.*<sup>9</sup> performed theoretical studies on the stable diaminocarbenes synthesised by Arduengo<sup>5</sup> and Denk<sup>10</sup> and proved the contrary. Electron delocalisation does occur in cyclic unsaturated imidazol-2-ylidene systems, especially compared to their saturated analogues.<sup>9</sup>

(7) Dixon, D. A., Arduengo, A. J.; *J. Phys. Chem.*, **1991**, *95*, 4180.

(8) Cioslowski, J., *In. J. Quantum Chem.* **1993**, 309.

(9) Heinemann, C., Muller, T., Apeloig, Y., Schwarz, H. *J. Am. Chem. Soc.* **1996**, *118*, 2023.

(10) Denk, M., Lennon, R., Hayashi, R., West, R., Belyakov, A. V., Verne, H. P., Haaland, A., Wagner, M., Metsler, N.; **1994**, *116*, 2691.



However, aromaticity of these unsaturated cyclic ylidenes is less prominent compared to its corresponding salt or to benzene.

These findings are also supported by the theoretical study of Frenking *et al.*<sup>11</sup> where he ascribed the ability to isolate the 1,3-bis(2,4,6-trimethylphenyl)imidazol-2-ylidene specifically to the 'strong  $\pi$ -donor stabilisation of the carbene p-orbital by the nitrogen lone pairs'<sup>12</sup>.

#### *Bond lengths and angles*

An interesting characteristic of the N-C-N bond angles of diaminocarbenes is that it is consistently smaller than the corresponding salt precursor, whether it is cyclic ( $100^\circ$ - $102^\circ$  vs  $107^\circ$ )<sup>12</sup> or acyclic ( $121^\circ$  vs  $133^\circ$ )<sup>13</sup>.

The N-C bond of the carbene (1.35-1.38Å) is longer compared to the imidazolium ion precursors (1.28-1.33Å) and some double bond character can be found in considering the values of these bond lengths<sup>14</sup>.

#### *<sup>13</sup>C NMR shifts*

It is important to mention the down field chemical shift of the carbene carbon atom compared to its value in the protonated form. The <sup>13</sup>C NMR values for imidazol-2-ylidenes N-C-N carbene carbons are found between 210-220ppm<sup>14</sup>. This value shifts upfield when complexed to a metal.

---

(11) Boehme, C.; Frenking, G. *J. Am. Chem. Soc.* **1996**, *118*, 2039.

(12) (a) Alder, R. W.; Allen, P. R.; Murray, M.; Orpen, A. G. *Angew. Chem., Int. Ed. Engl.* **1996**, *35*, 1121; (b) Arduengo, A. J.; Krafczyk, R.; Schmutzler, R. *Tetrahedron* **1999**, 14523.

(13) Alder, R. W.; Blake, M. E.; Bufali, S.; Butts, C. P.; Orpen, A. G.; Schutz, J.; Williams, S. J. *J. Chem. Soc., Perkin Transactions 1* **2001**, 1586.

(14) Bertrand, G., Ed.; *Carbene Chemistry*; New York, **2002**.

## 2.3 Methods towards the synthesis of imidazol-2-ylidenes

Different methods to form the imidazolylidene (free carbene) have been investigated and a few examples are shown here.

Anhydrous reaction conditions are necessary for all methods.

### 2.3.1 Deprotonation by strong bases<sup>15</sup>

Non-protic solvents are used, for example thf or ethers and strong bases (pKa above 14) are employed, such as NaH and <sup>t</sup>BuOK.

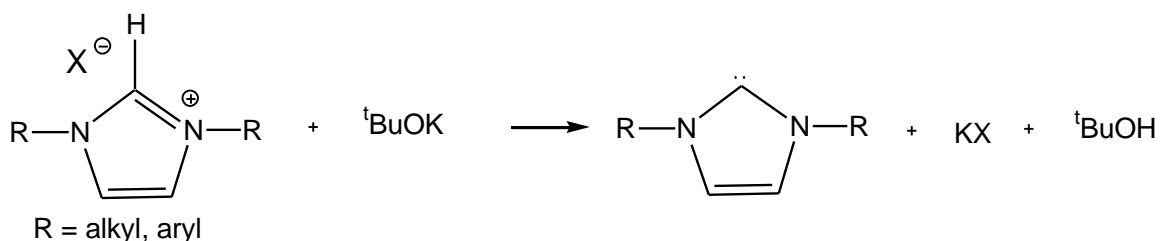


**Figure 2.2:** Deprotonation to form an imidazol-2-ylidene

(15) (a) Herrmann, W. A. *Angew. Chem., Int. Ed. Engl.* **2002**, *41*, 1290; (b) Arduengo III, A. J.; Goerlich, J. R.; Marshall, W. J. *J. Am. Chem. Soc.* **1995**, *117*, 11027; (c) Douthwaite, R. E.; Häussinger, D.; Green, M. L. H.; Silcock, P. J.; Gomes, P. T.; Martius, A. M.; Danopoulos, A. A. *Organomet.* **1999**, *18*, 4584; (d) Amyes, T. L.; Diver, S. T.; Richard, J. P.; Rivas, F. M.; Koth, K. J. *Am. Chem. Soc.* **2004**, *126*, 4366; (e) Waltman, A. W.; Ritter, T.; Grubbs, R. H. *Organometallics* **2006**, *25*, 4238.

### 2.3.2 Deprotonation by the radical anion superoxide<sup>16</sup>

In this method the base is formed *in situ* – dioxygen is reduced by a Fe<sup>I</sup> 19-electron complex to form a radical superoxide anion.

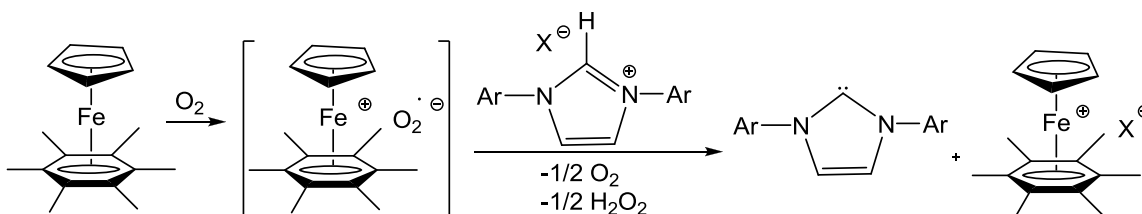


**Figure 2.3:** Radical anion superoxide base route

### 2.3.3 Chemical or electrochemical reduction<sup>7a, 17</sup>

Boiling thf and excess potassium are used in this method.

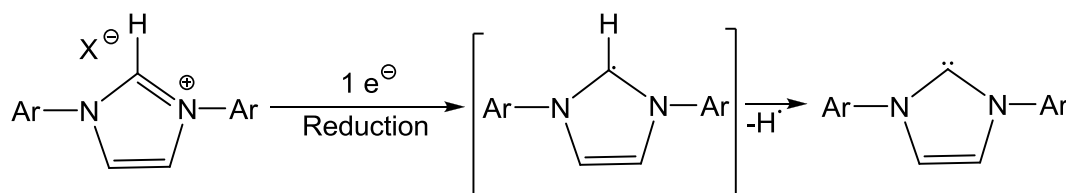


**Figure 2.4:** Imidazolylidene formation *via* reduction

(16) Méry, D.; Aranzaes, R.; Astruc, D. *J. Am. Chem. Soc.* **2006**, *128*, 5602.

(17) Gorodetsky, B.; Ramnial, T.; Branda, N. R.; Clyburne, J. A. C. *Chem. Commun.* **2004**, 1972.

### 2.3.4 Reduction of thiones with metal<sup>18</sup>

The same reagents as in section 2.3.3 are used.

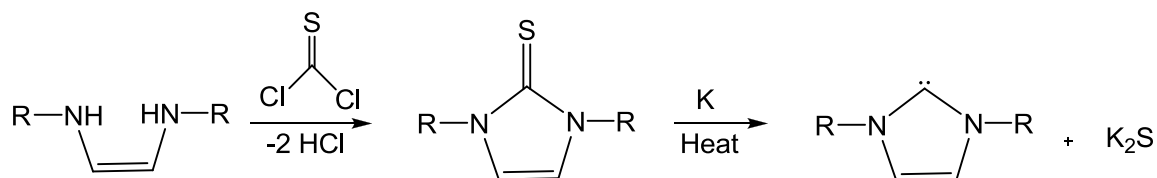


**Figure 2.5:** Reduction of imidazole-2-thiones

## 2.4 Applications

A useful application of free NHCs includes their use as organocatalysts<sup>19</sup>. Processes like *trans*-esterification and acylation reactions, ring opening reactions, 1,2-addition reactions, generation of homoenolates<sup>20</sup> (Figure 2.6), etc., have been reported where free NHCs have been employed as such.

(18) (a) Kuhn, N.; Kratz, T. *Synth.* **1993**, 561; (b) Hahn, F. E.; Wittenbecher, L.; Boese, R.; Bläster, D. *Chem. Eur. J.* **1999**, 5, 1931; (c) Denk, M. K.; Thadani, A.; Hatano, K.; Lough, A. J. *Angew. Chem., Int. Ed. Engl.* **1997**, 36, 2607; (d) Benac, B. L.; Burgess, E. M.; Arduengo III, A. J. *Org. Synth.* **1986**, 64, 92; (e) Arduengo III, A. J. U.S Patent 5,162,482, **1992**; (f) Arduengo III, A. J. *Acc. Chem. Res.* **1999**, 32, 913.

(19) Enders, D.; Niemeier, O.; Alexander, H. *Chem. Rev.* **2007**, 107, 5606.

(20) Marion, N.; Díez-González, S.; Nolan, S. P. *Angew. Chem., Int. Ed. Engl.* **2007**, 46, 2988.

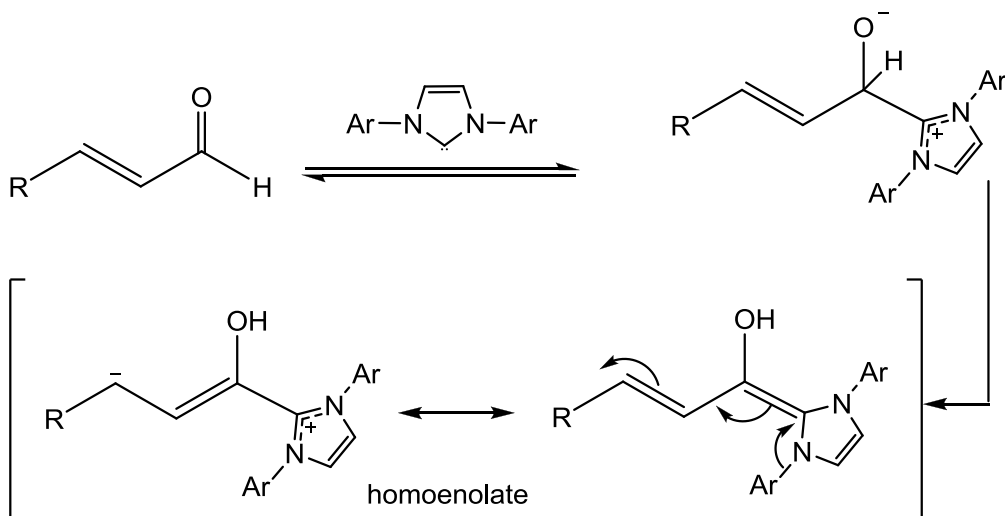


**Figure 2.6:** NHC-catalysed synthesis of homoenolates

## 2.5 Side reactions

Some interesting side reactions were described in literature and will be discussed briefly.

In the 2001 article of Denk<sup>21</sup> the hydrolysis of NHCs is described with formamide formation *via* ring opening, resulting in an acyclic product (Figure 2.10).

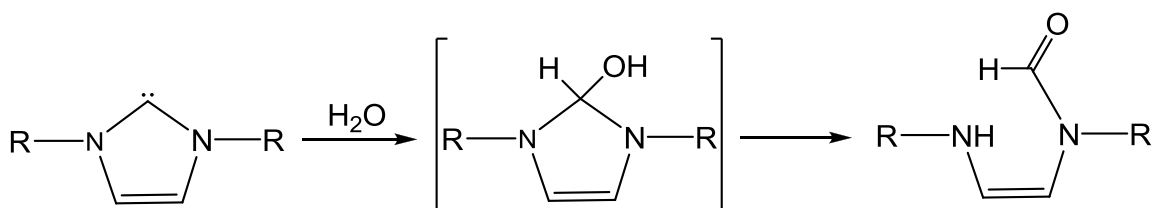


**Figure 2.7:** Hydrolysis pathway of NHCs

(21) Denk, M. K.; Rodenzo, J. M.; Gupta, S.; Lough, A. *J. Organomet. Chem.* **2001**, 617, 618, 242.

Vinyl formation also occurred as a side reaction when bases such as lithium diisopropylamide (LDA) and lithium tetramethylpiperidide (LiTMP) are used (Figure 2.8)<sup>14</sup>. The deprotonation of a methylene group yields a vinyl group, and once again an acyclic decomposition product is obtained. Reports suggested that with weaker bases this competing deprotonation can be minimized.

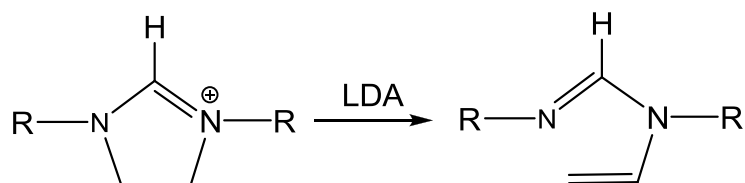


**Figure 2.8:** Vinyl formation of NHCs

Diaminocarbene dimerisation has also been observed as a side reaction (Figure 2.9).

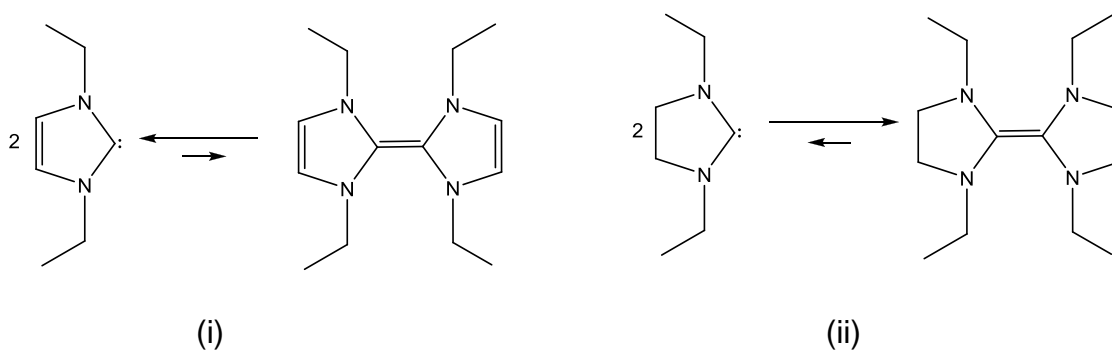


**Figure 2.9:** Diaminocarbene dimerisation: (i) type I and (ii) type II

It is found that type I shows very little dimerisation affinity<sup>22</sup> due to its stability attributed to the aromaticity in the compound<sup>23</sup>. This leads to a high entropy of dissociation value which makes it difficult for adequate experimental determination of the diaminocarbene bond dissociation energy<sup>24</sup>.

Furthermore, 1,2 H-migration from the nitrogen atoms in the imidazole ring can also occur after ylidene formation (Figure 2.10)<sup>25</sup>. Substituents on the N-atoms (either large or small R-groups) can prevent migration and this minimizes the range of products that can be obtained.

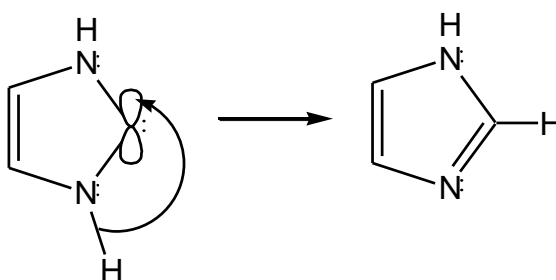


**Figure 2.10:** H-migration from the N-atom

(22) (a) Arduengo III, A. J.; Krafczyk, R. *Chem. Ztg.* **1998**, 32, 6; (b) Arduengo III, A. J.; Harlow, R. L.; Kline, M. *J. Am. Chem. Soc.* **1991**, 113, 361; (c) Arduengo III, A. J.; Dias, H. V. R.; Harlow, R. L.; Kline, M. *J. Am. Chem. Soc.* **1992**, 114, 5530; (d) Arduengo III, A. J.; Davidson, F.; Dias, H. V. R.; Goerlich, J. R.; Khasnis, D.; Marshall, W. J.; Prakasha, T. K. *J. Am. Chem. Soc.* **1997**, 119, 12742; (e) Arduengo III, A. J.; Goerlich, J. R.; Krafczyk, R.; Marshall, W. J. *Angew. Chem., Int. Ed. Engl.* **1998**, 37, 1963; (f) Herrman, W. A.; Köcher, C.; Goossen, L. J.; Artus, G. R. J. *Chem. Eur. J.* **1996**, 2, 1627.

(23) (a) Boehme, C.; Frenking, G. *J. Am. Chem. Soc.* **1996**, 118, 2039; (b) Heinemann, C.; Müller, T.; Apeloig, Y.; Schwarz, H. *J. Am. Chem. Soc.* **1996**, 118, 2023; (c) Sauers, R. R. *Tetrahedron Lett.* **1996**, 37, 149; (d) Olsson, M. H. M.; Boroski, P. *Theor. Chim. Acta* **1996**, 93, 17; (e) Arduengo III, A. J.; Dias, H. V. R.; Dixon, D. A.; Harlow, R.; Klooster, W. T.; Koetze, T. F. *J. Am. Chem. Soc.* **1994**, 116, 6812.

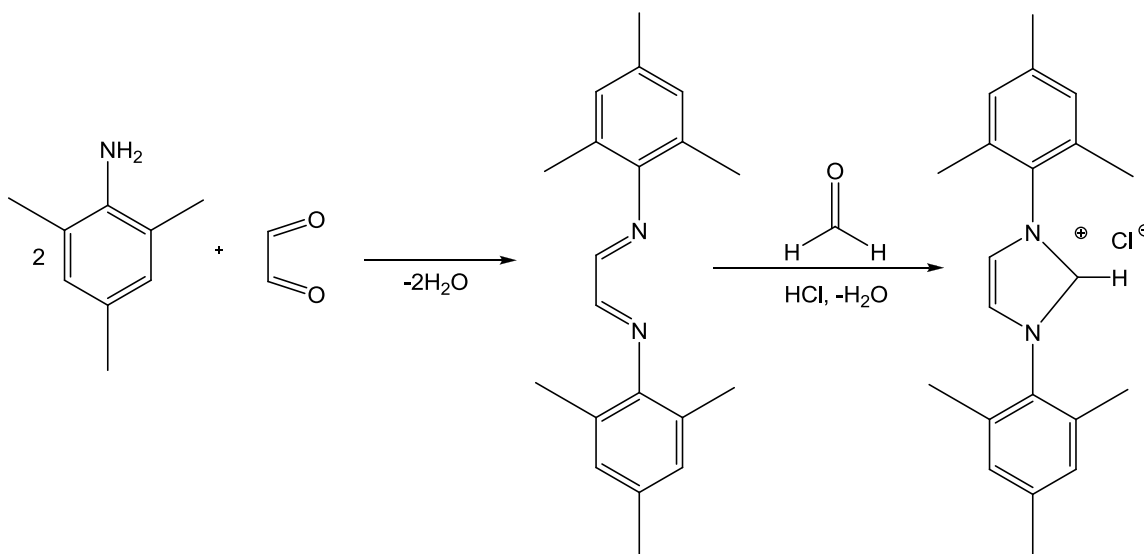
(24) Liu, Y.; Lindner, P. E.; Lemal, D. M. *J. Am. Chem. Soc.* **1999**, 121, 10626.

(25) (a) Heinemann, C.; Thiel, W. *Chem. Phys. Lett.* **1994**, 217, 11; (b) McGibbon, G.A.; Heinemann, C.; Lavorato, D. J.; Schwarz, H. *Angew. Chem., Int. Ed. Engl.* **1997**, 36, 1478; (c) Maier, G.; Endres, J.; Reisenauer, H. P. *Angew. Chem., Int. Ed. Engl.* **1997**, 36, 1709.

## 2.6 Synthesis, results and discussion

### 2.6.1 Synthesis of 1,3-bis(2,4,6-trimethylphenyl)imidazolium chloride (IMesHCl)

Synthesising the appropriate salt (precursor) is done by a relatively easy and reliable two step method<sup>26</sup>. In the first step a primary amine (2,4,6-trimethyl aniline, 0.07mol, 10ml) and glyoxal (4ml, 40% solution) are reacted and by removal of water the corresponding Schiff base (glyoxal-bis(2,4,6-trimethylphenyl)imine) is formed. The second step involves condensation with formaldehyde (0.04mol, 0.6g) and by addition of 2.5ml of a HCl/dioxane solution (4ml 32% HCl in 6ml dioxane) the imidazolium salt is formed after stirring the mixture for 4-7 days (Figure 2.11). The beige precipitate was washed with cold diethylether and thf to yield a white powder.

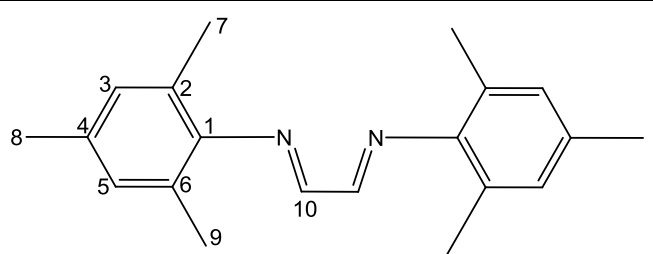


**Figure 2.11:** Synthetic route of the imidazol precursor

(26) (a) Arduengo III, A. J.; Krafczyk, R.; Schmutzler, R. *Tetrahedron* **1999**, *55*, 14523; (b) Jafarpour, L.; Stevens, E. D.; Nolan, S. P. *J. Organomet. Chem.* **2000**, *606*, 49; (c) Hintermann, L. *J. Org. Chem.* **2007**, *3*, 22; (d) de Frémont, P.; Scott, N. M.; Stevens, E. D.; Ramnial, T.; Lightbody, O. C.; MacDonald, C. L. B.; Clyburne, J. A. C.; Nolan, S. P. *Organometallics* **2005**, *24*, 6301.

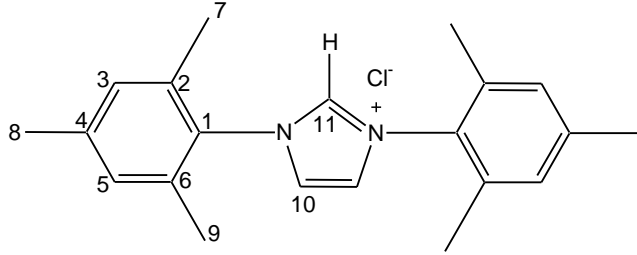


**Table 2.1:** NMR data for glyoxal-bis(2,4,6-trimethylphenyl) imine (imine) in CDCl<sub>3</sub>

	
Atom number	<sup>1</sup> H NMR (ppm)
7,9	2.11 (s, 12H)
8	2.14 (s, 6H)
3,5	6.76 (m, 4H)
10	8.06 (s, 2H)
<sup>13</sup> C NMR (ppm)	
7,9	18.3
8	20.8
3,5	126.7
2,6	129.4
4	134.1
1	148.2
10	163.6

The chemical shifts in the <sup>1</sup>H and <sup>13</sup>C NMR spectra of the imine are given in Table 2.1. The spectra were recorded in CDCl<sub>3</sub>. The assignment of the chemical shifts of the atoms of this Schiff base was based on the assignments found in literature<sup>26</sup>. In the <sup>1</sup>H NMR spectrum, singlet signals were found for protons 7, 8 and 9.

**Table 2.2:** NMR data for 1,3-bis(2,4,6-trimethylphenyl)imidazolium chloride (IMesHCl) in CDCl<sub>3</sub>

	
Atom number	<sup>1</sup> H NMR (ppm)
7,9	2.08 (s, 12H)
8	2.27 (s, 6H)
3,5	6.93 (s, 4H)
10	7.69 (s, 2H)
11	10.51 (s, 1H)
<sup>13</sup> C NMR (ppm)	
7,9	17.9
8	21.4
3,5	125.2
10	130.1
2,6	131.0
1	134.4
4	139.5
11	141.4

The chemical shifts in the <sup>1</sup>H and <sup>13</sup>C NMR spectra of the imidazolium chloride salt are given in Table 2.2. The spectra were recorded in CDCl<sub>3</sub>. The aromaticity of the imidazol ring makes it an electron withdrawing group on the mesityl ring and the deshielding effect of this substituent is evident from the downfield shift of the *p*-methyl protons.

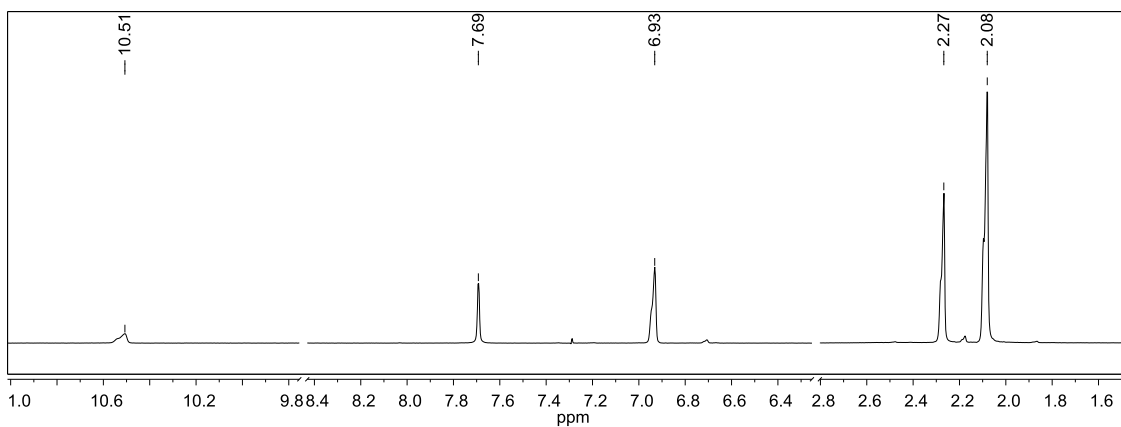


Figure 2.12: <sup>1</sup>H NMR spectrum of IMesHCl in CDCl<sub>3</sub>

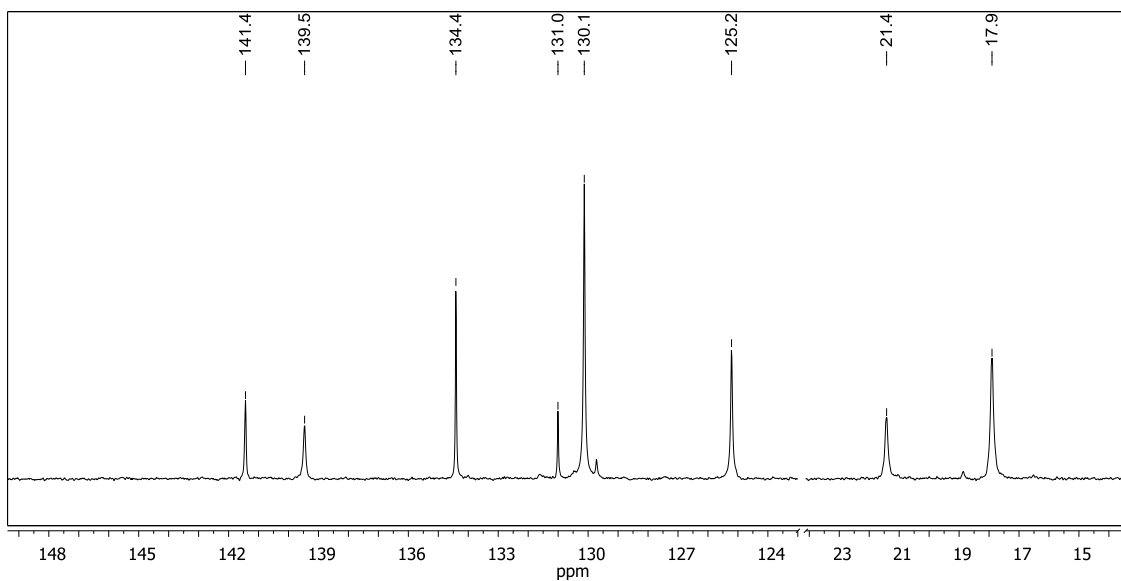


Figure 2.13: <sup>13</sup>C NMR spectrum of IMesHCl in CDCl<sub>3</sub>

### 2.6.2 Isolation of 1,3-bis(2,4,6-trimethylphenyl)imidazol-2-ylidene (IMes)

Deprotonation by strong bases was the method chosen to form the ylidene used in this study, as described by Arduengo<sup>27</sup>. Relatively high yields of the isolated free carbene was reported.

The chloride salt (3.6mmol, 1.24g) was deprotonated by 3.6mmol of strong base in 15ml of thf. The ylidene was extracted in toluene and after the solvent was removed a yellow oil resulted.

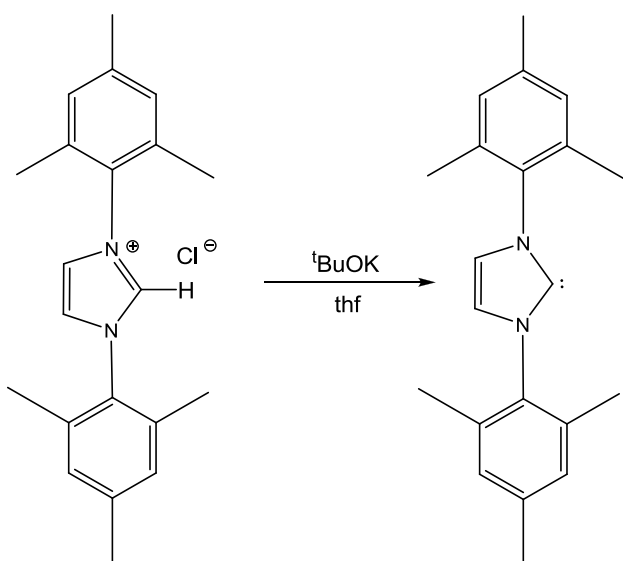


Figure 2.14: Deprotonation according to Arduengo

When the NMR analysis data obtained were compared with literature<sup>27</sup>, it appeared that the ylidene was either not formed or it underwent side reactions before or during analysis. The peaks related to the ylidene could not be unambiguously assigned and it is unclear from the data if the ylidene was still present as there was no signal found in the expected range of 220ppm shift in

(27) Arduengo, III, A. J.; Dias, H. V. R.; Harlow, R. L.; Kline, M. *J. Am. Chem. Soc.* **1992**, *114*, 5530.

the  $^{13}\text{C}$  NMR to confirm the presence of the carbene carbon. Also seen in the spectrum are resonances found in the range of 163ppm and these correspond well to the signals obtained for the C10 atoms in the Schiff base (see Table 2.1). In the  $^1\text{H}$  NMR spectrum a signal of 9.55ppm was observed and this resonance value is very close to the H11 value of the protonated form of the ligand. In the second attempt to isolate the ylidene, extraction was done with benzene instead of toluene. Similar results were obtained.

These observations lead us to believe that fragmentation occurs during analysis due to the highly reactive nature of the carbene and that the reaction should only be attempted in a glove box.

It is known in practice that upscaling and downscaling procedure amounts may influence the outcome of the results and yield of the product. Based on this the procedure was repeated without downscaling. Yet again similar NMR results were obtained in which the chemical shifts resemble the fragmented ligand and not the ylidene.

Repeating the procedure using another base, nBuLi (a stronger base than  $^t\text{BuOK}$ ), yielded similar results and the ylidene could not be isolated.

After this attempt it was decided not to isolate the ylidene, instead *in situ* formation of the free carbene was attempted. The deprotonation step was done in thf to form the ylidene and this step was directly followed by quenching of the ylidene with a metal substrate. This was done to limit the time allowed for side reactions to occur and in the process prepare the target metal complexes with NHC ligands. Results obtained will be discussed in subsequent chapters.

## Chapter 3: Monometal NHC complexes and experimental results

### 3.1 Introduction

#### 3.1.1 Monometal NHC complexes of group VI, VIII and IX transition metals

Even though NHC complexes (*N*-heterocyclic ligand coordinated to a metal) have been known for more than 40 years, their potential as catalysts has only been studied in the last 15 years<sup>1</sup>. Table 3.1 summarises some of the catalytic processes where NHC complexes are used.

Table 3.1<sup>2</sup>: Some of the catalytic processes employing NHC complexes

Catalytic process	NHC complex metal
Olefin metathesis and organic transformations	Ru
Cross-coupling reactions	Pd
Telomerisation and aryl amination reactions	Pd
Metal-mediated and -catalysed oxidations	Co, Ni, Pd
Hydrosilation of alkenes and alkynes	Pt
Rearrangement, cycloadditions, coupling, oligomerisation, polymerisation and hydrogenation	Ni
Asymmetric catalysis	Cu, Rh, Pd, Ru
Hydrogenation	Ir, Rh
Conjugate additions, reduction of carbonyl compounds, allylic alkylations, synthesis of esters, carbene delivery agents, carbene transfer reactions	Cu, Ag, Au

(1) Arnold, P. L., Pearson, S. *Coordination Chemistry Reviews*. **2007**, 251, 596.

(2) Bertrand, G., Ed.; *Carbene Chemistry*; New York, **2002**.

These complexes are generally synthesised by addition of the NHC to the metal substrate in toluene or thf at room temperature. The NHC Pt<sup>0</sup> complex (Figure 3.1) is synthesised in this way.

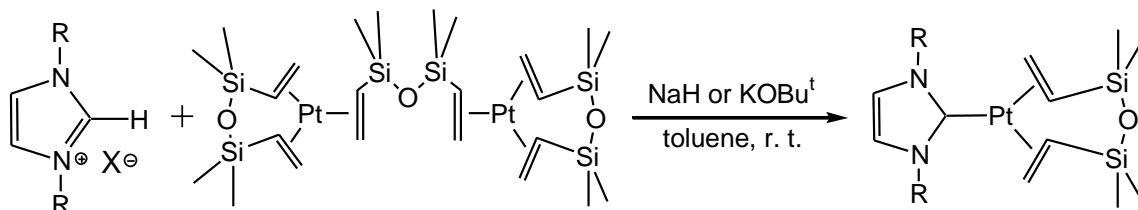


**Figure 3.1:** Synthetic route of [(NHC)Pt(dvtms)] complexes<sup>1</sup>

This complex contains a divinyltetramethylsiloxane (dvtms) ligand and catalyses selective hydrosilylation of alkenes and alkynes (Figure 3.2).

The <sup>13</sup>C NMR chemical shifts of the carbene carbons of these complexes or catalysts range from approximately 170 – 200ppm<sup>3</sup> and vary with other ligands attached to the metal. These resonances are relatively high field compared to the <sup>13</sup>C NMR shifts of for example the carbene carbon in Fischer carbene complexes containing group VII transition metals which resonate at around 240 - 300ppm.<sup>4</sup>

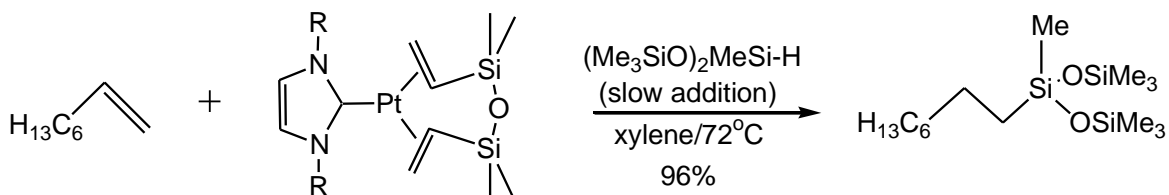


**Figure 3.2:** Hydrosilylation of oct-1-ene by [(ICy)Pt(dvtms)]<sup>1</sup>

(3) Schuster, O.; Yang, L.; Raubenheimer, H. G.; Albrecht, M. *Chem. Rev.* **2009**, 109, 3445.

(4) Bezuidenhout, D. I.; Liles, D. C.; van Rooyen, P. H.; Lotz, S. *J. Organomet. Chem.* **2007**, 692, 774

Synthesis of group VI transition metal NHC complexes has also been studied and examples are illustrated in Figure 3.3<sup>5</sup>.

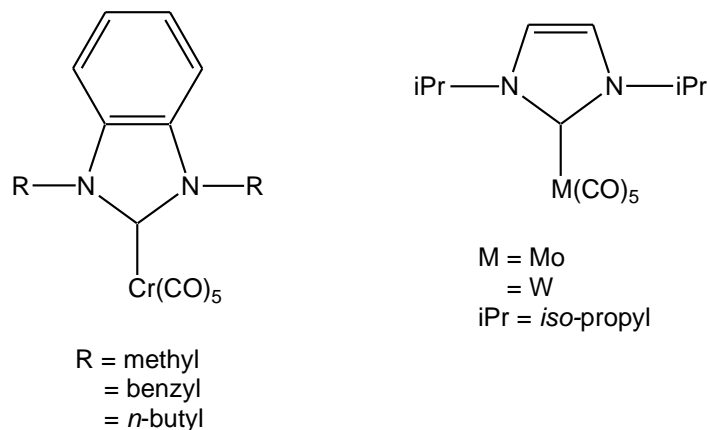


**Figure 3.3:** Examples of Group VI NHC complexes

### 3.1.2 Monometal NHC complexes of Group VII transition metals

Surprisingly little is known about NHC complexes of Group VII transition metals, especially considering that NHC complexes have been known for many years. In 1984, Burger et al.<sup>6</sup> synthesised a manganese complex (Figure 3.4) in thf at cold temperatures. Purification was performed on a silica-gel column (hexane/Et<sub>2</sub>O 2:1) to give a deep yellow product. The carbon bound to the metal contains a hydrogen atom bound to it, which means that conjugation between the N-C-N does not exist for this compound, and is different (although with line structures looks very similar to NHC complexes) to the target complexes prepared in this study.

(5) Seongjin, K., Choi, S. Y., Lee, Y. T., Park, K. H., Sitzmann, H., Chung, Y. K. *J. Organomet. Chem.* **2007**, 692, 5390.

(6) Burger, U., Perret, C., Bernardinelli, G., Kundig, E. P. *Helv. Chim. Acta* **1984**, 67, 2063.



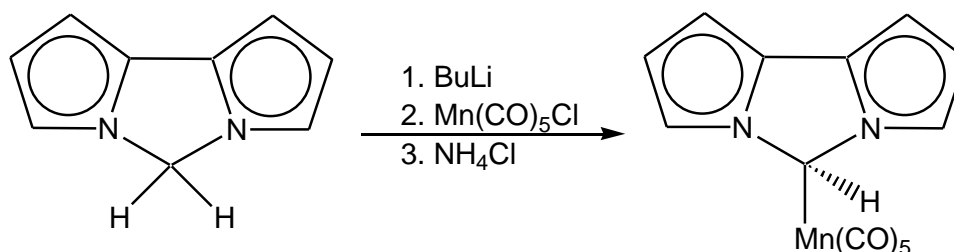


**Figure 3.4:** Synthesis of the pentacarbonyl(5H-dipyrrolo[1,2-c:2',1'-e]imidazol-5-yl)manganese complex

Group VII complexes of this type  $[MX(CO)_4NHC]$  only recently became known when Lui *et al.*<sup>7</sup> and Chen<sup>8</sup> created a stable NHC complex (Figure 3.5) from the isocyanide complex via intramolecular cyclisation (see later: Chapter 4). It led to one of the first Re(I) NHC complexes reported. Luminescent properties have been found for Re(I) tricarbonyl NHC complexes which make them interesting targets for future research<sup>9</sup>.

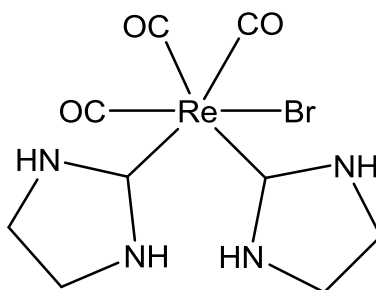


**Figure 3.5:** A Re(I) NHC complex synthesised from the isocyanide precursor

(7) Liu, C., Chen, D., Lee, G., Peng, S., Liu, S. *Organometallics* **1996**, 15, 1055.

(8) Chen, L., Chen, M., Chen, J., Wen, Y., Lu, K. *J. Organomet. Chem.* **1992**, 425, 99.

(9) Braband, H.; Kückmann, T. I.; Abram, U. *J. Organometallics* **2005**, 690, 5421.

Few examples of these Group VII transition metal complexes in low oxidation states are known. However, Re(V) and Tc(V) NHC complexes have been found to be very stable and this is reflected in the number of structurally characterised complexes<sup>10</sup>. Re(V) and Tc(V) complexes have potential applications in medicine used for cancer therapy as well as in diagnostic and therapeutic nuclear medicine<sup>9</sup>.

Solubility problems have been encountered for Re(VI) complexes and Re(VII) are found to be very unstable<sup>11</sup>. Rhenium NHC complexes in high oxidation states (6+, 7+) are synthesised by treatment of the metaloxide with the ylidene in thf.

Mn(I) NHC complexes are also very rare but the known examples were synthesised either by reaction of isocyanides with propargylamine (as with the Re(I) analogues, Figure 3.5) or by tautomerisation of imidazoles<sup>12</sup> (Figure 3.6).

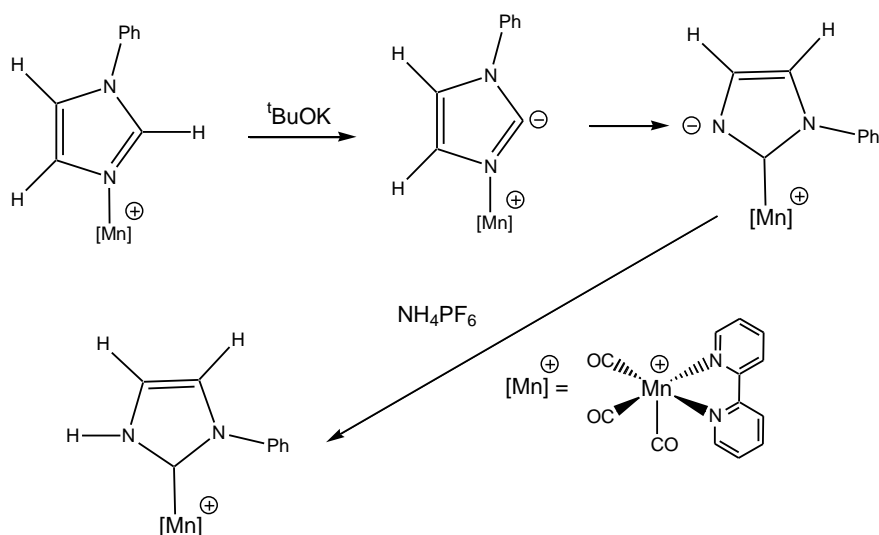


**Figure 3.6:** Isomerisation of imidazole ligands to the NHC Mn(I) complex

(10) (a) Alberto, A. *Comprehensive Coordination Chemistry II*, Amsterdam. **2004**, 5, 127; (b) Abram, U. *Comprehensive Coordination Chemistry II*, Amsterdam. **2004**, 5, 271.

(11) Herrmann, W. A.; Öfele, K.; Elison, M.; Kühn, F. E.; Roesky, P. W. *J. Organomet. Chem.* **1994**, 13, C1.

(12) Ruiz, J., Perandones, B. F. *J. Am. Chem. Soc.* **2007**, 129, 9298.

Mn(II) NHC complexes were also identified and can be synthesised by simple addition of the ylidene to  $MnX_2$  in  $thf^{13}$  (Figure 3.7).

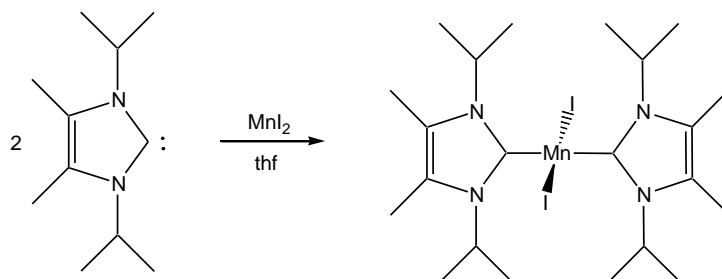


**Figure 3.7:** Synthetic pathway towards a Mn(II) NHC complex

### 3.2 The focus of this study

The only examples found of Group VII transition metal complexes of the type  $[MX(CO)_4L]$  ( $L=NHC$ ) are those prepared by Hahn *et al.* in 2009<sup>14</sup> (Figure 3.8).

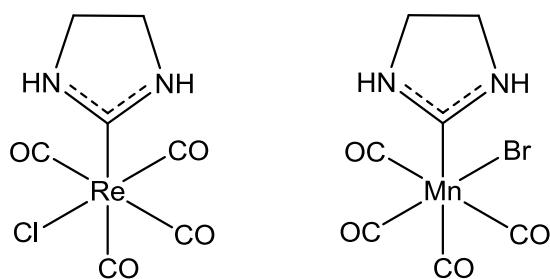


**Figure 3.8:** Literature examples of  $[MX(CO)_4L]$

(13) Chai, J., Zhu, H., Peng, Y., Roesky, H. W., Singh, S., Schmidt, H., Noltemeyer, M. *Eur. J. Inorg. Chem.* **2004**, 2673.

(14) Kaufhold, O., Stasch, A., Pape, T., Hepp, A., Edwards, P. G., Newmand, P. D., Hahn, F. E. *J. Am. Chem. Soc.* **2009**, 131, 306.

These complexes were prepared by stirring a thf solution of  $[MX(CO)_5]$  ( $M = Mn, Re$ ) and  $H_2NCH_2CH_2N=PPh_3$  (phosphinimine) for 24 hours. The  $^{13}C$ -NMR spectrum of the Mn complex displayed a resonance at 219ppm for the carbene carbon and the carbonyl carbon signals ranged from 210-212ppm. For the Re analogue these values were found to be 193ppm and 184-186ppm respectively. Four IR bands for the carbonyl stretches of both complexes were found in the range  $2100-1920cm^{-1}$ , corresponding to a *cis*- $[ML_2(CO)_4]$  system<sup>15</sup>.

In this study the synthesis of Re(I) and Mn(I) NHC complexes  $[MX(CO)_4L]$  was attempted. Figure 3.9 represents the target complexes containing the 1,3-bis(2,4,6-trimethylphenyl) imidazol-2-ylidene (IMes) ligand.

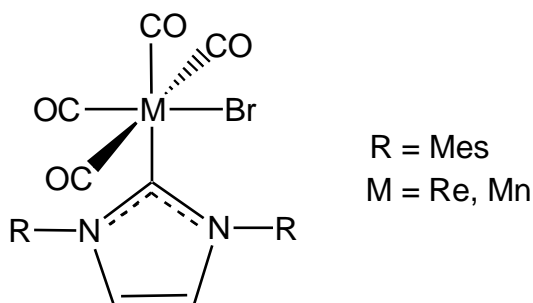


**Figure 3.9:** Proposed monometal NHC complexes

(15) Angelici, R. J., Ed.; *Reagents for Transition Metal Complex and Organometallic Synthesis*, 28, New York. **1990**.

### 3.3 Results and discussion

The synthetic approach toward monometal NHC complexes is illustrated in Figure 3.10.



Figure 3.10: Synthetic pathway towards monometal NHC complexes

#### 3.3.1 Decarbonylation

Decarbonylation is achieved by either reacting the metal substrate with  $\text{Me}_3\text{NO}$  (Figure 3.11) or by employing ultra violet (UV) radiation (Figure 3.12)

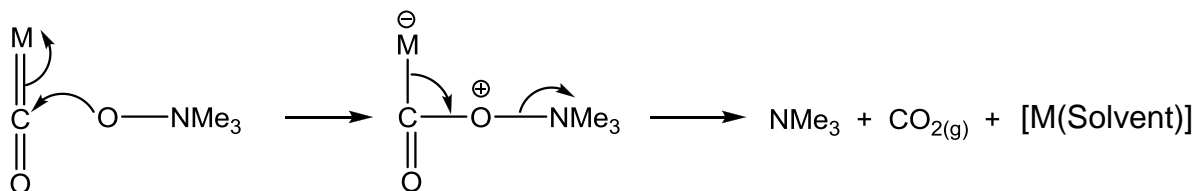


Figure 3.11: Mechanism of the reaction with  $\text{Me}_3\text{NO}$

By employing  $\text{Me}_3\text{NO}$ , a labile solvent molecule (e.g. thf) coordinates to the vacant site which can then be substituted by a  $\text{IMes}$  molecule. Alternatively, the free NHC can directly bind to the open coordination site which resulted from UV radiation.

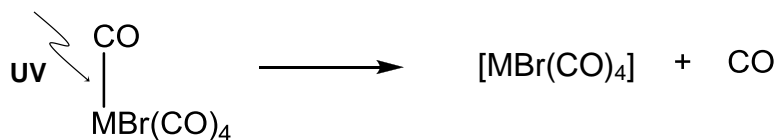


Figure 3.12: Labilisation of the carbonyl-metal bond with UV radiation

### 3.3.2 Deprotonation of ligand

The ylidene was prepared by deprotonation of the appropriate chloride salt with different strong bases (e.g.  $n\text{BuLi}$ ,  $t\text{BuOK}$ ) (Figure 3.13).

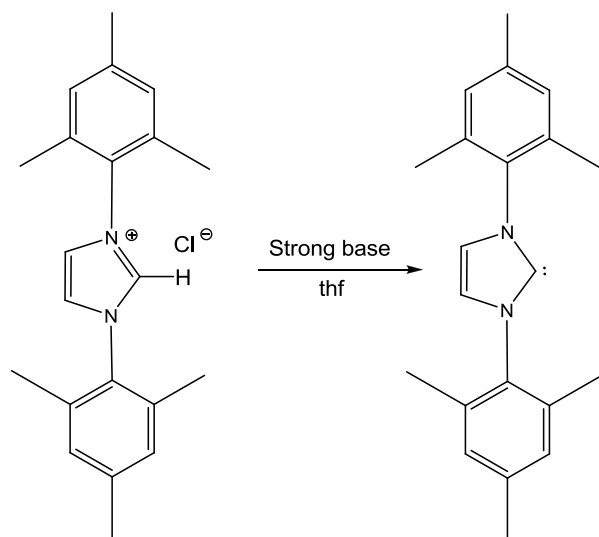
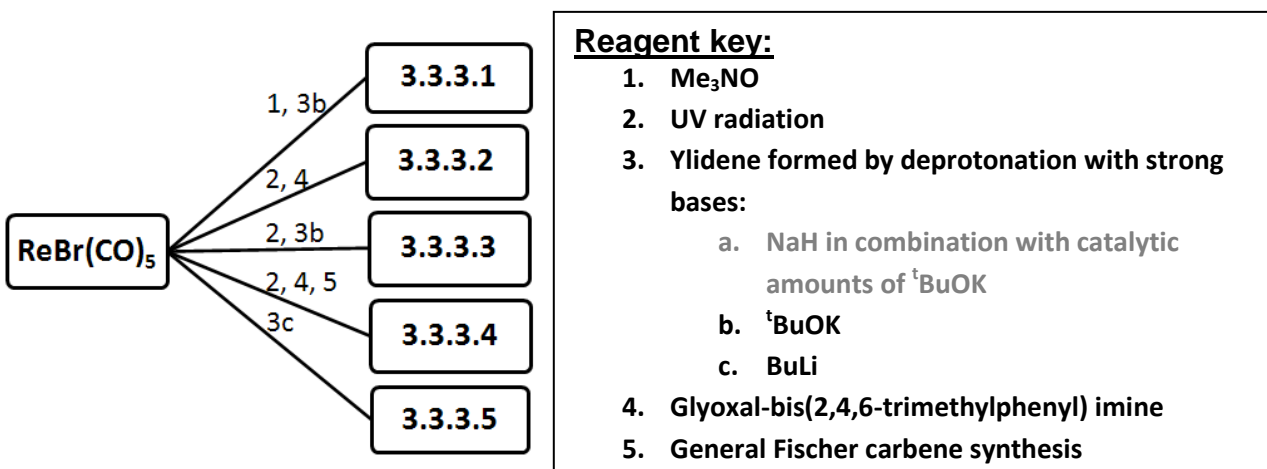


Figure 3.13: Deprotonation with strong bases to produce the ylidene

### 3.3.3 Complex formation by employing $[\text{ReBr}(\text{CO})_5]$

Scheme 3.1 and 3.2 give an overview of the synthetic routes followed and will be discussed.



Scheme 3.1: Synthetic overview of reactions attempted with  $[\text{ReBr}(\text{CO})_5]$  as metal substrate.

$^1\text{H}$  NMR,  $^{13}\text{C}$  NMR and IR spectroscopic data are reported on all reaction products. Most chemical shifts obtained in the  $^1\text{H}$  NMR spectra were broad and J coupling values could not be assigned, unless otherwise stated.

### 3.3.3.1 Route 1 followed by route 3b

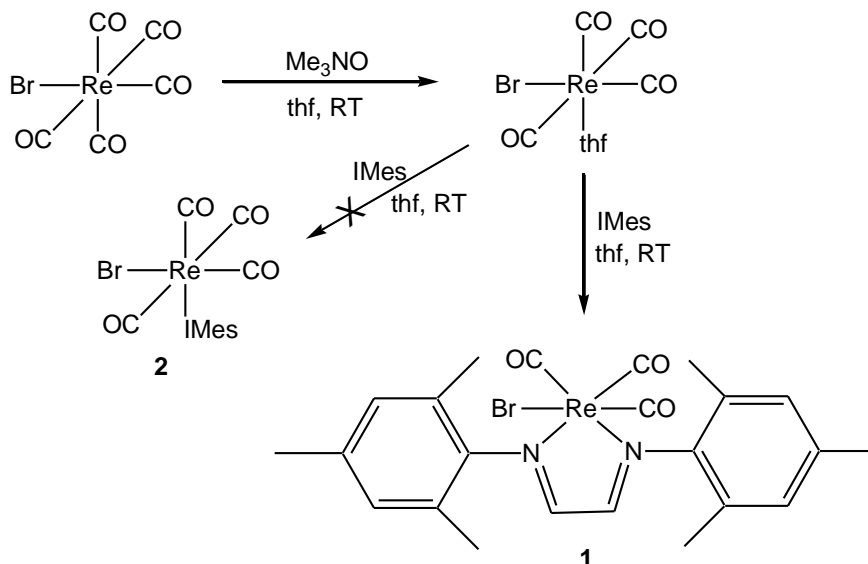


**Figure 3.14:** Illustration of the reaction route followed

$[\text{ReBr}(\text{CO})_5]$  (3mmol, 1.2g) was dissolved in 20ml  $\text{thf}$  and  $\text{Me}_3\text{NO}$  (3mmol, 0.2g) added to the solution; it was stirred for 2 hours.  $\text{IMesHCl}$  (3mmol, 1.0g) was suspended in  $\text{thf}$  and deprotonated with  ${}^t\text{BuOK}$  (3 mmol, 0.33g) to form the ylidene which was then added to the decarbonylised metal substrate solution. The mixture turned a dark-red colour and the  $\text{thf}$  solvent was removed by reduced pressure. Column chromatography was employed to purify the residue and a highly polar fraction was collected with  $\text{thf}$ . After the removal of the solvent a dark purple powder was obtained (**1**). It was crystallised from a saturated chloroform solution and the structure obtained is presented in Figure 3.21.

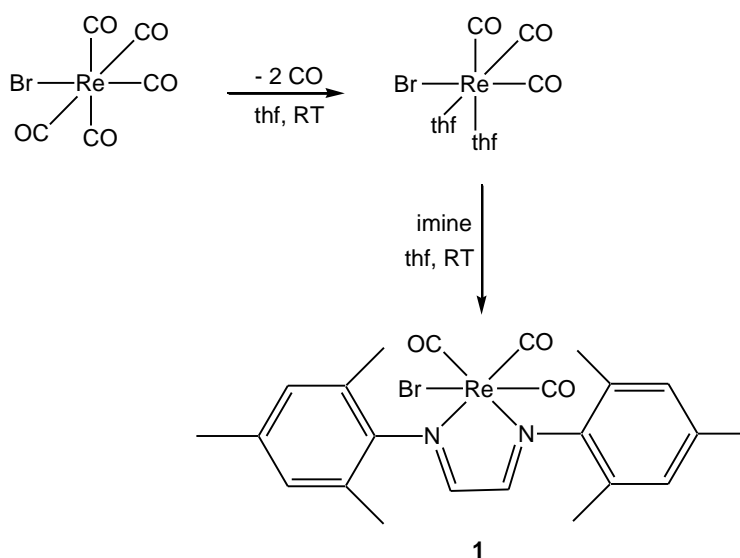
Isolation of this compound from this reaction is unexpected. Decarbonylation resulted in the loss of two carbonyl ligands and in addition, the ylidene fragmented to form the imine precursor of the salt, glyoxal-bis(2,4,6-trimethylphenyl)imine. This imine is attached to the metal through the nitrogen atoms. A yield of ~25% was obtained.



Following these results, it was decided to design a test reaction where the imine was added instead of the ylidene. The synthesis and results will be discussed in the next section (3.3.3.2).

### 3.3.3.2 Route 2 followed by 4

The same method as described in section 3.3.3.1 was followed to synthesise the  $[\text{ReBr}(\text{CO})_3(\text{imine})]$  complex, except that decarbonylation was performed by UV radiation for 1 hr in thf and the imine (3mmol, 1.0g) was added instead of the  $\text{IMesHCl}$ . This method was found to be a relatively easy and clean method to prepare the  $[\text{ReBr}(\text{CO})_3(\text{imine})]$  complex. The synthetic pathway is presented in Figure 3.15.

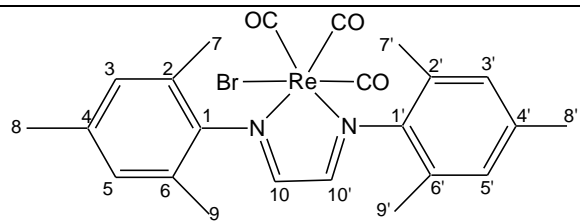


**Figure 3.15:** Illustration of the reaction route followed and the target molecule. The complex (**1**) was isolated in a higher yield (~40%) and full spectroscopic analysis was done.

#### NMR spectroscopy

The chemical shifts in the  $^1\text{H}$  and  $^{13}\text{C}$  NMR spectra of complex **1** are given in Table 3.2 and the spectra are recorded in  $\text{C}_6\text{D}_6$ .

**Table 3.2:** NMR data for complex **1** in C<sub>6</sub>D<sub>6</sub>

	
<b>1</b>	
<b>Atom number</b>	<b><sup>1</sup>H NMR (ppm)</b>
8'	2.03 (s, 3H)
8	2.04 (s, 3H)
9'	2.08 (s, 3H)
9	2.09 (s, 3H)
7'	2.63 (s, 3H)
7	2.64 (s, 3H)
5, 5'	6.61 (m, 2H)
3, 3'	6.68 (m, 2H)
10, 10'	7.19 (s, 2H)
<b><sup>13</sup>C NMR (ppm)</b>	
8, 8'	20.6
7'	20.3
9, 9'	18.8, 19.0
7	21.2
5, 5'	129.5
3, 3'	129.6
2, 2', 6, 6'	130.5
4, 4'	137.6, 137.7
1, 1'	148.7, 148.9
10, 10'	166.1, 166.8
M-CO	195.3, 203.8

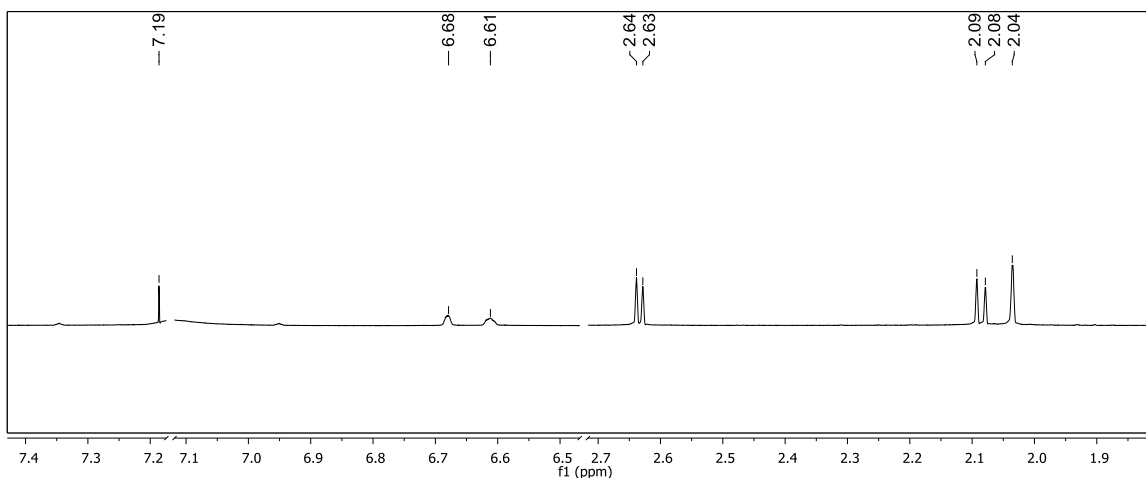


**Figure 3.16:** <sup>1</sup>H-NMR spectrum of complex **1**

The nitrogen atoms are electron withdrawing and this effect can not only be seen on the methyl substituents of the mesityl (Mes) groups in complex **1**, but also by the deshielding effect it has on H10, 10' of the complex. The coordinated nitrogen atoms withdraw electron density from the metal and the necessity of electron density withdrawal from the alkyl substituents on the nitrogen atoms is reduced. This results in the shielding of the N-alkyl substituents and more upfield NMR values are observed for H3, 3', 5, 5', 7, 7' and 10, 10' compared to the uncoordinated imine ligand. Different signals for the protons are observed due to the different environments surrounding these protons after complexation with the [ReBr(CO)<sub>5</sub>] substrate. The pattern for 8, 8' is observed as two overlapping singlets. This is ascribed to the fact that 8, 8' are very little affected by the different chemical environments.

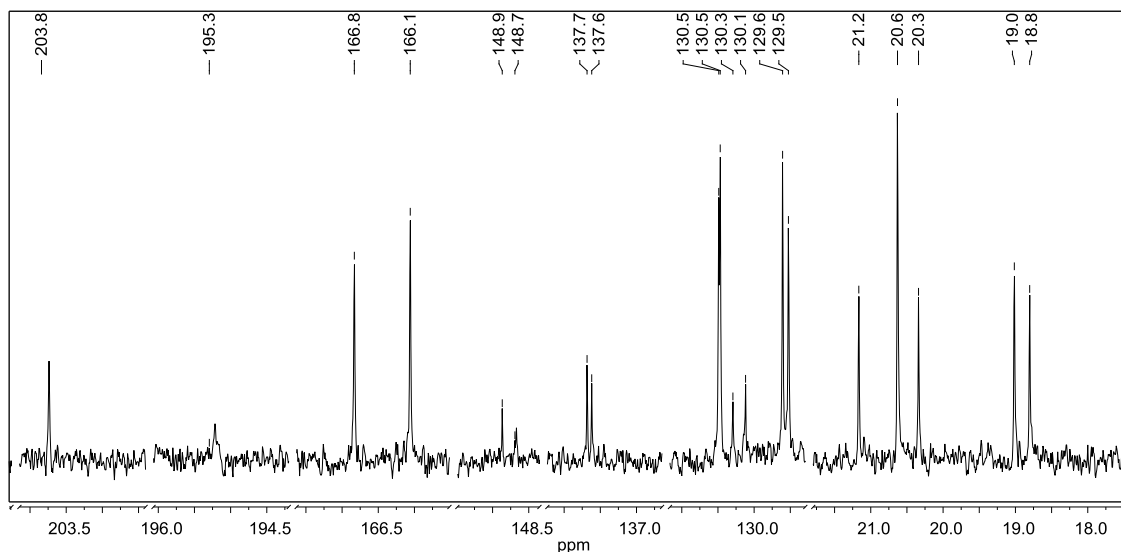


**Figure 3.17:**  $^{13}\text{C}$ -NMR spectrum of complex **1**

Complexation of the  $[\text{ReBr}(\text{CO})_5]$  substrate to the imine limits rotation of the mesityl groups around the N-C1 bond. This introduces different environments to the carbons of the imine and can be seen in the multiple peaks detected for the carbons. The electron withdrawing effect of the nitrogen atoms can also be observed in the downfield shift of the substrate carbonyl ligands which shift from 177 and 176ppm to 195 and 203ppm upon complexation.

### Infrared Spectroscopy

This technique is also employed for characterisation in solution. It is very useful to determine the stretching vibrational frequencies of terminal carbonyl ligands which lie in a range between  $1850$  and  $2120\text{cm}^{-1}$ <sup>16</sup>. The carbonyl vibrations are independent from other stretching vibrational frequencies in the molecule which makes it an even more attractive qualitative method for analysis.

There is a correlation between the bond order of the C-O bond and its vibration: the more backbonding from the metal to the carbonyl ligand, the stronger the

(16) Braterman, P. S. *Metal Carbonyl Spectra*, Academic Press Inc., London, **1975**.

M-C bond and in turn results in a weaker C-O bond and a lower stretching frequency.

The geometric arrangement (i.e. symmetry) of the carbonyl ligands around the metal determines the number and intensities of the carbonyl stretching frequencies<sup>15</sup>. The carbonyl stretching modes of *fac* and *mer* isomers of the monometal tricarbonyl complexes are summarised in Figure 3.18 and Figure 3.19.

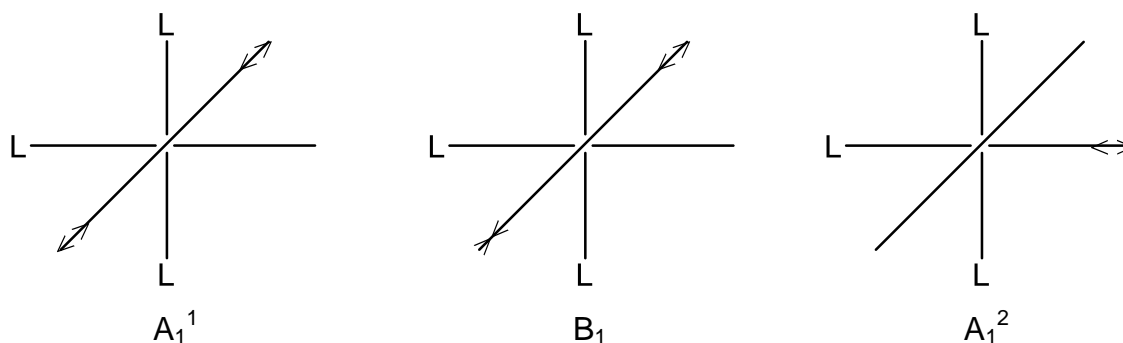


**Figure 3.18:** Normal  $\nu_{\text{CO}}$  modes for *mer*-[M(CO)<sub>3</sub>L<sub>3</sub>]

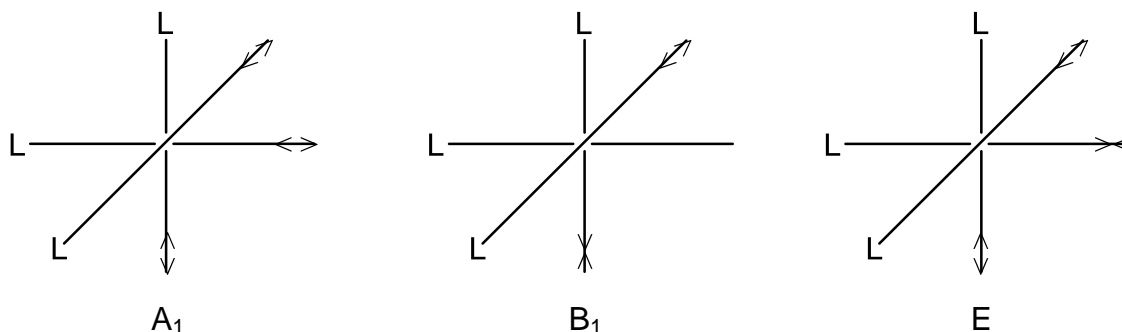


**Figure 3.19:** Normal  $\nu_{\text{CO}}$  modes for *fac*-[M(CO)<sub>3</sub>L<sub>3</sub>]

The *mer*-[M(CO)<sub>3</sub>L<sub>3</sub>] complex displays a three-band pattern, namely  $A_1^1$ ,  $B_1$  and  $A_1^2$  of which all are IR (infrared) and Raman active. However, for the *fac*-[M(CO)<sub>3</sub>L<sub>3</sub>] system only  $A_1$  and  $E$  are IR active when all three L ligands are equal.

The IR spectrum of complex **1** isolated in this reaction indicates three IR vibrations which might lead us to believe that the complex has a *mer* conformation, but X-ray diffraction analysis indicates a *fac* geometry for this complex. These contrary observations can be explained by looking at the intensity pattern of the carbonyl stretches in the spectrum<sup>17</sup>. For the *mer* geometry of a  $[M(CO)_3BrL_2]$  type complex a weak band near  $2050\text{cm}^{-1}$  and two strong bands between  $2000\text{cm}^{-1}$  and  $1890\text{cm}^{-1}$  are expected. In the case of the *fac* conformation all three bands are strong and appear between  $2050\text{cm}^{-1}$  and  $1900\text{cm}^{-1}$ . Considering this information together with the  $C_s$  symmetry of this complex and the different ligands complexed to the metal, a *fac* geometry is assigned to this complex.

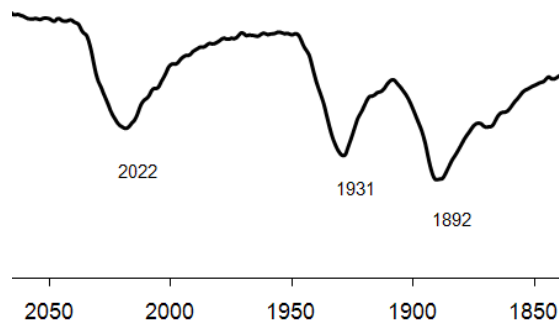


**Figure 3.20:** The carbonyl region of the IR spectrum obtained for complex **1**

### Mass Spectrometry

A molecular ion peak ( $M^+$ ) was observed in the mass spectrum for this complex with a low intensity. Mass spectral data are given in Table 3.3.

(17) (a) Wuyts, L. F.; van der Kelen, G. P. *Inorg. Chim. Acta.* **1977**, 23, 19; (b) Edwards, D. A.; Marshalsea, J. J. *Organomet. Chem.* **1977**, 131, 73.

**Table 3.3:** Mass spectral data of complex **1**

<b>m/z</b>	<b>Intensity (%)</b>	<b>Fragment ion</b>
642	1.5	[M] <sup>+</sup>
614	1	[M-CO] <sup>+</sup>
586	0.5	[M-2CO] <sup>+</sup>

### X-ray diffraction

The molecular structure of this complex confirmed the structural assignment made from the analyses in solution. For solid state analysis this complex was crystallised from a saturated chloroform solution to yield dark purple crystals. The ORTEP<sup>18</sup> + POV-Ray<sup>19</sup> plot of the geometry of the structure is given in Figure 3.21. Structural properties of **1** will be discussed in Chapter 5.

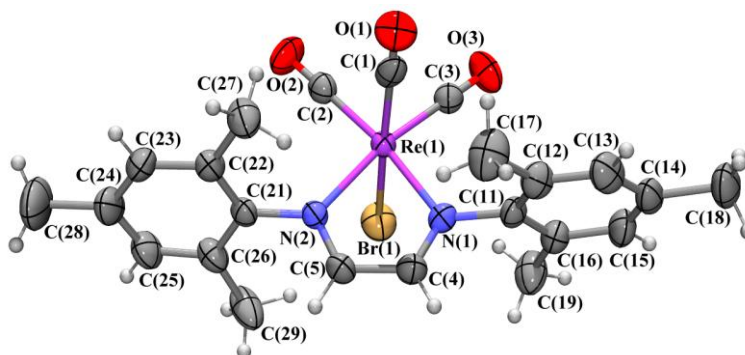


**Figure 3.21:** ORTEP + POV-Ray drawing of the molecular structure of complex **1**

(18) Farrugia, L. J., *J. Appl. Crystallogr.* **1997**, *30*, 565

(19) The POV-Ray Team, POV-Ray **2004**, URL: <http://www.povray.org/download/>.

### 3.3.3.3 Route 2 followed by 3b

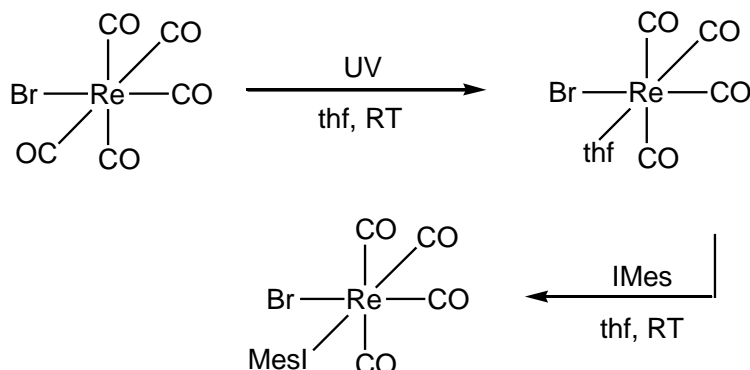


**Figure 3.22:** Illustration of the reaction route followed and the target molecule

$\text{ReBr}(\text{CO})_5$  (2.5mmol, 1.02g) was dissolved in thf and irradiated with UV light for 1 hr, while IMesHCl (2.5mmol, 0.75g) also dissolved in thf was deprotonated by  $t\text{BuOK}$  (2.5mmol, 0.28g). The formed ylide was added to the decarbonylated metal substrate and the mixture stirred for 4hrs at RT. Column chromatography was employed for purification and a red-orange fraction was collected by elution with a hexane:dcm mixture (1:1). However, complete characterisation has not been possible due to decomposition or fragmentation of the product during analysis which could be seen in the multiple peaks featuring in certain ranges of the  $^{13}\text{C}$  NMR.

Although no spectroscopic evidence for the target complex was obtained, indications for the formation of the imine ligand are present. These include the C10, 10'  $^{13}\text{C}$  NMR shifts at 166ppm and the  $^1\text{H}$  NMR shift around 8ppm.



### 3.3.3.4 Route 2 followed by 4 and 5

Recent studies in our labs have focused on the synthesis of Fischer carbene complexes using transition metal substrates in oxidation state +1 containing carbonyl ligands, example  $[\text{Mn}_2(\text{CO})_{10}]$  and  $[\text{ReBr}(\text{CO})_5]^4$ . Employing complex **1** as starting material it presents a metal substrate with not only carbonyl ligands but also nitrogen atoms attached to the Re atom. The ability to replace yet another carbonyl ligand with a Fischer carbene was investigated.

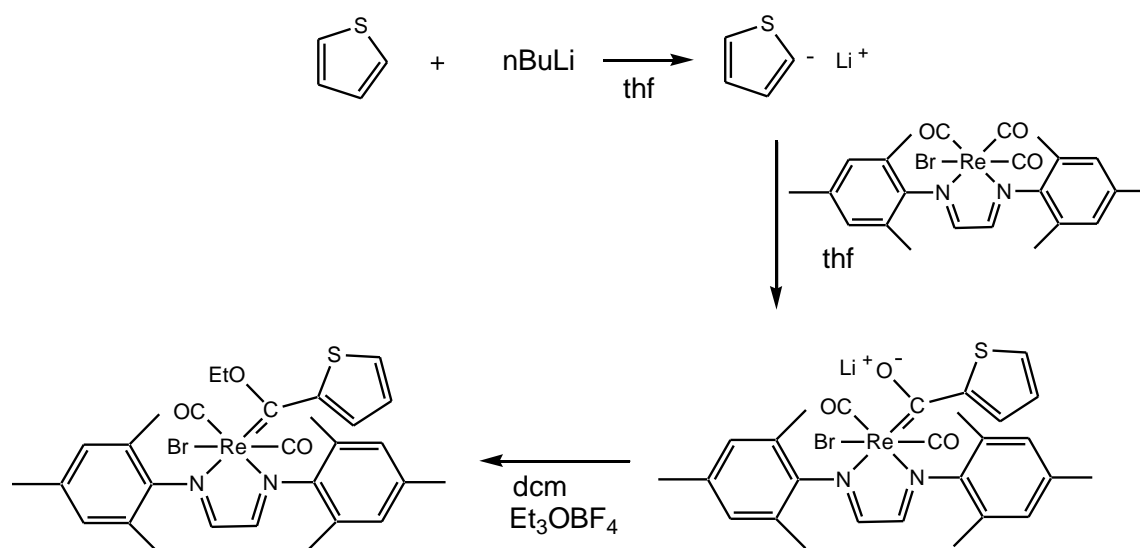


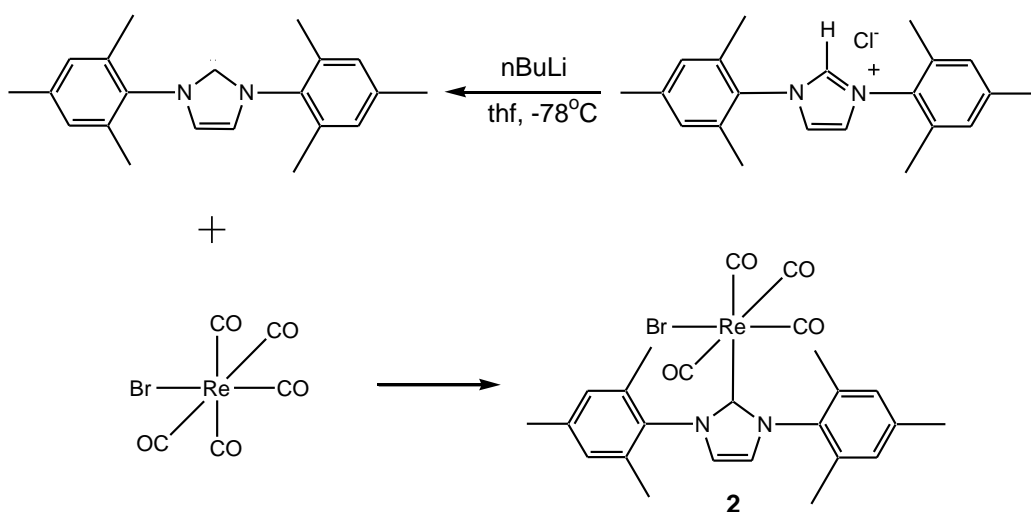
**Figure 3.23:** Reaction pathway towards Fischer carbene

A thiophene (0.6mmol, 0.05ml) solution in 15 ml  $\text{thf}$  was cooled down to  $-78^\circ\text{C}$  after which  $n\text{BuLi}$  (0.6mmol) was added. The mixture was stirred for 30 min at  $-78^\circ\text{C}$  and another 30 min at RT. The solution was again cooled to  $-78^\circ\text{C}$  and the metal substrate (complex **1**, 0.6mmol, 0.36g) added. The reaction mixture was left to stir for 1hr after which it was allowed to warm to RT. After the  $\text{thf}$  solvent was replaced with  $\text{dcm}$  solvent the reaction mixture was cooled to  $-78^\circ\text{C}$  and  $\text{Et}_3\text{OBF}_4$  (0.6mmol, 0.1g) added. It was allowed to stir for 30min and then 30min at  $-35^\circ\text{C}$ . Solvents were removed and the residue was filtered through silica gel.

IR:  $\nu_{\text{CO}}$  ( $\text{cm}^{-1}$ ) 2030, 1940 and 1910: unassigned

From the spectroscopic characterisation it was obvious that the target complex was not formed. Although carbonyl signals could be observed in both the IR and the  $^{13}\text{C}$  NMR spectra, no structure could unambiguously be assigned. A useful suggestion would be to model the target complex with computational methods to investigate the possibility of formation.

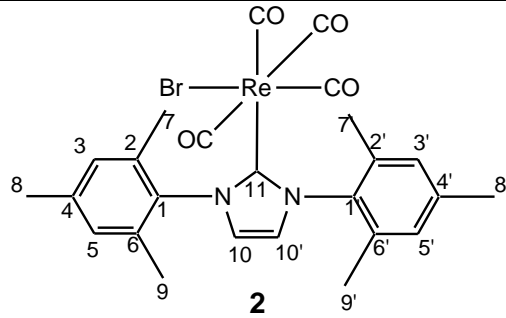
### 3.3.3.5 Route 3c



**Figure 3.24:** Illustration of the reaction route followed and the target molecule

A solution of 20ml thf and IMesHCl (2mmol, 0.7g) was stirred and cooled to  $-78^\circ\text{C}$ .  $n\text{BuLi}$  (2.1mmol, 1.5ml) was added and left to stir for 20 min after which the metal substrate,  $[\text{ReBr}(\text{CO})_5]$  (2mmol, 0.8g) was added. The reaction mixture was stirred at  $-78^\circ$  for 1 hr and then allowed to warm to RT. Thf solvent was removed under reduced pressure and purification was performed using cold ( $-40^\circ\text{C}$ ) column chromatography with florasil as resin. Starting materials (SM) were separated from the product by elution with hexane followed by dcm. The polar fraction eluted with thf and after the solvent was removed, NMR analysis was performed on the yellow-brown oil.

**Table 3.4:** NMR data for complex **2** in C<sub>6</sub>D<sub>6</sub>

	
Atom number	<sup>1</sup> H NMR (ppm)
8, 8'	1.90 (br, 6H)
7, 7', 9, 9'	2.08 (br, 12H)
5'	7.03 (m, 1H)
5	7.04 (m, 1H)
3'	7.05 (m, 1H)
3	7.07 (m, 1H)
10, 10'	7.30 (s, 2H)
<sup>13</sup> C NMR (ppm)	
8, 8'	17.3
9, 9'	21.2
7, 7'	22.0, 22.1
5, 5'	124.8
3, 3'	125.1
10, 10'	129.7
2, 2', 6, 6'	133.7
4, 4'	134.3
1, 1'	142.4
11	196.2
CO's	183.6, 186.1, 186.5

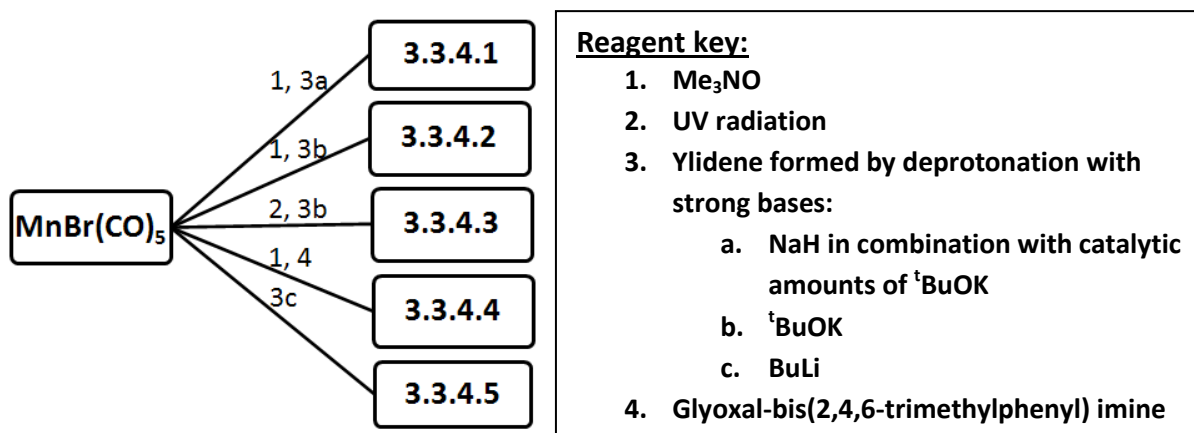
Signals expected for the target molecule could be observed but could not unambiguously be assigned due to multiple resonance peaks present.

A three band pattern is observed in the IR spectra of this complex and the values fall within the expected range for a *cis*-[ReBr(CO)<sub>4</sub>L] type complex<sup>20</sup>, however overlap of the A<sub>1</sub>(2) and B<sub>1</sub> is seen.

IR:  $\nu_{\text{CO}}$  (cm<sup>-1</sup>) 2126, 2035, 1970

Purification is influenced by the *in situ* fragmentation of products and this lead to difficulty in the overall spectroscopic analyses.

### 3.3.4 Complex formation by employing [MnBr(CO)<sub>5</sub>]



Scheme 3.2: Synthetic overview of reactions attempted with [MnBr(CO)<sub>5</sub>] as metal substrate.

(20) Chen, L. C.; Chen, M. Y.; Chen, J. H.; Wen, Y. S.; Lu, K. L. *J. Organomet. Chem.* **1992**, 425, 99.

$^1\text{H}$  NMR,  $^{13}\text{C}$  NMR and IR spectroscopy have been reported on all reaction products. Most chemical shifts obtained in the  $^1\text{H}$  NMR spectra were broad and J coupling values could not be assigned, unless otherwise stated.

### 3.3.4.1 Route 1 followed by 3a

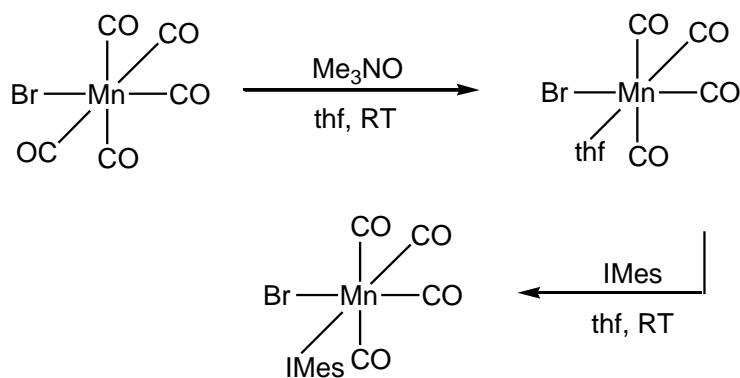


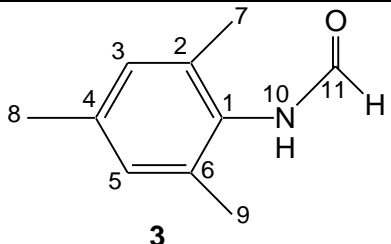
Figure 3.25: Illustration of the reaction route followed and the target molecule

$[\text{Mn}(\text{CO})_5\text{Br}]$  (3mmol, 0.74g) and  $\text{Me}_3\text{NO}$  (2.8mmol, 0.21g) was stirred in  $\text{thf}$  and it resulted in a red solution.  $\text{IMesHCl}$  (3mmol, 1.02g) was deprotonated in  $\text{thf}$  by addition of base (3mmol, see route 3a) and the ylide was added to the solution and stirred overnight.  $\text{thf}$  solvent was removed and purification was done on an aluminium oxide 90 ( $\text{Al}_2\text{O}_3$ ) column. Elution with dichloromethane ( $\text{dcm}$ ) and  $\text{thf}$  yielded starting material and a yellow fraction respectively. The yellow fraction was crystallized from a saturated chloroform solution. An unexpected organic product, mesitylformamide (**3**,  $\text{C}_{10}\text{H}_{13}\text{O}$ ), was obtained.

## NMR spectroscopy

The chemical shifts in the  $^1\text{H}$  and  $^{13}\text{C}$  NMR spectra of the **3** are given in Table 3.5 and the spectra are recorded in  $\text{C}_6\text{D}_6$ .

Table 3.5: NMR data of **3** in  $\text{C}_6\text{D}_6$

	
<b>Atom number</b>	<b><math>^1\text{H}</math> NMR (ppm)</b>
7, 8, 9	2.24 (br, 9H)
10	3.85 (br, 1H)
3,5	6.65 (br, 2H)
11	8.32 (br, 1H)
	<b><math>^{13}\text{C}</math> NMR (ppm)</b>
7,9	18.8
8	21.2
3,5	129.2
2,6	130.2
4	135.3
1	137.6
11	208.6

Rotation of the mesityl group results in a broad  $^1\text{H}$  NMR peak observed for the methyl groups 7, 8 and 9. These methyl protons are not situated in significantly different chemical environments.

## X-ray diffraction

The molecular structure of this complex confirms the data collected from NMR studies. The light yellow crystals were analysed with single crystal XRD. ORTEP<sup>16</sup> + POV-Ray<sup>17</sup> plots of the structure is given in Figure 3.26.

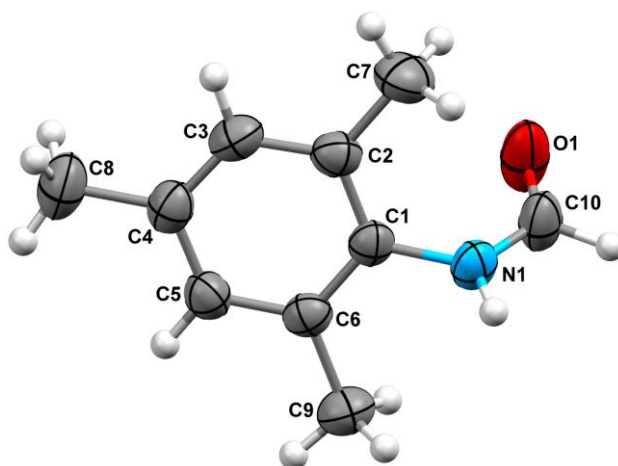


Figure 3.26: Mesitylformamide (**3**) obtained as side-product

The reaction pathway for the mesitylformamide formation is proposed in Figure 3.27.

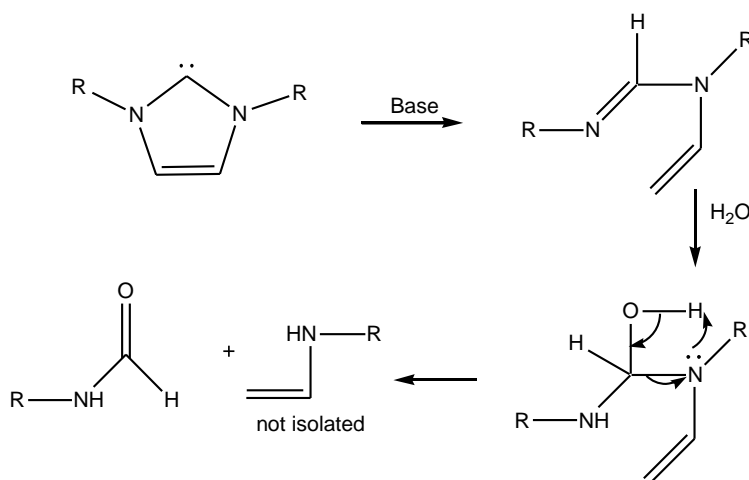
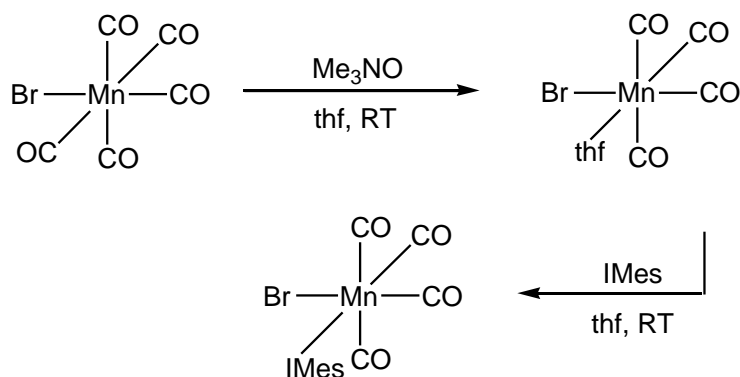


Figure 3.27: The proposed reaction pathway for the formation of **3**.

After ylidene formation the molecule is prone to undergo side reactions as described in Chapter 2. The strong base results in vinyl formation<sup>2</sup> and the hydrolysis<sup>21</sup> of the molecule results in the dissociation of the NC – N bond. The vinyl fragment was not isolated.

### 3.3.4.2 Route 1 followed by 3b



**Figure 3.28:** Illustration of the reaction route followed and the target molecule

The same synthetic procedure was followed as described in section 3.3.4.1 with the exception of the use of  $^t\text{BuOK}$  only as base (route 3b). The residue was purified with column chromatography on  $\text{Al}_2\text{O}_3$ . Starting material eluted with a hexane/dcm (1:1) mixture and a yellow-brown fraction eluted with dcm only.

According to the spectroscopic evidence of the  $^1\text{H}$  NMR and  $^{13}\text{C}$  NMR data there is a strong indication that the target complex formed. However, the IR spectrum resembled that of the starting material and due to the absence of the metal carbonyl signals in the  $^{13}\text{C}$  NMR, the presence of the target complex could not be confirmed.

No further spectroscopic data was obtained for this fraction.

(21) Nolan, S. -P., Ed.; *N-Heterocyclic Carbenes in Synthesis*. WILEY-VCH Verlag GmbH & Co. KGaA, Weinheim. **2006** and references therein.



### 3.3.4.3 Route 2 followed by 3b

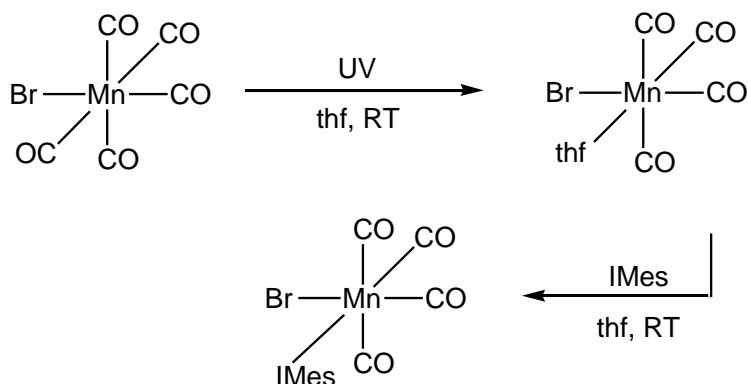


Figure 3.29: Illustration of the reaction route followed and the target molecule

The method employed with  $[\text{ReBr}(\text{CO})_5]$  and UV radiation was applied to  $[\text{MnBr}(\text{CO})_5]$ .  $[\text{MnBr}(\text{CO})_5]$  (2.5mmol, 0.62g) was dissolved in thf and irradiated with UV light for 1 hr, while  $\text{IMesHCl}$  (2.5mmol, 0.75g), also dissolved in thf, was deprotonated by  ${}^t\text{BuOK}$  (2.5mmol, 0.28g). The formed ylide was added to the decarbonylated metal substrate and the mixture stirred for 4hrs at RT. Column chromatography was employed for purification with a hexane:dcm mixture (1:1). Three fractions were collected during purification.

The first yellow fraction proved unstable and decomposition with colour change from yellow to brown was detected shortly after collection. IR spectroscopic analysis indicates three strong bands corresponding to a  $\text{MXL}_5$  system, but with significantly different frequencies than the starting material  $[\text{MnBr}(\text{CO})_5]$ . However, the stretching frequencies correspond to the values found for  $[\text{Mn}_2(\text{CO})_{10}]$ .

The second fraction was identified as unreacted metal substrate and the third fraction had a light blue colour but the immediate decomposition of this compound precluded the possibility of any analysis.

This reaction was repeated with longer reaction times but the yields did not improve and analysis showed similar results.

#### 3.3.4.4 Route 1 followed by 4

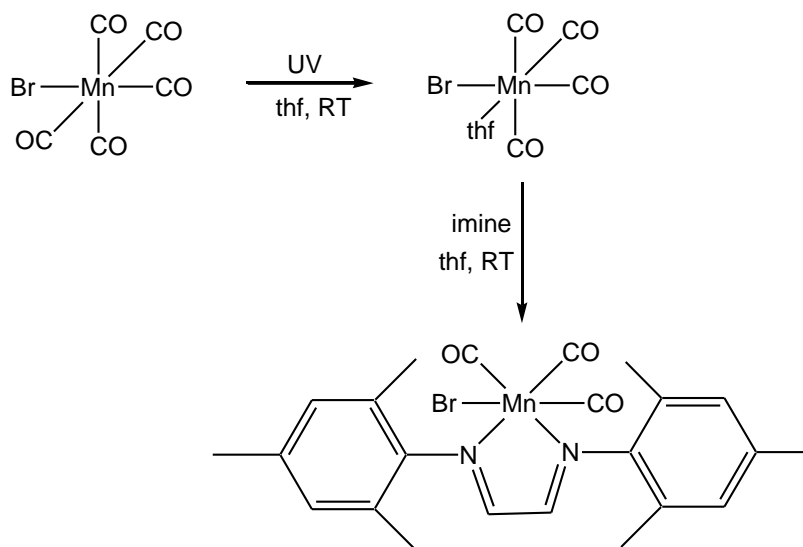


**Figure 3.30:** Illustration of the reaction route followed and the target molecule

$[\text{MnBr}(\text{CO})_5]$  (1.5mmol, 0.41g) was dissolved in 20ml of thf and  $\text{Me}_3\text{NO}$  (1.5mmol, 0.1g) added to the solution. A dark red colour was observed. The imine (1.5mmol, 0.5g) was added to the decarbonylised metal substrate solution. Strong colour changes occurred in approximately 1-5 minutes: the deep red solution obtained after decarbonylation turned dark brown almost immediately after addition of the imine. Thf solvent was removed by reduced pressure and a bright yellow residue was left.

After the high reactivity of this reaction was noticed it was decided that decarbonylation might not be needed. However, when the method was repeated without decarbonylation, the strong colour changes were still observed.

In an attempt to limit reactivity the reaction was repeated by first adding solid samples of the substrate and imine together. 15ml of thf was added followed by direct solvent evaporation. A bright yellow powder was obtained yet again. Hexane was used to attempt extraction of the product and a bottle green compound was extracted. The green solution was collected and the solvent removed which again resulted in a bright yellow powder. Manganese in oxidation state +6 ( $\text{MnO}_4^{2-}$ ) is known to give a green colour and it also strongly absorbs UV radiation at 610nm<sup>22</sup>. The UV/visible spectrum of this compound was recorded to confirm the presence of this compound (Figure 3.31).

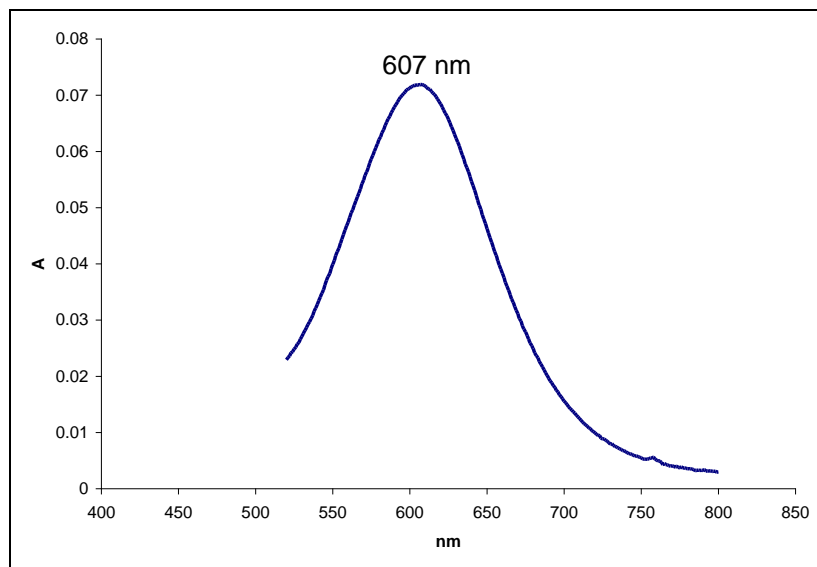
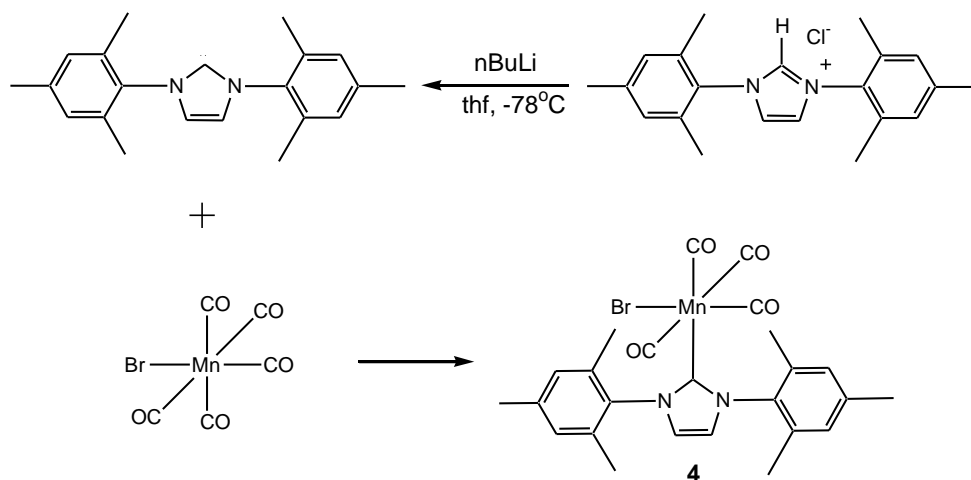


Figure 3.31: UV spectrum of sample obtained from the hexane extraction

---

(22) (a) Carrington, A., Symons, M. C. R. *J. Chem. Soc.* **1956**, 3373; (b) Lee, D. G., Chen, T. J. *Am. Chem. Soc.* **1993**, 115, 11231.

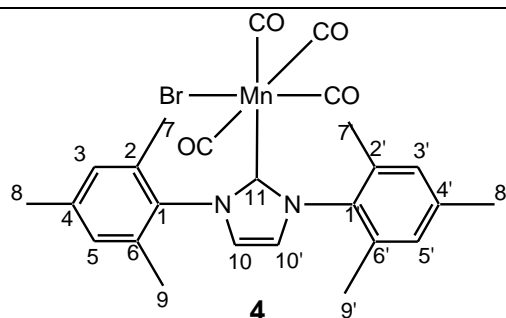
### 3.3.4.5 Route 3c



**Figure 3.32:** Illustration of the reaction route followed and the target molecule

A solution of 20ml thf and IMesHCl (2mmol, 0.7g) was stirred and cooled to  $-78^\circ\text{C}$ .  $n\text{BuLi}$  (2.1mmol, 1.5ml) was added and left to stir for 20 min after which the metal substrate,  $[\text{MnBr}(\text{CO})_5]$  (2mmol, 0.8g) was added. The reaction mixture was stirred at  $-78^\circ$  for 1hr and then allowed to warm to RT. Thf solvent was removed under reduced pressure and purification was performed by cold ( $-40^\circ\text{C}$ ) column chromatography with florasil as resin. SMs were separated from the product by gradient elution with hexane and subsequently dcm. The polar fraction eluted with thf and after the solvent was removed, NMR analysis was performed.

Table 3.6: NMR data of **4** in CDCl<sub>3</sub>



Atom number	<sup>1</sup> H NMR (ppm)
8, 8', 9, 9'	2.15 (br, 12H)
7, 7'	2.34 (br, 6H)
3, 3', 5, 5'	7.02 (br, 4H)
10	7.12 (br, 2H)
	<sup>13</sup> C NMR (ppm)
8, 8'	17.6
9, 9'	21.0
7, 7'	23.1
5, 5'	124.2
3, 3'	126.1
10, 10'	129.8
2, 2', 6, 6'	134.2
4, 4'	136.9
1, 1'	139.8
11	218.5
CO's	209.9, 212.1, 213.7

The chemical shifts in the <sup>1</sup>H and <sup>13</sup>C NMR spectra of the **4** are given in Table 3.6 and the spectra are recorded in CDCl<sub>3</sub>. Compared to the NMR shifts obtained for

**2**, these values are consistently found slightly more upfield and can be attributed to the fact that complex **2** is analysed in C<sub>6</sub>D<sub>6</sub> compared to complex **4** which was analysed in CDCl<sub>3</sub>.

Signals expected for the target molecule could be observed. The four band IR vibrational pattern observed here was expected since this complex resembles a *cis*-[M(CO)<sub>4</sub>L<sub>2</sub>] type complex. The values indicated are also in the accepted range for this type of complex<sup>23</sup>.

IR:  $\nu_{\text{CO}}$  (cm<sup>-1</sup>) 2077, 2009, 1999, 1979

Purification is influenced by the *in situ* fragmentation of products.

### 3.4 Conclusion

Much is still to be discovered on the behaviour and reactions of monometals with free N-heterocyclic carbenes. Different results were obtained and varied with deprotonation method, decarbonylation method and the metal substrate used. Spectroscopic analyses in solution (NMR and IR spectroscopy) are made difficult by the *in situ* decomposition of reaction products. This limited the analyses done on products synthesised.

Complexes **1-4** were novel compounds isolated and single crystals were obtained for **1** and **3**. A probable reaction pathway was proposed for the formation of these two complexes. It indicates the effect of trace amounts of water in the hydrolysis reaction of the free carbene. In the presence of strong base, these hydrolysed products can undergo C-N bond cleavage to form the observed product.

---

(23) MSc thesis filed under the supervision of S. Lotz, Universiteit van Pretoria: Bezuidenhout, D. I.

The synthetic route employing nBuLi as base (3c) proved to be the most promising route to synthesise the target complexes. Resonance signals of the carbene carbon as well as shifts in carbonyl resonances of these products could be observed, but purification remains a challenge.

Isolation of the target complexes can be considered as the main difficulty due to insolubility of target complexes and the presence of fragmentation products *via* the occurrence of side reactions. Side reactions also occur during purification with column chromatography and prevented complete characterisation.

# Chapter 4: Dimetal NHC complexes and experimental results

## 4.1 Introduction

The use of NHCs as ligands to synthesise novel and improved catalysts has expanded over the last 15 years. In a paper by Nolan *et al.*<sup>1</sup> applications of late transition metal catalysts are reviewed and can be divided into four categories: the heavy weights (Ru, Rh, Ni and Pd), the well-established (Ir, Pt, Cu and Au), the underdeveloped (Fe, Os, Co and Ag) and the nonexistent (Mn, Tc and Re). Even in this wide variety of complexes, there are not many examples of complexes that contain more than one metal. Dimetal complexes not exhibiting metal-metal bonds are illustrated in Figure 4.1. The ruthenium complex (Figure 4.1(i)) is used in the  $\beta$ -alkylation of secondary alcohols with primary alcohols<sup>2</sup> and the rhodium complex (Figure 4.1(ii)) in hydroformylation reactions<sup>3</sup>.

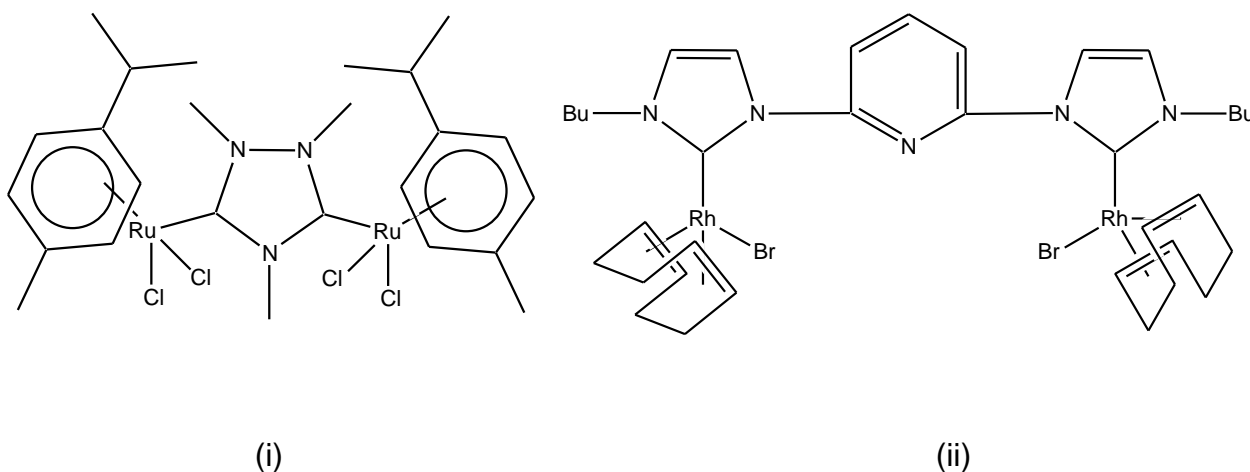


**Figure 4.1:** Dinuclear catalysts (non-metal-metal bonded complexes)

(1) Díez-González, S.; Marion, N.; Nolan, S. P.; *Chem. Rev.* **2009**, *109*, 3612.

(2) Viciano, M.; Sanaú, M; Peris, E. *Organometallics* **2007**, *26*, 6050.

(3) Poyatos, M.; Uriz, P.; Mata, J. A.; Claver, C.; Fernandez, E.; Peris, E. *Organometallics* **2003**, *22*, 440.



Surprisingly few examples of NHC complexes synthesized with dimetal substrates are known.

Figure 4.2 demonstrates metal-metal bonded dimetal complexes. The rhodium complex is used as catalyst in arylation reactions<sup>4</sup> and the nickel complex as catalyst in cross-coupling reactions<sup>5</sup>.

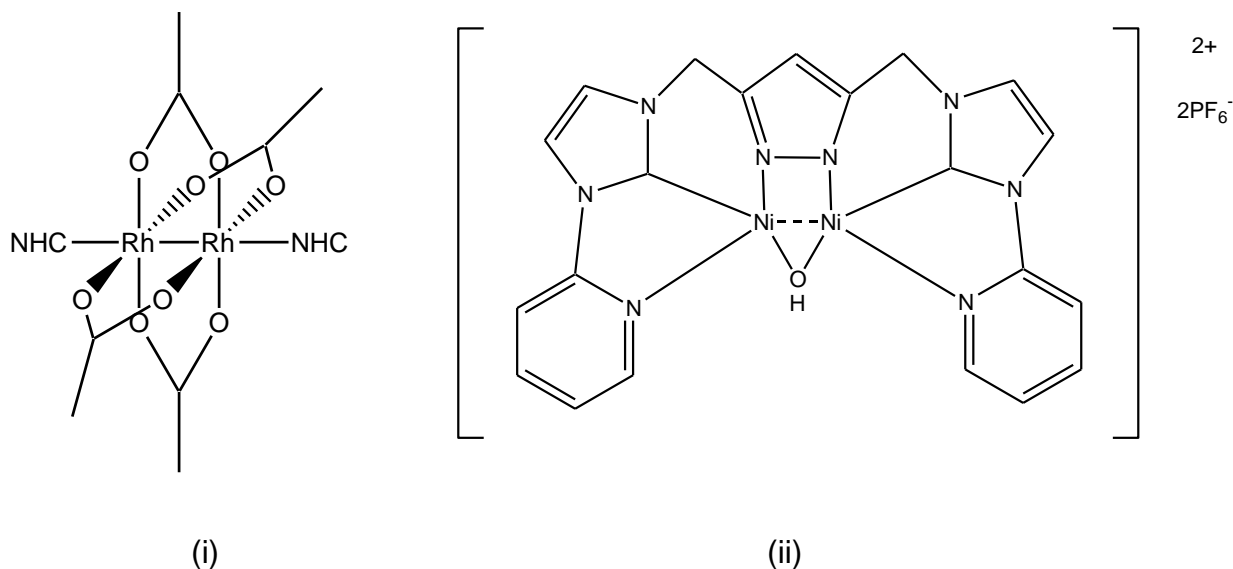


**Figure 4.2:** Dinuclear catalysts (metal-metal bonded complexes)

Another example reported in literature of this type of complex is the cobalt carbonyl dimer (Figure 4.3)<sup>6</sup> and was synthesised by van Rensburg *et al.*, simply by addition of the IMes (IMes = 1,3-bis(2,4,6-trimethylphenyl)imidazol-2-ylidene) dissolved in thf, to a warm solution of  $[\text{Co}_2(\text{CO})_8]$  in heptane under a CO blanket. The  $^{13}\text{C}$  NMR chemical shift of the carbene carbon atom is found to resonate at 183.2ppm. This complex is very interesting because it is one of the rare examples of a NHC dinuclear compound which contains both a metal-metal bond

(4) Gois, P. M. P.; Trindade, A. F.; Veiros, L. F.; André, V.; Duarte, M. T.; Afonso, C. A. M.; Caddick, S.; Cloke, F. G. N. *Angew. Chem., Int. Ed.* **2007**, *46*, 5750.

(5) Guo, N.; Stern, C. L.; Marks, T. J. *J. Am. Chem. Soc.* **2008**, *130*, 2246.

(6) Van Rensburg, H.; Tooze, R. P.; Foster, D. F.; Slawin, A. M. Z. *Inorg. Chem.* **2004**, *43*, 2468.

and carbonyl ligands, similar to the target compounds in this chapter.  $[\{\text{Co}(\text{CO})_3(\text{IMes})\}_2]$  was tested for modified cobalt hydroformylation but found to be unstable under these conditions<sup>7</sup>.

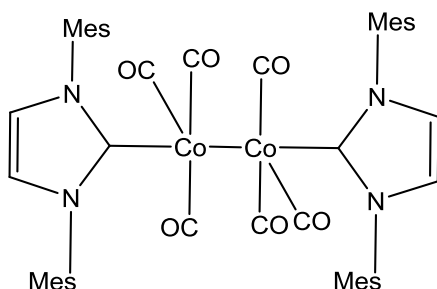


**Figure 4.3:** The first cobalt carbonyl-NHC dimer

Limited information on NHC dimetal complexes precludes the assumption that monometal NHC complexes are more prone to result in active catalysts than dimetal NHC complexes. This ambiguity led to the formulation of this project.

Various methods were used to synthesise the target molecules ( $[\text{Re}_2(\text{CO})_9\text{IMes}]$ ,  $[\text{Mn}_2(\text{CO})_9\text{IMes}]$ ) and derivatives thereof. Different approaches were explored and syntheses were repeated several times to attempt optimisation of reaction conditions and complete characterisation of the products. Insolubility of these compounds made it very difficult to handle, purify and to perform spectroscopic characterisation.

## 4.2 Approaches towards the NHC target molecules

### *The initial approach*

It was decided to follow the simplest route, in which the dimetal carbonyl substrate is decarbonylised and the deprotonated IMes added (Figure 4.4). As with the monometal complexes synthetic routes were varied by changing the solvent, base and temperature.

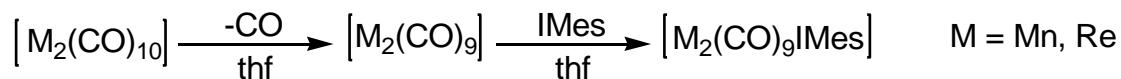


**Figure 4.4:** Illustration of the initial approach

*Using the imine complexes*

Following the results obtained in the reaction of  $[\text{ReBr}(\text{CO})_5]$  with the imine ligand (Imine = {glyoxal-bis(2,4,6-trimethylphenyl) imine}), it was thought worthwhile to attempt this synthesis with the dimetallic carbonyl substrates and subsequently use these dimetallic imine complexes as precursors in the synthesis of Fischer carbene complexes (Figure 4.5).

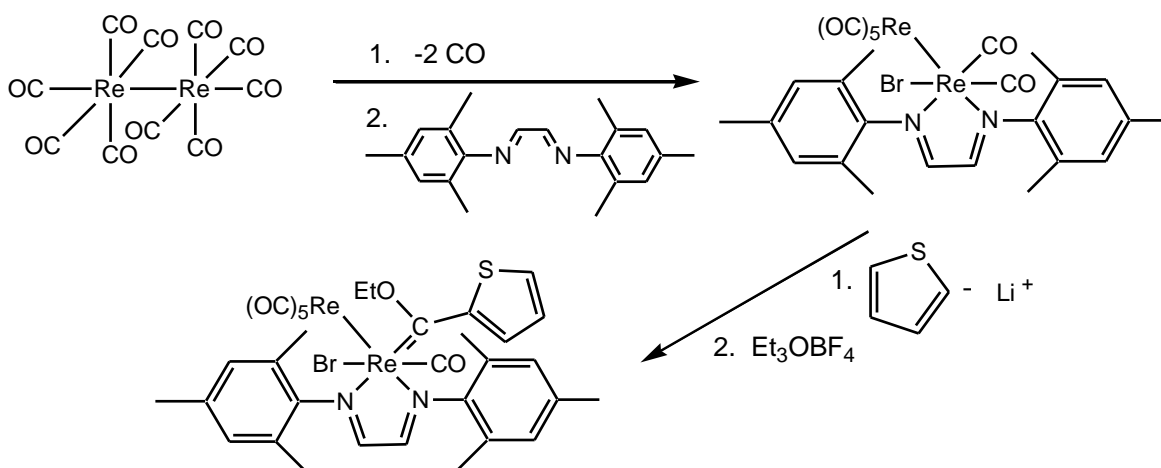


**Figure 4.5:** Fischer carbene synthesis from imine complexes

### The build-up approach

Another synthetic route, described by Ruiz *et al.*<sup>7</sup> was also employed, which involved building a less sterically demanding ligand on the metal substrate from the corresponding isocyanide complex (Figure 4.6).

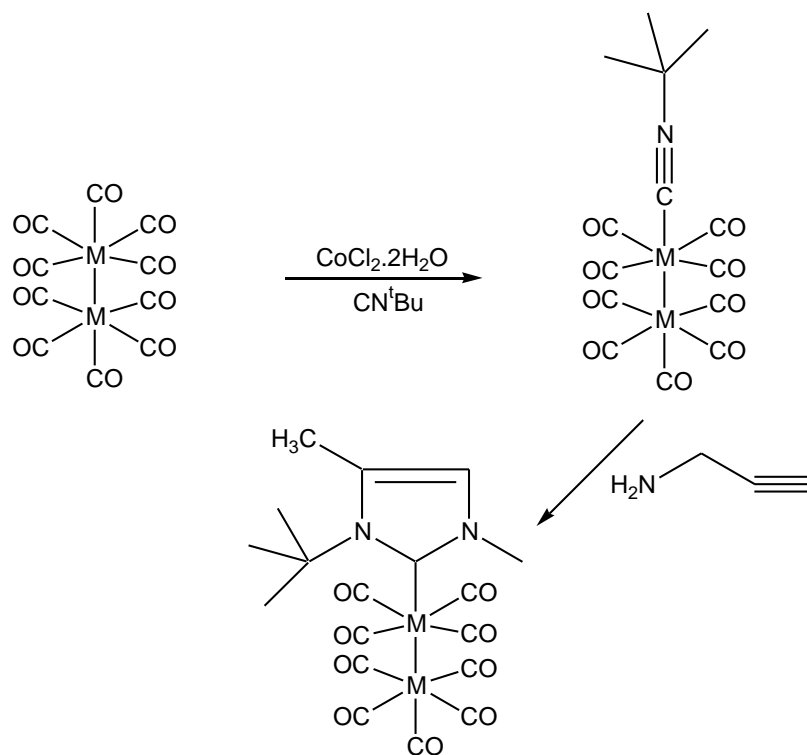


**Figure 4.6:** Illustration of the build-up approach employed by addition of propargylamine

### Employing Fischer carbenes

Synthesising complexes which contain not only an NHC ligand, but also a Fischer carbene ligand was attempted as well. The two approaches involved either the incorporation of an NHC ligand to a Fischer carbene complex (Figure 4.7), or, alternatively, a lithiated heteroarene was reacted with an NHC complex for Fischer carbene formation (Figure 4.8). In the former approach it was also possible to investigate the ability of the NHC ligand to replace the Fischer

(7) Ruiz, J., Garcia, G.; *J. Am. Chem. Soc.* **2005**, *127*, 8584.

carbene ligand in another attempt to synthesise an NHC complex. This is a successful method when chromium Fischer carbene complexes of the type  $[\text{Cr}\{\text{C}(\text{OEt})(\text{R})\}(\text{CO})_5]$  are employed in the synthesis of chromium NHC complexes (Figure 4.9).<sup>8</sup>

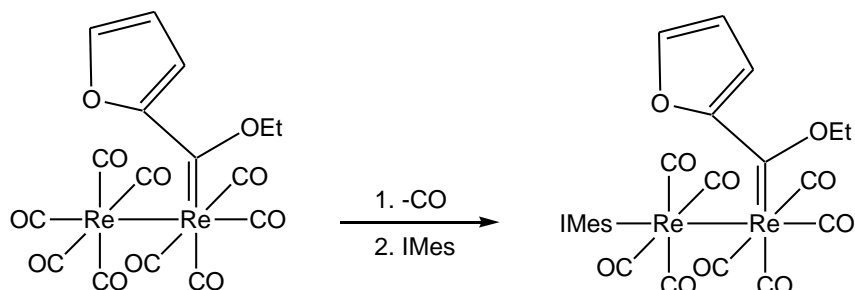


**Figure 4.7:** Utilizing a Fischer carbene complex as metal substrate in synthesising a complex containing both a Fischer carbene ligand and a NHC ligand. Geometric positions of these ligands are not definite

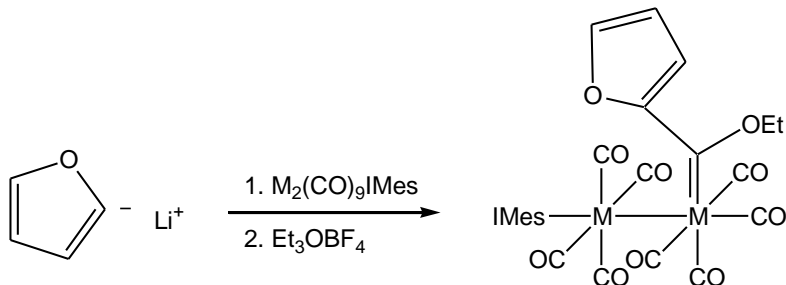


**Figure 4.8:** Reaction of a lithiated heteroarene with an NHC complex for Fischer carbene formation. Geometric positions of the ligands are not definite

(8) Kim, S., Choi, S. Y., Lee, Y. T., Park, K. H., Sitzmann, H. Chung, Y. K.; *Journal of Organometallic Chemistry*. **2007**, 692, 5390.

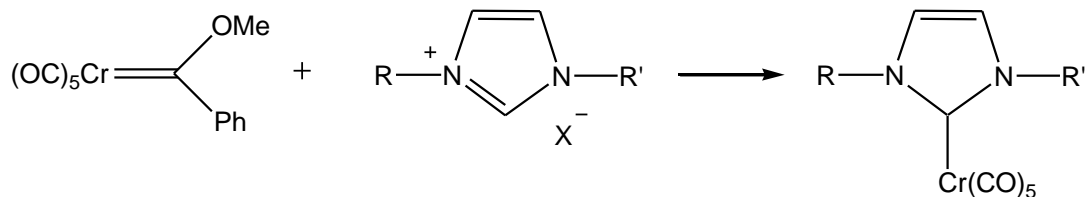


**Figure 4.9:** Employing chromium Fischer carbenes as a source of carbonyl chromium in synthesising chromium NHC complexes.

The section on employing Fischer carbenes will be described separately (Section 4.4.11).

Detailed descriptions of the synthesis method followed as well as the characterisation results obtained for each product will be presented.

### 4.3 Focus of this study

In an effort to prepare the target molecules  $[\text{Re}_2(\text{CO})_9\text{IMes}]$  and  $[\text{Mn}_2(\text{CO})_9\text{IMes}]$  (Figure 4.10), different approaches were explored. These target molecules are novel dimetallic Group VII metal complexes in a low oxidation state, and no literature precedents exist for their synthesis.

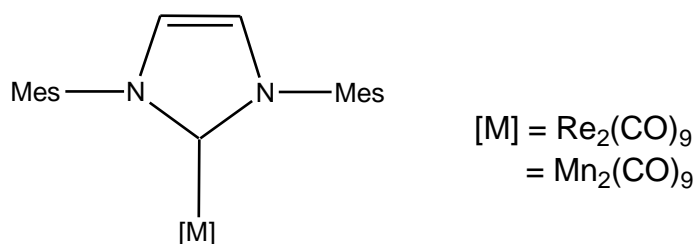
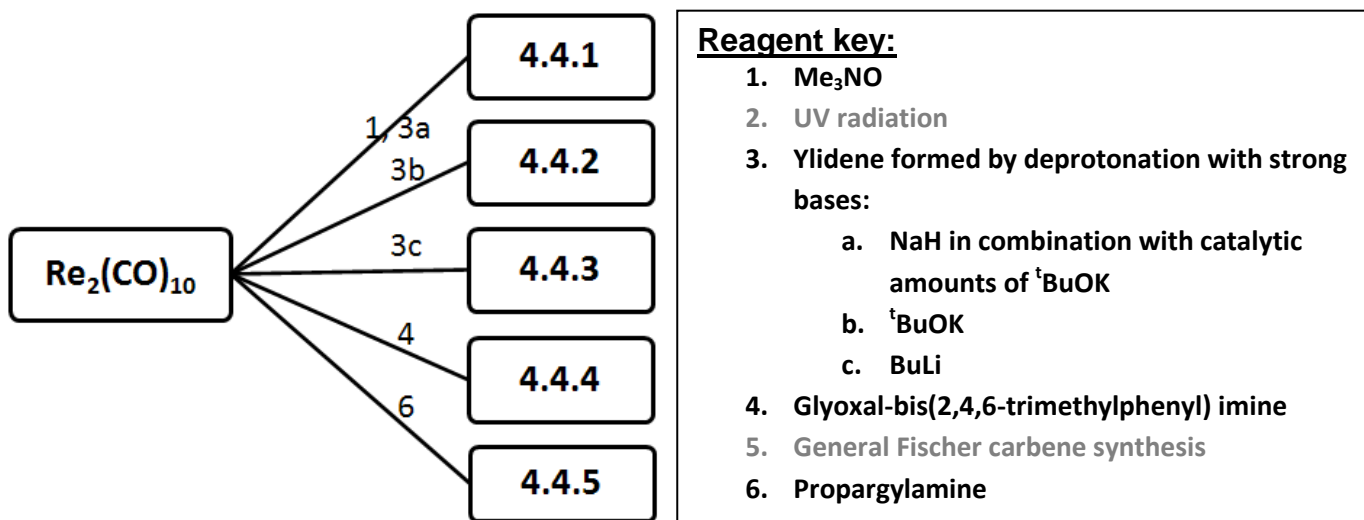


**Figure 4.10:** Template of the target molecules

#### 4.4 Synthesis, results and discussion of attempted NHC complexes

Scheme 4.1 and 4.2 give an overview of the synthetic routes followed and will be discussed.

*Complex formation by employing  $[\text{Re}_2(\text{CO})_{10}]$*



Scheme 4.1: Overview of reactions attempted with  $[\text{Re}_2(\text{CO})_{10}]$  as substrate

##### 4.4.1 Reaction route 1 followed by 3a

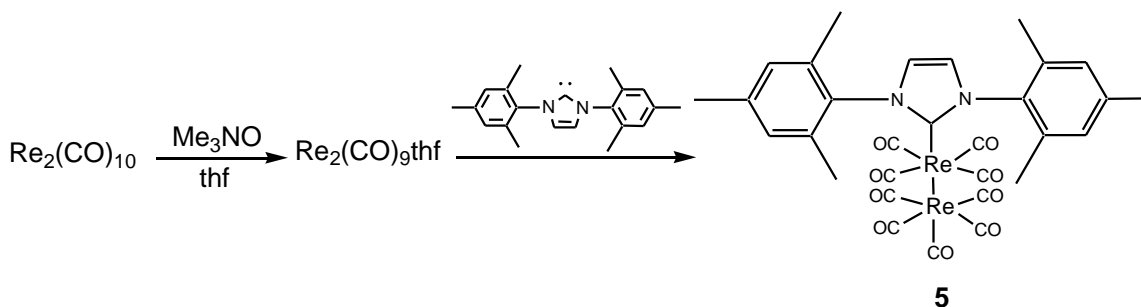


Figure 4.11: Illustration of the reaction route followed and the target molecule

[Re<sub>2</sub>(CO)<sub>10</sub>] (1.05mmol, 0.65g) was dissolved in 15ml thf and Me<sub>3</sub>NO (2mmol, 0.15g) added to promote decarbonylation. In a separate flask IMesHCl (IMesHCl = {1,3-bis(2,4,6-trimethylphenyl)-imidazolium chloride}) (2mmol, 0.68g) was dissolved in 10ml thf and deprotonated by 3a (see Reagent key, Scheme 4.1). The reaction mixture solution was filtered through celite and the ylide added dropwise. After two hours of stirring the volatiles were removed and the residue washed with hexane. IR analysis on the residue showed the presence of [Re<sub>2</sub>(CO)<sub>10</sub>], which could be due to incomplete separation of starting material during the hexane washings or due to incomplete reaction leaving the metal substrate uncomplexed. Four other vibrational frequencies were observed, but could not be assigned. The <sup>13</sup>C NMR indicates a double set of IMes signals. One set is attributed to unreacted IMesHCl and the other set to a partially decomposed IMes ligand. There are also traces of Me<sub>3</sub>NO and <sup>t</sup>BuOH (byproduct formed due to the base reaction). Chemical shifts in the NMR spectra could not be unambiguously assigned due to multiple signals observed. Expected chemical shifts of the target complex were found in the spectra and the IR spectra values (determined in dcm) are also found in the expected range.

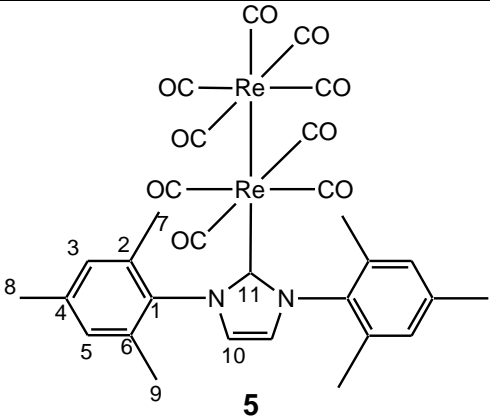
The proton NMR spectrum of this product displayed only broad unresolved peaks and no assignment was possible.

The IR vibrational six band pattern observed is accepted for an *ax*-[M<sub>2</sub>(CO)<sub>9</sub>L] type complex. The presence of [Re<sub>2</sub>(CO)<sub>10</sub>] was also visible from the spectrum.

IR: ν<sub>CO</sub> (cm<sup>-1</sup>) 2101, 2039, 1993, 1989, 1986, 1971.



Table 4.1



Atom number	<sup>13</sup> C NMR (ppm)
8	17.9
7, 9	20.4, 20.7
5	124.8
3	126.2
2, 6	129.6, 132.5
4	135.3
1	138.5
11	193.2
M-CO	186.6, 187.8

The reaction was repeated with longer stirring times and purification done with column chromatography. During purification a yellow fraction was isolated and after spectroscopic analysis not only  $[\text{Re}_3(\text{CO})_{14}\text{H}]$  was identified but also the *in situ* formation of  $[\text{Re}(\text{CO})_5\text{H}]$ . The formation of these complexes can be explained by following the proposed reaction pathway illustrated in Figure 4.12. Initiation of this pathway is due to a source of hydrogen atoms from either unreacted NaH still in the reaction mixture or during column chromatography in which the silica is slightly acidic and contains adsorbed  $\text{H}_2\text{O}$ . The hydrogen coordinates to the Re atom of the  $[\text{Re}_2(\text{CO})_{10}]$  complex and leads to the

dissociation of the Re-Re bond. The formation of the Re-H bond is more favoured since it forms a stronger and lower energy bond (10 - 14kJ/mol)<sup>9</sup> than the Re-Re bond (213 kJ/mol).<sup>10</sup> [HRe(CO)<sub>5</sub>] is formed as an intermediate and reacts further with the available decarbonylised [Re<sub>2</sub>(CO)<sub>9</sub>] complex to form the [Re<sub>3</sub>(CO)<sub>14</sub>H] complex.

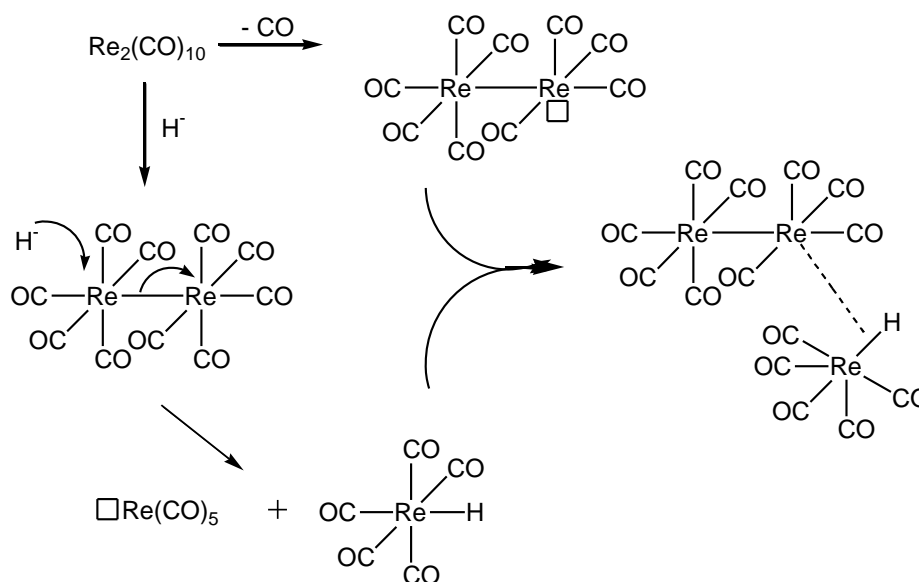


**Figure 4.12:** Proposed reaction pathway of the formation of [Re<sub>3</sub>(CO)<sub>14</sub>H]

The complex, [Re<sub>3</sub>(CO)<sub>14</sub>H], also known as the Fellmann-Kaesz complex was previously isolated in 1966<sup>11</sup> by Fellmann and Kaesz but its detailed structure reported in 1985<sup>12</sup>. Yang *et al.*<sup>12</sup> synthesised this complex by photolysis of a hexane solution containing [Re<sub>2</sub>(CO)<sub>10</sub>] and thiophene (Th). <sup>1</sup>H NMR and IR spectroscopy was employed to characterise this complex.

(9) Gusev, D. G., Nietlispach, D., Vymenits, A. B., Bakhmutov, V. I., Berke, H.; *Inorg. Chem.* **1993**, *32*, 3270.

(10) Gilbert, B. C., Parsons, A. F.; *J. Chem. Soc., Perkin Trans. II*, **2002**, 367.

(11) Fellman, W.; Kaesz, H. D. *Inorg. Nucl. Chem.* **1966**, *2*, 63.

(12) Yang, C. S.; Cheng, C. P. *J. Chin. Chem. Soc.* **1985**, *32*, 17

This spectroscopic analysis obtained by Yang *et al.* together with the crystal structure data obtained for this complex were used as guidance to confirm the formation of the Fellmann-KaesZ complex.

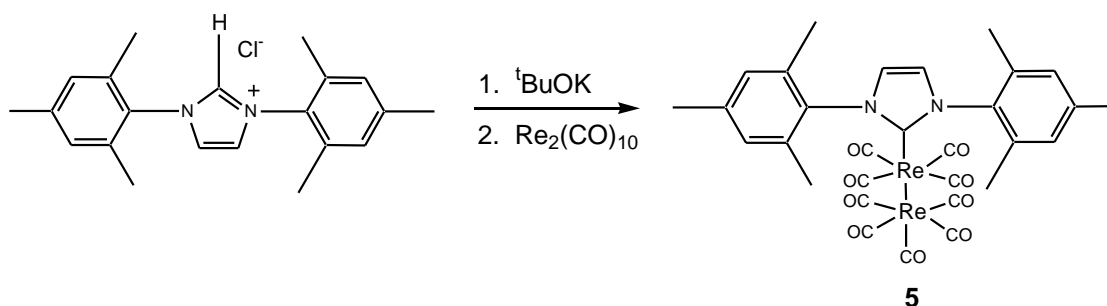
IR:  $\nu_{\text{CO}}$  ( $\text{cm}^{-1}$ ) 2147, 2099, 2038, 2011, 1988, 1980, 1935:  $[\text{Re}_3(\text{CO})_{14}\text{H}]$

$^1\text{H}$  NMR:  $\delta_{\text{C}}$  (ppm,  $\text{C}_6\text{D}_6$ ) -15.45 ( $[\text{Re}_3(\text{CO})_{14}\text{H}]$ )

$^1\text{H}$  NMR:  $\delta_{\text{C}}$  (ppm,  $\text{C}_6\text{D}_6$ ) -5.62 ( $[\text{Re}(\text{CO})_5\text{H}]$ )

Mass:  $m/z = 952$  ( $[\text{Re}_3(\text{CO})_{14}\text{H}]^+$ )

#### 4.4.2 Route 3b

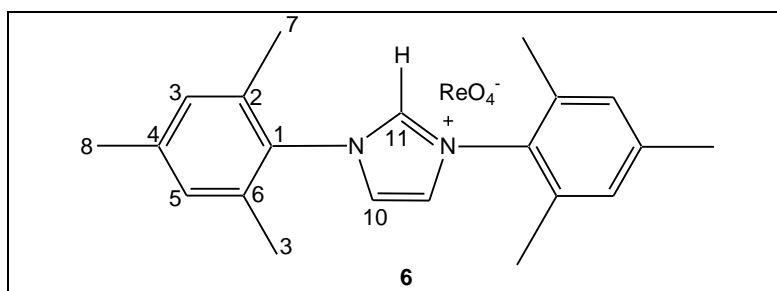


**Figure 4.13:** Illustration of the reaction route followed and the target molecule

IMesHCl (2mmol, 0.66g) was deprotonated with 3b in a thf solution. This mixture was added to a thf solution of  $[\text{Re}_2(\text{CO})_{10}]$  (1.06mmol, 0.68g) and stirred. Thin layer chromatography (Tlc) was used to monitor the reaction and due to the absence of product formation, the reaction mixture was heated in an oilbath at  $70^\circ\text{C}$  for an hour. The thf solvent was removed and left brown residue. The product was extracted with hexane and the hexane removed by reduced pressure. The deposit was purified with column chromatography. A dark yellow fraction was eluted with dcm. The  $^{13}\text{C}$  NMR spectrum revealed no carbonyl resonances and unassigned signals were observed. Further purification was

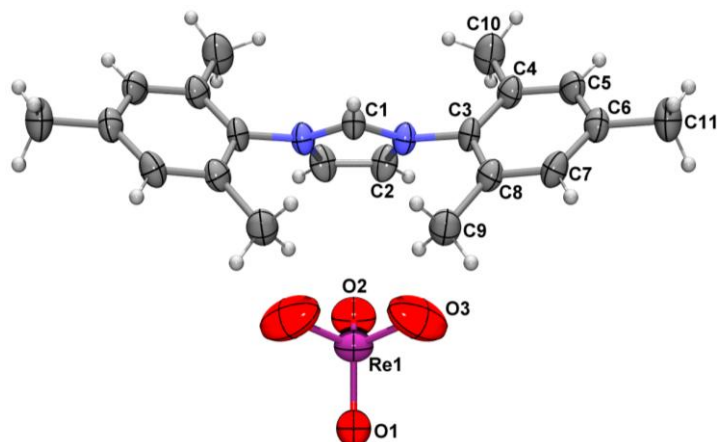
attempted by crystallisation by dissolving the fraction in dcm and layering it with hexane in a 1:1 ratio. The light brown crystals of  $\text{IMesH}[\text{ReO}_4]$  (**6**) were obtained.

Table 4.2: NMR data of **6** recorded in  $\text{C}_6\text{D}_6$

	
<b>Atom number</b>	<b><math>^1\text{H}</math> NMR (ppm)</b>
7,9	1.91 (br, 12H)
8	2.19 (br, 6H)
3,5	6.70 (br, 4H)
10	7.14 (s, 2H)
11	n. o.
	<b><math>^{13}\text{C}</math> NMR (ppm)</b>
7,9	17.8
8	20.9
3,5	121.8
2,6	126.9
4	128.9
1	129.6
11	141.2

The chemical shifts in the  $^1\text{H}$  and  $^{13}\text{C}$  NMR spectra of **6** were given in Table 4.2 and the spectra were recorded in  $\text{C}_6\text{D}_6$ . The NMR values reflect the same chemical shift pattern as the starting material (Table 2.2) at consistently upfield values, as it was recorded in  $\text{C}_6\text{D}_6$  compared to  $\text{CDCl}_3$  for the chloride salt.

*Crystal structure obtained*



**Figure 4.14:** ORTEP + POV-Ray drawing of the molecular structure of complex **6**

Formation of this complex is quite unexpected and the reaction pathway unexplained. The main aspect in the formation of this complex is the oxidation of the rhenium metal from +1 to +7 state which results in the  $[\text{ReO}_4]^{-1}$  anion. This anion replaces the  $\text{Cl}^-$  anion in the  $\text{IMesHCl}$  salt and, as will be further discussed (section 4.4.10), the preference for the larger anion is due to co-crystallization of similar size ions.

**4.4.3 Route 3c**

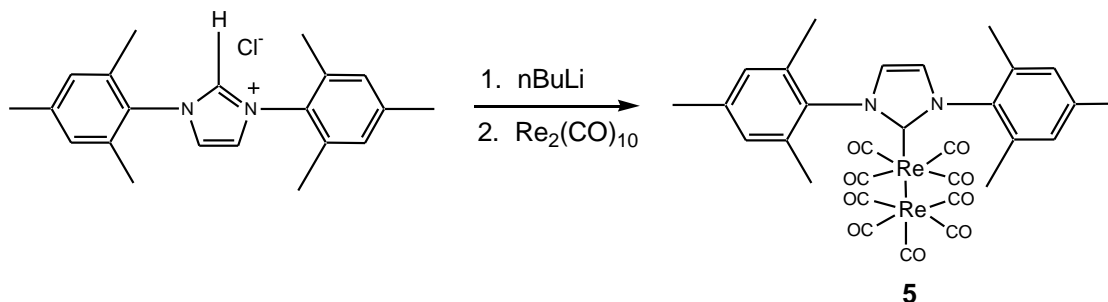


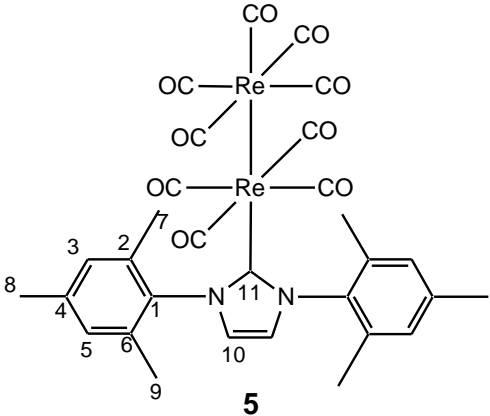
**Figure 4.16:** Illustration of the reaction route followed and the target molecule

A different deprotonation method involving very low temperatures was used in this attempt. 15ml of thf was cooled to  $-78^{\circ}\text{C}$  after which IMesHCl (2mmol, 0.7g) is added and stirred for 20min. After the addition of nBuLi (2.5mmol, 1.7 ml) the reaction was stirred for 1hr and allowed warm up to  $-30^{\circ}\text{C}$ . The mixture was again left to stir for 1hr and  $[\text{Re}_2(\text{CO})_{10}]$  (2mmol, 1.3g) added. While stirring, the reaction mixture was left to warm to RT and after 1hr the thf was removed by reduced pressure. Hexane was used to remove the unreacted  $[\text{Re}_2(\text{CO})_{10}]$  and the residue was dried under vacuum. Toluene and ether respectively was used in an attempt to extract the product from the residue after which IR spectroscopy was done in diethylether.

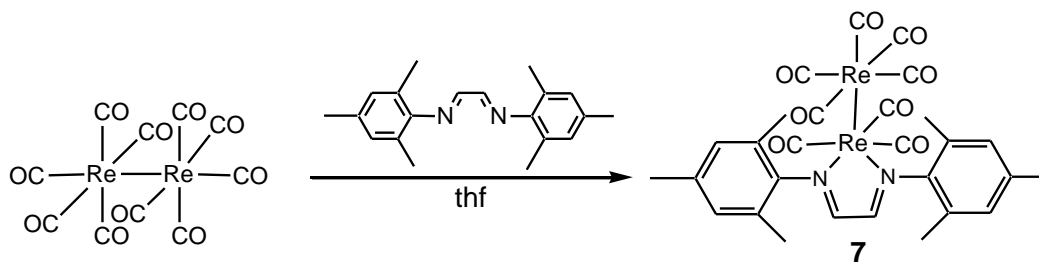
NMR signals expected for the target molecule could be observed but could not unambiguously be assigned due to multiple resonance peaks present.

The observed IR vibrational six band pattern is accepted for an  $ax\text{-}[\text{M}_2(\text{CO})_9\text{L}]$  type complex. Compared to the IR vibration values obtained for the same complex in Table 4.1 it is clear that there are similarities in the values obtained. The wavenumbers of the vibrations observed for complex **5** are as follows:  
IR:  $\nu_{\text{CO}}$  ( $\text{cm}^{-1}$ ) 2093, 2031, 1993, 1971, 1951, 1935

Table 4.3: NMR data of **5** recorded in C<sub>6</sub>D<sub>6</sub>

	
<b>Atom number</b>	<b><sup>1</sup>H NMR (ppm)</b>
8	2.11 (br, 6H)
7, 7', 9, 9'	2.15 (br, 12H)
3, 3', 5, 5'	6.70 (m, 2H)
10	8.05 (s, 2H)
	<b><sup>13</sup>C NMR (ppm)</b>
8	18.1
7, 9	20.6, 20.8
5	124.3
3	126.6
2, 6	129.7, 134.1
4	136.4
1	137.9
11	189.5
M-CO	n. o.

#### 4.4.4 Route 4

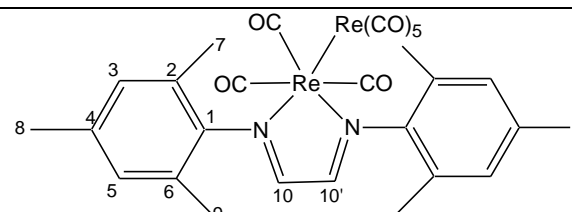


**Figure 4.17:** Illustration of the reaction route followed and the target molecule

A solution of  $[\text{Re}_2(\text{CO})_{10}]$  (1.5mmol, 0.98g) and imine (1.5mmol, 0.5g) in 20ml thf was stirred for different time lengths and the reaction monitored with Tlc. Volatiles were removed and purification done on a silica gel column. After the elution of the unreacted  $[\text{Re}_2(\text{CO})_{10}]$  with hexane, the solvent polarity was increased stepwise using dcm and later thf, after which two other fractions eluted. The first plum coloured fraction was identified as the target complex.



**Table 4.4:** NMR data of **7** recorded in C<sub>6</sub>D<sub>6</sub>

 <b>7</b>	
Atom number	<sup>1</sup> H NMR (ppm)
7, 9	2.00 (br, 12H)
8	2.06 (br, 12H)
5	6.55 (br, 2H)
3	6.67 (br, 2H)
10, 10'	7.86 (s, 2H)
<sup>13</sup> C NMR (ppm)	
8	19.0
9	20.5
7	20.6
5	127.8
3	129.0
2, 6	129.4
4	135.0
1	136.9
10	162.8
M-CO	197.9

IR:  $\nu_{\text{CO}}$  (cm<sup>-1</sup>) 2068, 2007, 1967, 1963

IR vibrational analysis show formation of a different carbonyl complex, however, the dominating species present is [Re<sub>2</sub>(CO)<sub>10</sub>].

Fraction two was a mixture of the target complex and decomposition products.

#### 4.4.5 Route 6

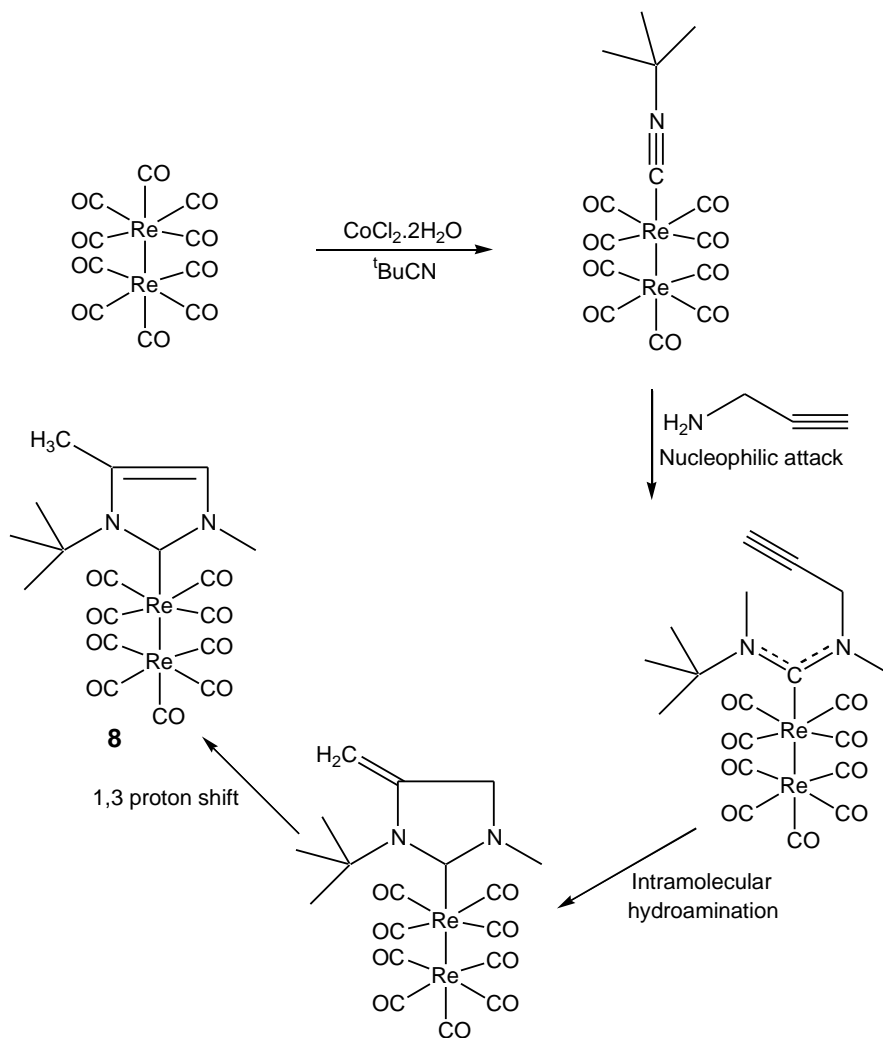


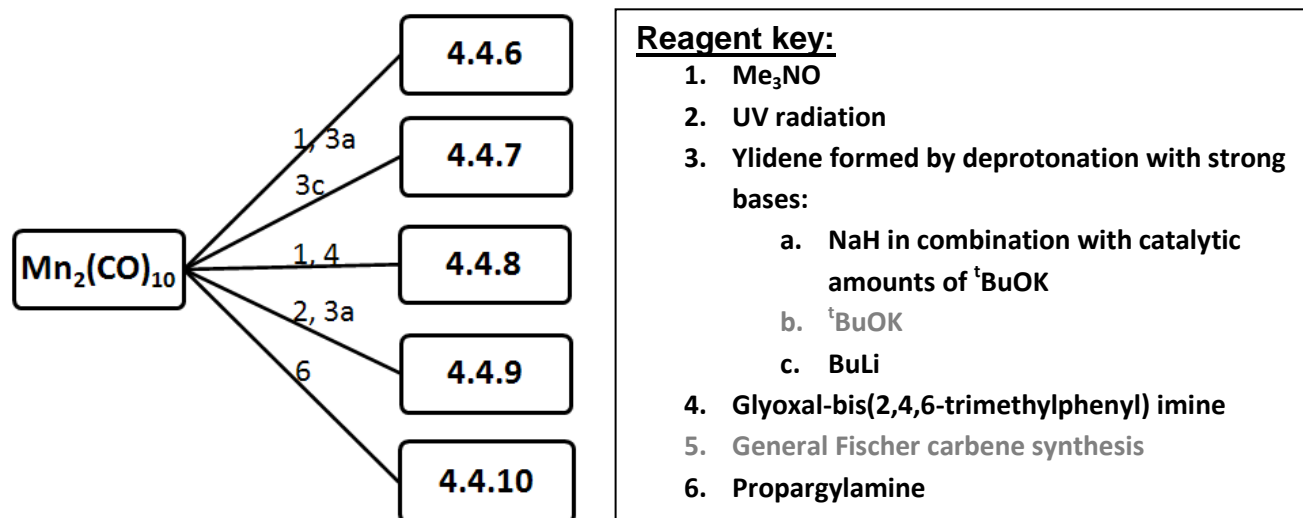
**Figure 4.17:** Illustration of the reaction route followed and the target molecule, **8**

$[\text{Re}_2(\text{CO})_{10}]$  (1.0mmol, 0.65g) and  $[\text{CoCl}_2 \cdot 2\text{H}_2\text{O}]$  (0.06mmol, 0.01g) were mixed in 10ml toluene. The mixture was refluxed after which  ${}^t\text{BuCN}$  (1.0mmol, 113 $\mu\text{l}$ ) was added. A blue-purple colour indicates the formation of the cobalt-isocyanide complex and after 48 hours the reaction colour changes to green which indicates completion. The solution was left to cool to RT and the catalyst adsorbed on 10g of silica gel. Toluene was used to extract the  $[\text{Re}_2(\text{CO})_9({}^t\text{BuCN})]$  product and filtered through silica gel to result in a pale yellow solution. The solvent was

removed under reduced pressure and a beige solid (approximately 50% yield) obtained.

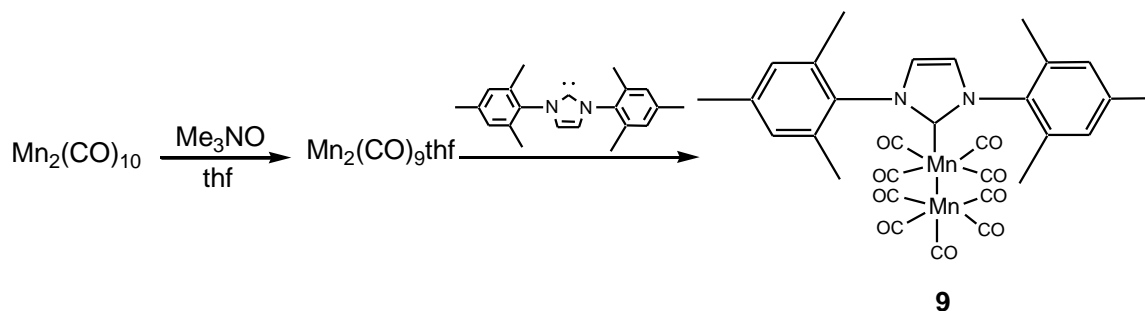
$[\text{Re}_2(\text{CO})_9(\text{}^t\text{BuCN})]$  (0.4mmol, 0.2g) was dissolved in 10ml thf and propargylamine ( $\text{C}_3\text{H}_5\text{N}$ ) (8.3mmol, 0.5ml) added. The mixture was left to stir for 24hrs after which the solvent was removed and a yellow oil resulted. 16ml of a 1:4 dcm:toluene mixture was added to the oil and stirred for 30min. The resultant precipitate was filtered off and the volume of the filtrate reduced to approximately 5ml. By addition of 10ml hexane a beige solid was formed and after decanting the excess solvent the solid was washed with hexane to yield the product,  $[\text{Re}_2(\text{CO})_9\text{NHC}]$  (**8**).

*Complex formation by employing  $[\text{Mn}_2(\text{CO})_{10}]$*



Scheme 4.2: Overview of reactions attempted with  $[\text{Mn}_2(\text{CO})_{10}]$  as metal substrate

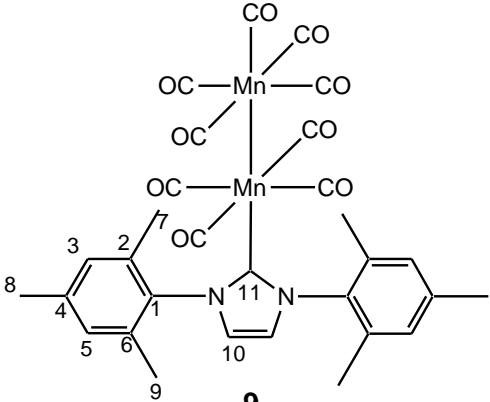
#### 4.4.6 Route 1 followed by 3a



**Figure 4.18:** Illustration of the reaction route followed and the target molecule

[Mn<sub>2</sub>(CO)<sub>10</sub>] (3mmol, 1.17g) was dissolved in 20ml of thf and Me<sub>3</sub>NO (3.2mmol, 0.27g) added. The reaction mixture was stirred for 30 min and the bright orange mixture filtered through celite. The ylidene (3mmol) in thf was added dropwise to the solution and stirred for 5hrs at RT. Thf was removed by reduced pressure and the residue washed with hexane until the hexane was clear. The spectroscopic analysis revealed traces of [Mn<sub>2</sub>(CO)<sub>10</sub>], product (**9**), and imine formation. Thf was used to do IR analysis.

Table 4.5: NMR data of complex **9** recorded in thf d<sub>8</sub>

	
<b>Atom number</b>	<b><sup>1</sup>H NMR (ppm)</b>
8	2.01 (s, 6H)
7, 9	2.11 (s, 12H)
3, 5	6.60 (br, 4H)
10	7.36 (s, 2H)
	<b><sup>13</sup>C NMR (ppm)</b>
8	18.3
7, 9	20.9
5	123.7
3	127.0
2, 6	130.2, 133.6
4	135.0
1	137.8
11	n. o.
CO's	197.9

IR:  $\nu_{\text{CO}}$  (cm<sup>-1</sup>) 2091, 2027, 1996, 1930 (br)

A IR vibrational five band pattern was expected for a  $ax-[Mn_2(CO)_9L]$  type complex<sup>13</sup> but the two bands with the lowest wavenumber ( $\nu$ ) overlap to give the four band pattern.

In an attempt to isolate the product the reaction was repeated. After the residue was washed with hexane it was dried under vacuum and benzene was used in an effort to extract the product. Spectroscopic analysis showed that a small amount of the imine is extracted but the  $^{13}C$  NMR signals cannot be unambiguously assigned. No metal carbonyl signals could be observed.

#### 4.4.7 Route 3c

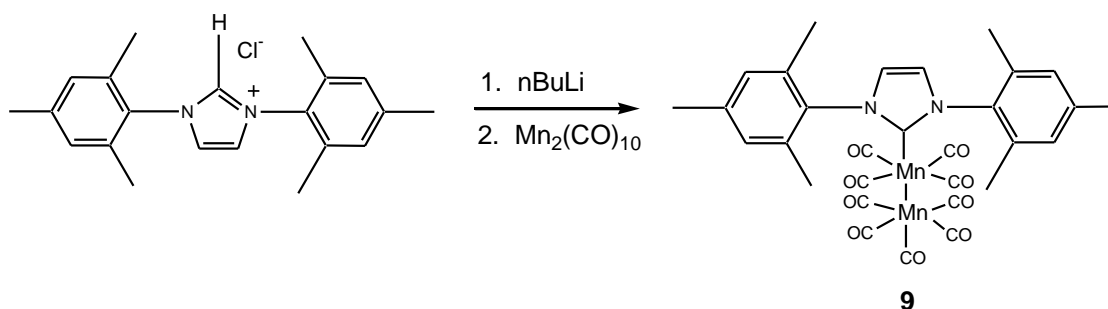


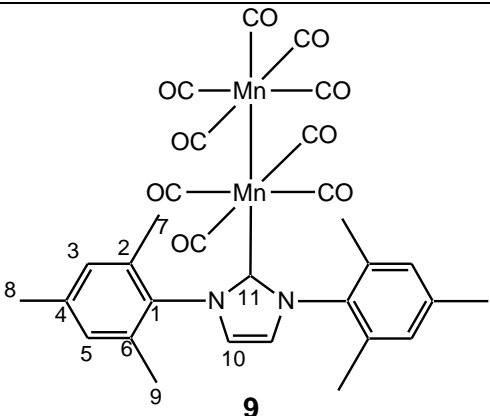
**Figure 4.19:** Illustration of the reaction route followed and the target molecule, **9**

20ml of thf was cooled to  $-78^{\circ}C$  and IMesHCl (2mmol, 0.7g) added. nBuLi (2.5mmol, 1.7ml) was added and the reaction mixture left to stir for 1hr after which it was allowed to warm to  $-30^{\circ}C$  and stirred for 1hr at this temperature.  $[Mn_2(CO)_{10}]$  (2mmol, 0.7g) was added to the solution and the mixture was left to warm to RT while stirring. Thf was removed by reduced pressure and washed with hexane and ether respectively. The hexane fraction contained most of the unreacted  $[Mn_2(CO)_{10}]$  while the orange target product,  $[Mn_2(CO)_9IMes]$ , was extracted in ether. This ether fraction contained traces of unreacted  $[Mn_2(CO)_{10}]$

(13) Ziegler, M. L.; Haas, H.; Sheline, R. K. *J. Inorg. Nuclear Chem.* **1962**, *24*, 1172.

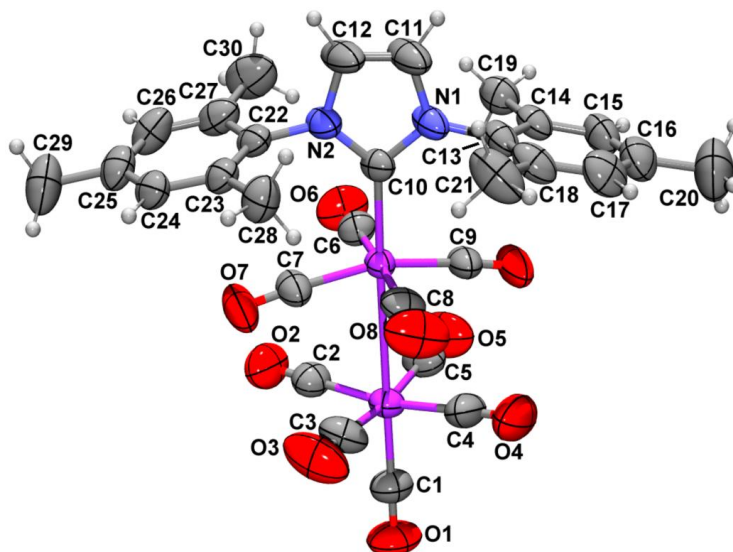
and was further purified by crystallisation from the ether. IR analyses was also done in ether.

Table 4.6: NMR data of **9** recorded in C<sub>6</sub>D<sub>6</sub>

	
<b>Atom number</b>	<b><sup>1</sup>H NMR (ppm)</b>
8	2.07 (br, 6H)
7, 9	2.13 (br, 12H)
3, 5	6.72 (br, 4H)
10	7.59 (br, 2H)
	<b><sup>13</sup>C NMR (ppm)</b>
8	17.7
7, 9	21.0
5	124.1
3	129.8
2, 6	136.0
4	137.0
1	139.9
11	226.0
M-CO	208.9, 212.1

IR:  $\nu_{\text{CO}}$  (cm<sup>-1</sup>) 2077, 2028, 2000, 1961, 1938

The IR vibrational spectrum obtained for this complex shows the expected  $ax-[Mn_2(CO)_9L]$  five band pattern and the wavenumbers fall well within the range prescribed by literature<sup>13</sup>.



**Figure 4.20:** ORTEP + POV-Ray drawing of the molecular structure of complex **9**.

The proposed reaction pathway is illustrated in Figure 4.21. The ylide is formed by the deprotonation of the precursor chloride salt and displaces a labile carbonyl ligand to coordinate to the metal atom.

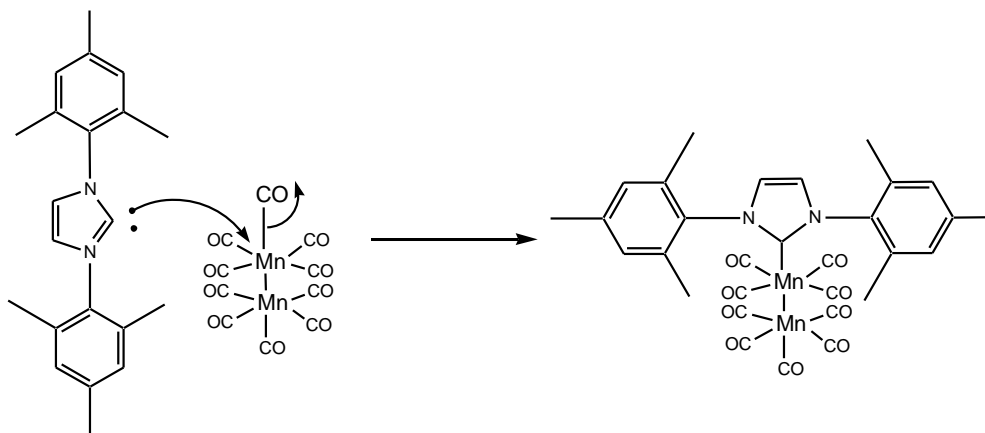


**Figure 4.21:** The proposed reaction pathway of complex **9**



Usually, the electronic favoured site of coordination of a carbene ligand is the equatorial position. This means that the carbene ligand is placed *trans* to a  $\pi$ -acceptor (carbonyl ligand) instead of the remaining  $M(CO)_5$ -moiety<sup>14</sup>. In the complex displayed in Figure 4.20 the *axial* position is the preferred position of the carbene ligand over the expected equatorial position. This indicates that the steric effects in this complex play a dominant role compared to the electronic effect.

#### 4.4.8 Route 1 followed by 4

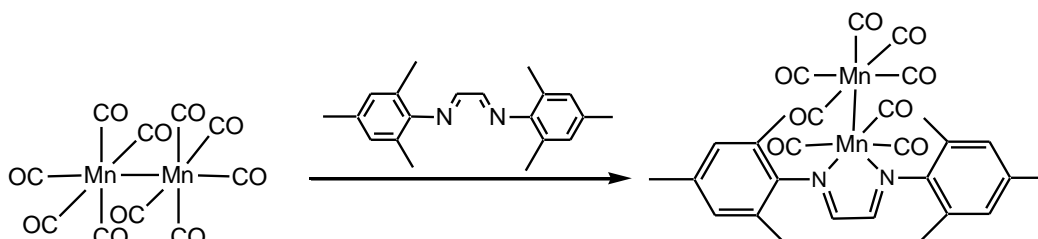
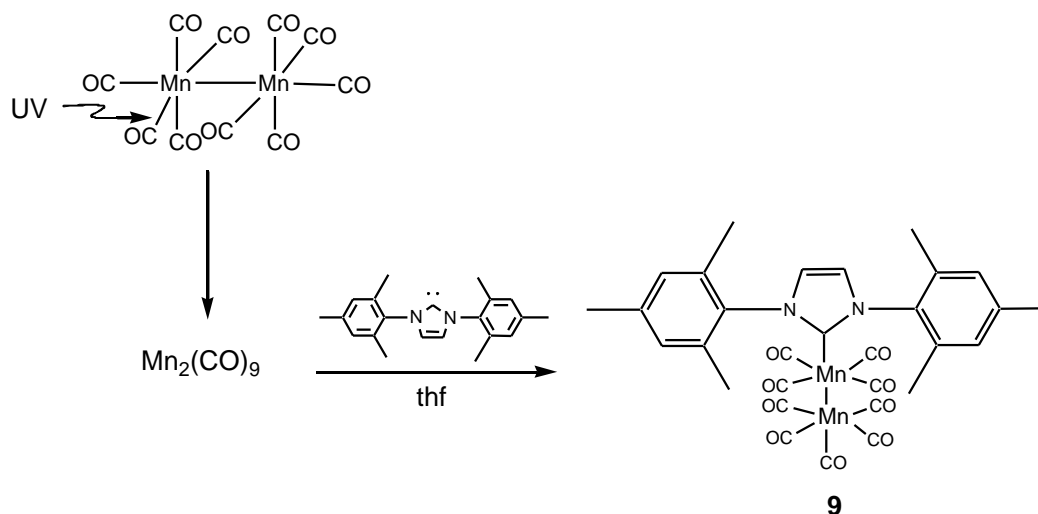


**Figure 4.22:** Illustration of the reaction route followed and the target molecule

A solution of  $[Mn_2(CO)_{10}]$  (2mmol, 0.78g) and  $Me_3NO$  (4mmol, 0.3g) was stirred in 20ml of thf for 1hr. Imine (2mmol, 0.66g) was added to this deep orange solution and stirred overnight. No products could be isolated. Reaction conditions were varied by increasing energy by heating and employing different reaction times, but did not result in product formation.

(14) Bezuidenhout, D. I.; Liles, D. C.; van Rooyen, P. H.; Lotz, S. J. *J. Organomet. Chem.* **2007**, 692, 774.

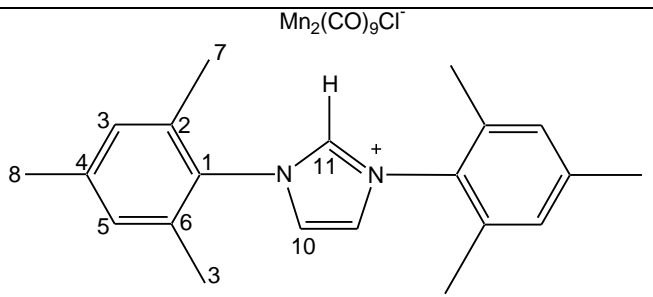
#### 4.4.9 Route 2 followed by 3a



**Figure 4.23:** Illustration of the reaction route followed and the target molecule

$[\text{Mn}_2(\text{CO})_{10}]$  (3mmol, 1.23g) was dissolved in 15ml of thf and radiated with UV for 4hrs. In a separate flask MesHCl (3mmol, 1.7g) was deprotonated in 20ml thf via the base indicated by 3a. This solution was added to the  $[\text{Mn}_2(\text{CO})_{10}]$  mixture and stirred for 3hrs while it was monitored with Tlc. After no product formation could be observed the reaction mixture was refluxed for 2hrs. As soon as the Tlc plate indicated the presence of additional products the heat was removed and reduced pressure was applied to remove the thf. Purification was attempted with silica column chromatography and a hexane/dcm (1:1) as eluent. One fraction was collected. With spectroscopic analysis no product formation could be observed, only IMesHCl resonance signals were detected. Further purification was attempted by crystallisation by dissolving the fraction in dcm and layering it with hexane in a 1:1 ratio. A single crystal was isolated and X-ray diffraction revealed the molecular structure to be the salt IMesH $[\text{Mn}_2(\text{CO})_9\text{Cl}]$ , **10**.

**Table 4.7:** NMR data of complex **10** recorded in C<sub>6</sub>D<sub>6</sub>

 <b>10</b>	
<b>Atom number</b>	<b><sup>1</sup>H NMR (ppm)</b>
7,9	1.75 (br, 12H)
8	2.42 (br, 6H)
3,5	6.98 (br, 4H)
10	7.65 (s, 2H)
11	9.40 (s, 1H)
	<b><sup>13</sup>C NMR (ppm)</b>
7,9	17.5
8	20.3
3,5	127.2
2,6	128.9
4	129.9
1	135.8
2	137.1
11	140.1
M-CO	n. o.

The chemical shifts obtained for this salt are similar to the chemical shifts of the two other analogues (Table 2.2 and Table 4.2)

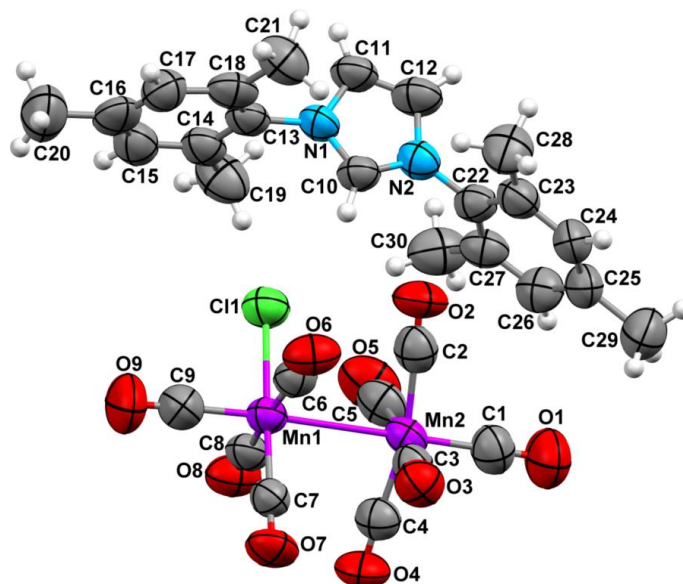


**Figure 4.24:** ORTEP + POV-Ray drawing of the molecular structure of complex **10**

The IMesHCl salt has two moieties: the chlorine anion and the IMesH cation. There is an obvious size difference between these two ions, where the chlorine atom is much smaller than the IMesH cation. The crystal structure of complex **10** is a typical example of the preferred co-crystallisation of similar size ions as seen for the  $[\text{ReO}_4]^{-1}$  complex **6**. The formation of this chloro complex is ascribed to the abstraction of a chloride ion from the IMesHCl salt. The increased size of the  $[\text{Mn}_2(\text{CO})_9\text{Cl}]^{-}$  anion is a better match for the large IMesH cation which results in co-crystallisation.

This reaction was repeated and the time of radiation with UV light was extended to 7hrs. No heat was applied and after purification two fractions were collected of which only one was suitable for spectroscopic analysis. No product formation was observed.

#### 4.4.10 Route 6

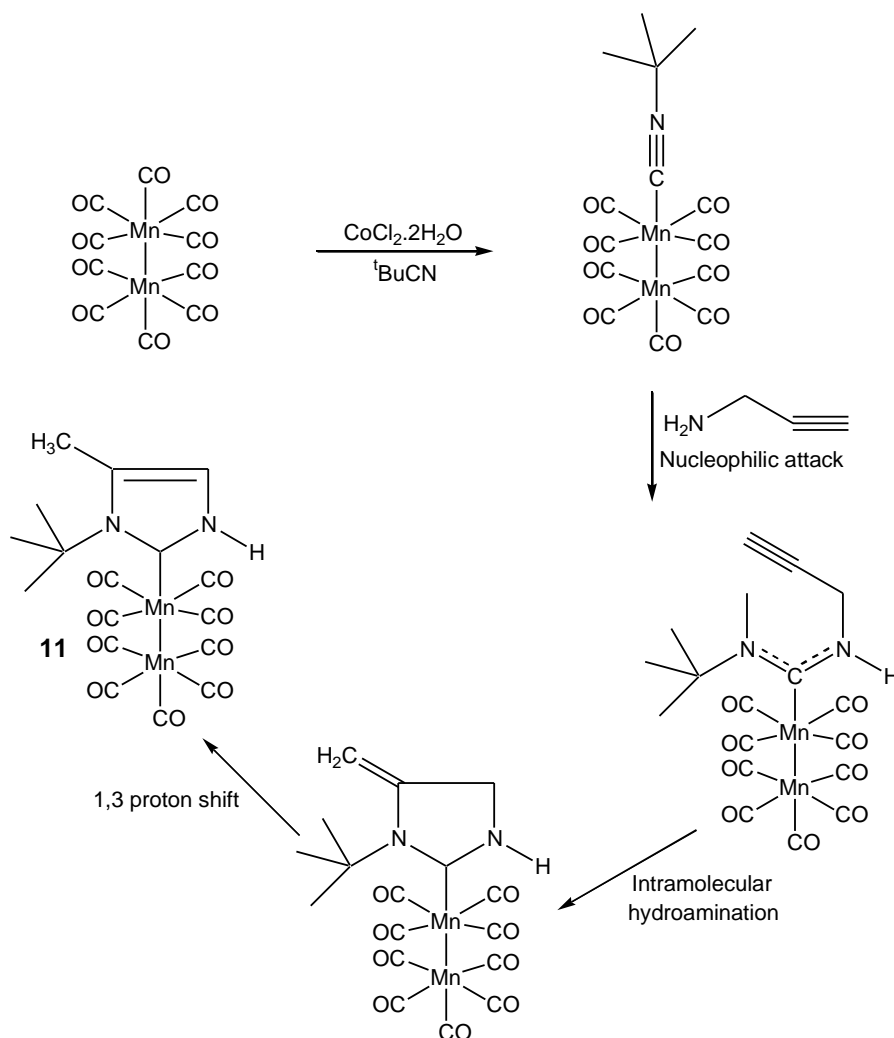


**Figure 4.25:** Illustration of the reaction route followed and the target molecule, **11**

The same synthetic method was used as described in Section 4.4.5.

$[\text{Mn}_2(\text{CO})_{10}]$  (1.0mmol, 0.39g) and  $[\text{CoCl}_2 \cdot 2\text{H}_2\text{O}]$  (0.06mmol, 0.01g) were mixed in 10ml of toluene. The mixture was refluxed after which  ${}^t\text{BuCN}$  (1.0mmol, 113 $\mu\text{l}$ ) was added and stirred for 48hrs. The solution was left to cool to RT and the catalyst adsorbed on 10g of silica. Toluene was used to extract the  $[\text{Mn}_2(\text{CO})_9({}^t\text{BuCN})]$  product and filtered through silica. The solvent was removed under reduced pressure and approximately 50% yield of the beige product

obtained.  $[\text{Mn}_2(\text{CO})_9(\text{tBuCN})]$  (0.32mmol, 0.14g) was dissolved in 10ml of thf and propargylamine ( $\text{C}_3\text{H}_5\text{N}$ ) (6.6mmol, 0.4ml) added. The mixture was left to stir for 24hrs after which the solvent was removed and 16ml of a 1:4 dcm:toluene mixture added. After 30min, the resultant precipitate was filtered off and the volume of the filtrate reduced to approximately 5ml. By addition of 10ml hexane an orange solid was formed and after decanting the excess solvent the solid was washed with hexane to yield the product.

**Table 4.8:** NMR data of complex **11** recorded in  $\text{CDCl}_3$

<b>Atom number</b>	<b><math>^1\text{H}</math> NMR (ppm)</b>
3	1.35 (s, 9H)
4	2.10 (br, 3H)
N-H	5.92 (br, 1H)
6	6.89 (br, 1H)
	<b><math>^{13}\text{C}</math> NMR (ppm)</b>
3	22.7
4	31.9
6	68.1
5	71.9
2	72.2
1	224.2
M-CO	215.6, 207.4

IR:  $\nu_{\text{CO}}$  ( $\text{cm}^{-1}$ ) 2080, 2036, 2022, 1990, 1974, 1916

The IR vibrational spectrum obtained for this complex shows the expected  $ax\text{-}[\text{Mn}_2(\text{CO})_9\text{L}]$  six band pattern and the wavenumbers fall well within the range described by literature<sup>13</sup>.

#### 4.4.11 Employing Fischer carbenes to synthesise biscarbene complexes containing NHCs

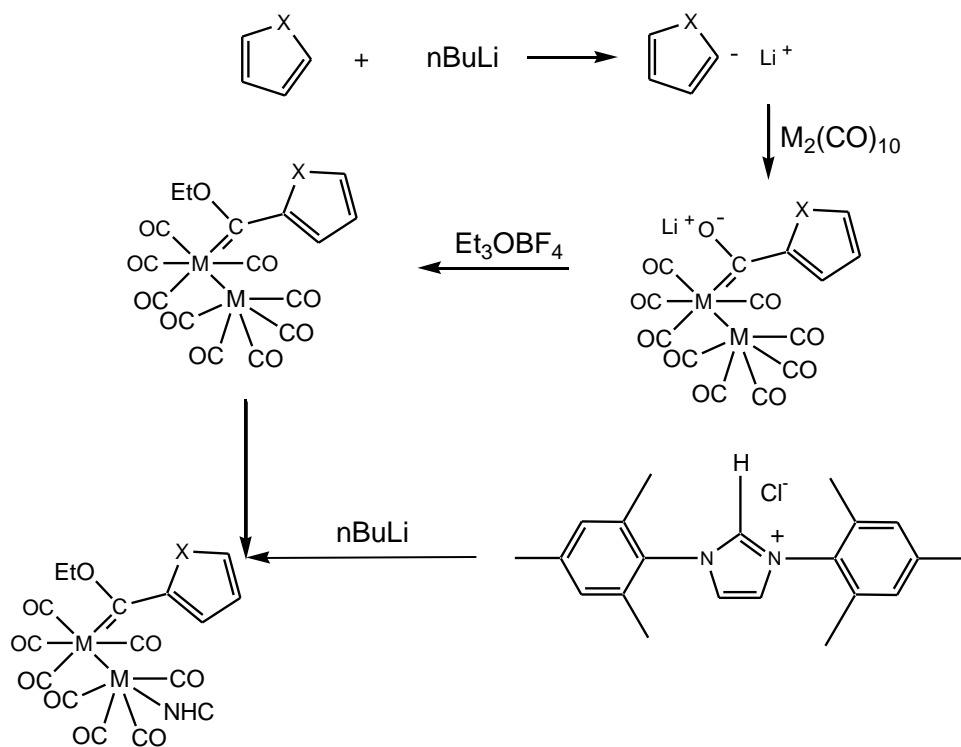


**Figure 4.26:** General reaction pathway to attempt the synthesis of biscarbene complexes ( $X = \text{S}, \text{O}$ ;  $M = \text{Re}$ )

### General Fischer carbene synthesis

The general Fischer carbene synthesis methodology<sup>15</sup> was used to synthesise the target complexes. The heteroarenes used are thiophene (Th, X=S) and furan (Fu, X=O). Metal substrates used were  $[\text{Re}_2(\text{CO})_{10}]$  and  $[\text{Mn}_2(\text{CO})_{10}]$ .

Heteroarene (2mmol) was dissolved in 20ml thf and cooled down to  $-20^\circ\text{C}$ . nBuLi (2mmol, 1.3ml) was added and the reaction left to stir for 1hr. The mixture was further cooled down to  $-70^\circ\text{C}$  and the metal decacarbonyl (2mmol) added. After 1hr the reaction was allowed to warm to RT and stirred for another 30min. The thf solvent was removed by reduced pressure and replaced with dcm. This solution is cooled to  $-30^\circ\text{C}$  and  $\text{Et}_3\text{OBF}_4$  (2mmol) added. The mixture was stirred for 1hr and allowed to warm to RT after which it was stirred for another 30 min. A short silica gel filter was used to remove the lithium salts and further purification was done with column chromatography. Approximately 50% yield was obtained for both the thienyl and furyl Fischer carbene complexes.

### General NHC synthesis

In a separate flask IMesHCl (1mmol, 0.34g) was dissolved in thf and cooled to  $-78^\circ\text{C}$ . nBuLi (1mmol, 0.7ml) was added and stirred for 20min after which the Fischer carbene (1mmol) was added. The substrates (Fischer carbenes) used for NHC synthesis were  $eq\text{-}[\text{Re}_2(\text{CO})_9\text{C}(\text{OEt})\text{Th}]$  and  $eq\text{-}[\text{Re}_2(\text{CO})_9\text{C}(\text{OEt})\text{Fu}]$  respectively. The solution was stirred at  $-78^\circ\text{C}$  for 1hr, 30min at  $-30^\circ\text{C}$  and then allowed to warm to RT. The solvents were removed and purification was done with cold column chromatography on florasil. The unreacted starting material was eluted with dcm and the polar fraction collected with thf.

After NHC synthesis spectroscopic analyses were performed and are presented for each complex separately. The solvents used to perform NMR analysis are indicated and thf was used as solvent to record an IR spectrum.

---

(15) Bezuidenhout, D. I.; van der Watt, E.; Liles, D. C.; Landman, M.; Lotz, S. *Organometallics*. **2008**, *27*, 2447.



## Results

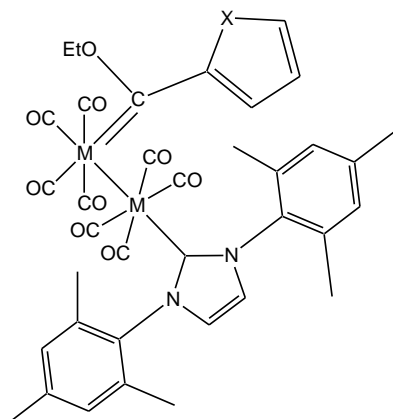
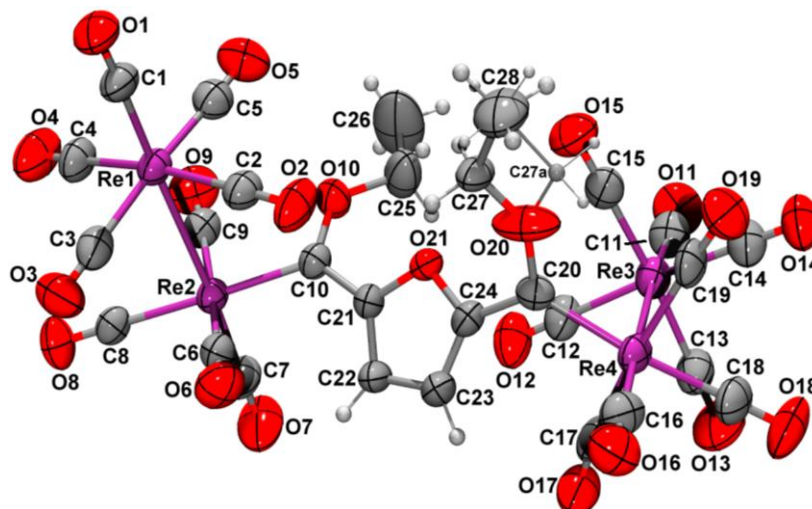


Figure 4.27: Structural presentation of the target compounds (M=Re; X=O,S). Presented configurations are not definite

Synthesis of these complexes proved to be more challenging than expected. No target complexes could be isolated. However, synthesis towards the  $[\text{Re}_2(\text{CO})_8\text{IMesC}(\text{OEt})\text{Fu}]$  target complex lead to the isolation of a novel Fischer biscarbene complex, **12**, and yet another side product, **13**.

During purification of the Fischer carbene not only the product  $[\text{Re}_2(\text{CO})_9\text{C}(\text{OEt})(\text{Fu})]$  but also a novel biscarbene complex  $[\text{Re}_2(\text{CO})_9\text{C}(\text{OEt})\text{C}_4\text{H}_2\text{O}(\text{OEt})\text{Re}_2(\text{CO})_9]$  was isolated. This red-purple biscarbene was crystallised by dissolving the fraction in dcm and layering it with hexane in a 1:1 ratio (Figure 4.29). Spectroscopic data obtained for complex **12** will be discussed before continuing to the results obtained for complex **13**.



**Figure 4.28:** ORTEP + POV-Ray drawing of the molecular structure of complex **12**

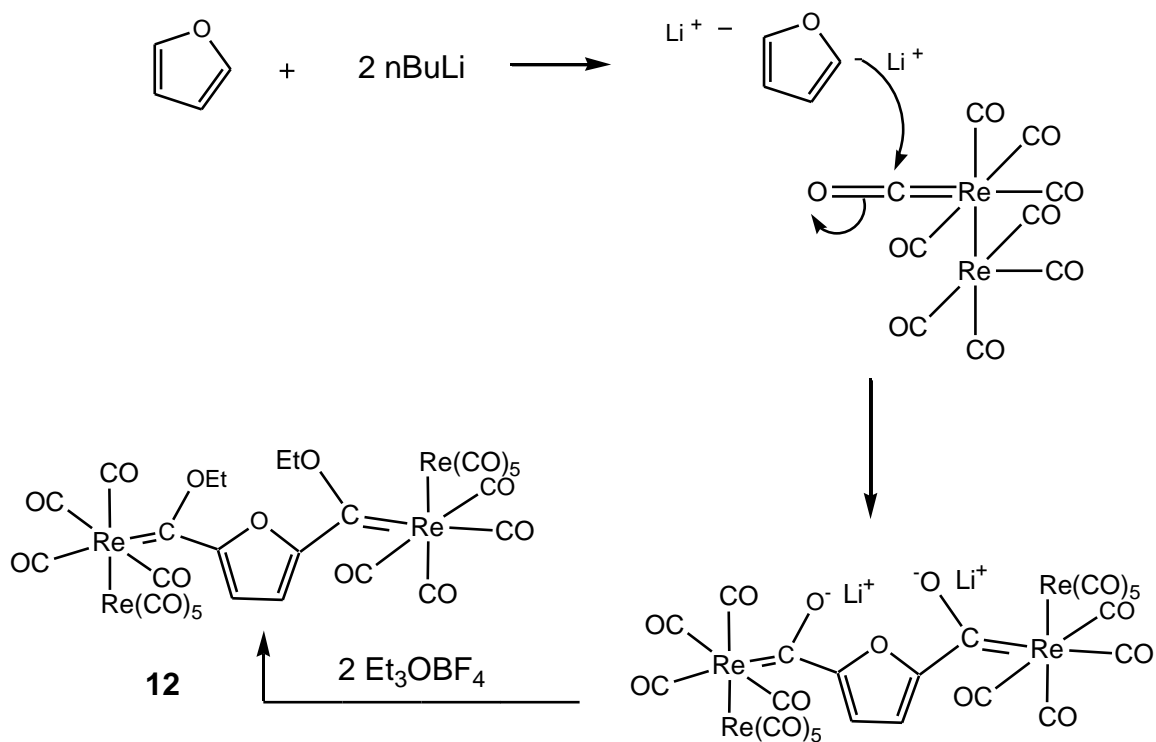
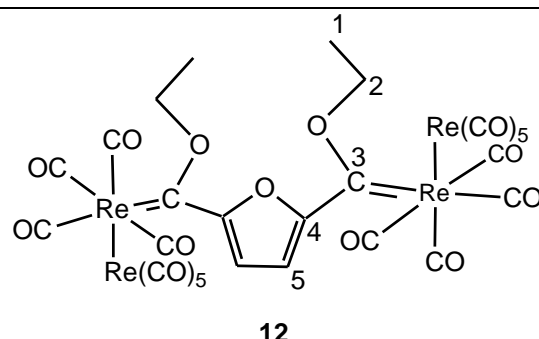


**Figure 4.29:** Proposed reaction pathway of the novel biscarbene complex **12**

**Table 4.9:** NMR data of complex **12** recorded in CDCl<sub>3</sub>



Atom number	<sup>1</sup> H NMR (ppm)
1	1.59 (t, J = 7.5 Hz, 6H)
2	4.48 (q, J = 7.5 Hz, 4H)
5	7.44 (s, 2H)
	<sup>13</sup> C NMR (ppm)
1	14.6
2	78.2
5	117.3
4	166.8
3	286.1
M-CO	193.0

The proposed reaction pathway is illustrated in Figure 4.29. The formation of this bis-carbene complex is ascribed to the dilithiation of the furan precursor, so that the 2,2'-furyl acts as a bridging ligand between the two [Re<sub>2</sub>(CO)<sub>9</sub>] fragments. The spectrum obtained from IR analysis is displayed in Figure 4.30.

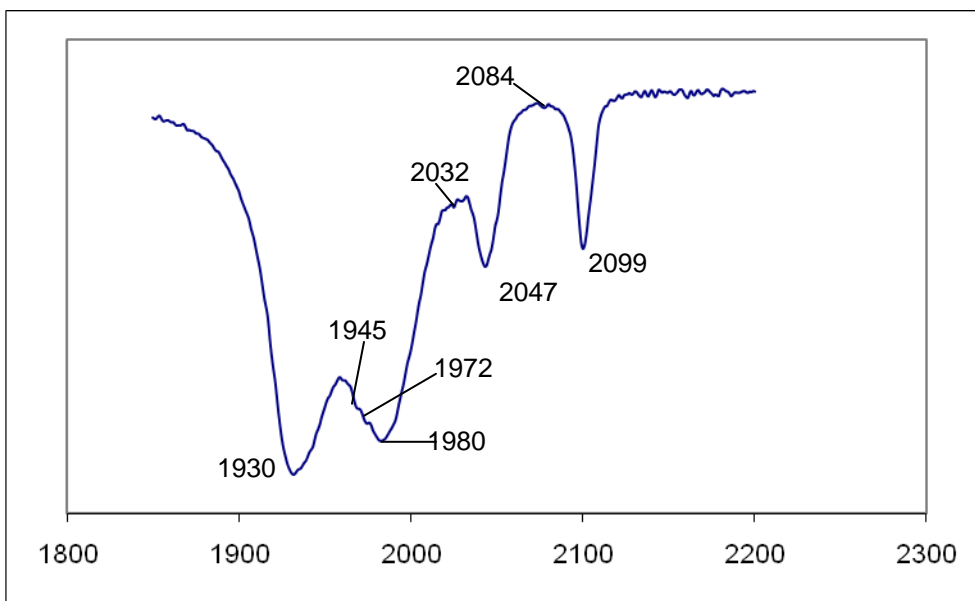


**Figure 4.30:** IR spectrum of complex **12**

IR:  $\nu_{\text{CO}}$  ( $\text{cm}^{-1}$ ) 2099, 2084, 2047, 2032, 1980, 1978, 1972, 1945, 1930

The vibrational stretching pattern as well as the range of values found for complex **12** compares well with the literature data obtained for its thiophene analogue<sup>16</sup>.

#### *Fischer-NHC biscarbene complex*

Following the purification of the Fischer carbene complex and isolation of complex **12**, NHC synthesis was continued as described above. From the thf fraction spectroscopic data was obtained and the complex **13** illustrated in Figure 4.31 crystallised from the fraction at cold temperature ( $\sim 5^{\circ}\text{C}$ ).

(16) PhD thesis filed under the supervision of S. Lotz: Olivier, A. J. : PhD thesis, **2010**.

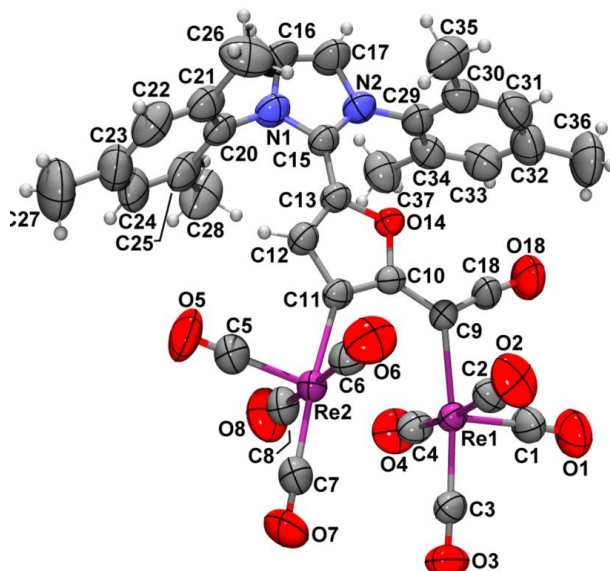


Figure 4.31: ORTEP + POV-Ray drawing of the molecular structure of complex **13**

Table 4.10: NMR data of complex **13** recorded in C<sub>6</sub>D<sub>6</sub>

Atom number	<sup>1</sup> H NMR (ppm)
H <sub>a</sub>	-15.48 (s, 1H)
7, 9	2.06, 2.07 (br, 12H)
8	2.19 (br, 6H)
13	n. o.
3, 5	6.70 (s, 4H)
10	7.63 (s, 2H)



Atom number	<sup>13</sup> C NMR (ppm)
7, 9	16.9
8	20.6
3, 5	125.5
2, 6	129.3
10	130.4
4	136.7
1	141.9
13	147.0
15	148.8
12	159.2
11	164.4
14	n. o.
17	249.8
16	275.4
M-CO	n. o.

IR:  $\nu_{\text{CO}}$  ( $\text{cm}^{-1}$ ) 2086, 1970, 1948, 1937, 1932, 1903, 1883, 1876

### Discussion on the formation of complex 13

Formation of this complex is quite unique and involves four reaction sites. In the diagram (Figure 4.32) these locations are indicated and will be discussed separately. The order of occurrence is not clear at this stage and ligands of the different intermediates and products involved are omitted when not actively part of the pathway demonstrated.

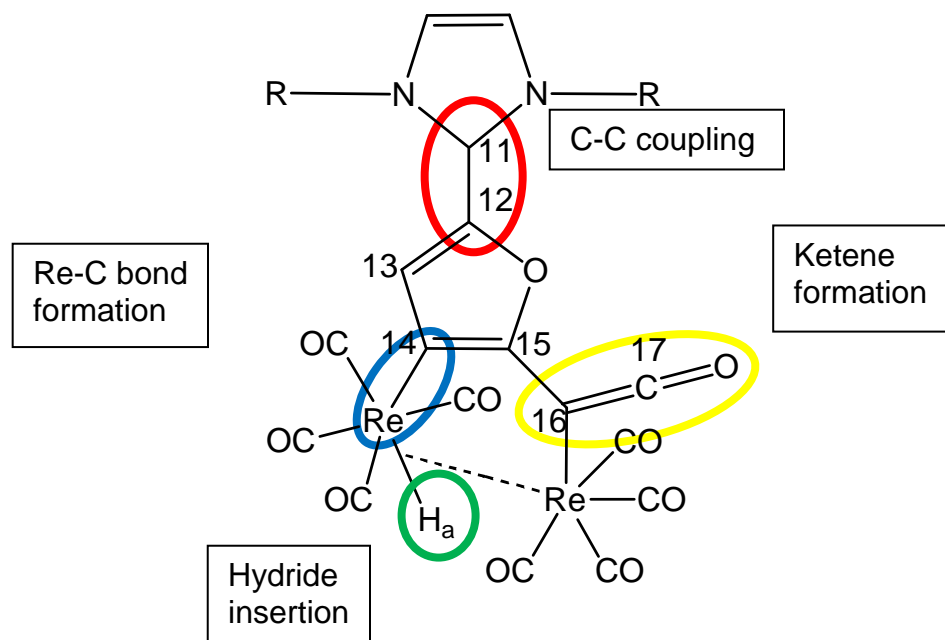


**Figure 4.32:** The proposed reaction sites of complex 13

Rhenium complexes can mimic transition metal Lewis acids to catalyze Friedel-Crafts C-C bond formation<sup>17</sup>. The catalytic activity of the rhenium complexes is initiated by decarbonylation under heating<sup>18</sup> to form the active species [ReBr(CO)<sub>4</sub>]. The mechanism of how the coupling occurs in this complex remains unclear.

Figure 4.33 illustrates a reaction pathway of C-C bond formation in this complex.

(17) (a) Beck, W.; Sunkel, K. *Che. Rev.* **1988**, 88, 1405; (b) Murahashi, S. I.; Takaya, H. *Acc. Chem. Res.* **2000**, 33, 225.

(18) (a) Jolly, P. W.; Stone, F. G. A. *J. Chem. Soc.* **1965**, 5259; (b) Zingales, F.; Sartorelli, U.; Canziani, F.; Raveglia, M. *Inorg. Chem.* **1967**, 6, 154.

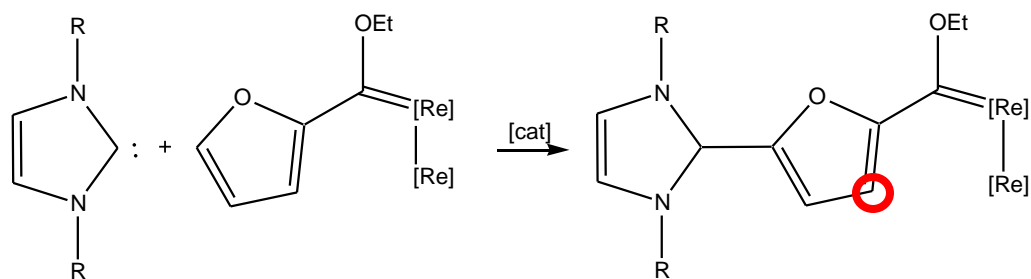


**Figure 4.33:** C-C bond formation in complex **13**

In the complex above the most activated position on the furan ring is indicated. This is attributed to the electron withdrawing effect of the carbene ligand on the ring<sup>19</sup>. Subsequent C-H activation leads to hydride migration and Re-Re bond breaking (Figure 4.34).

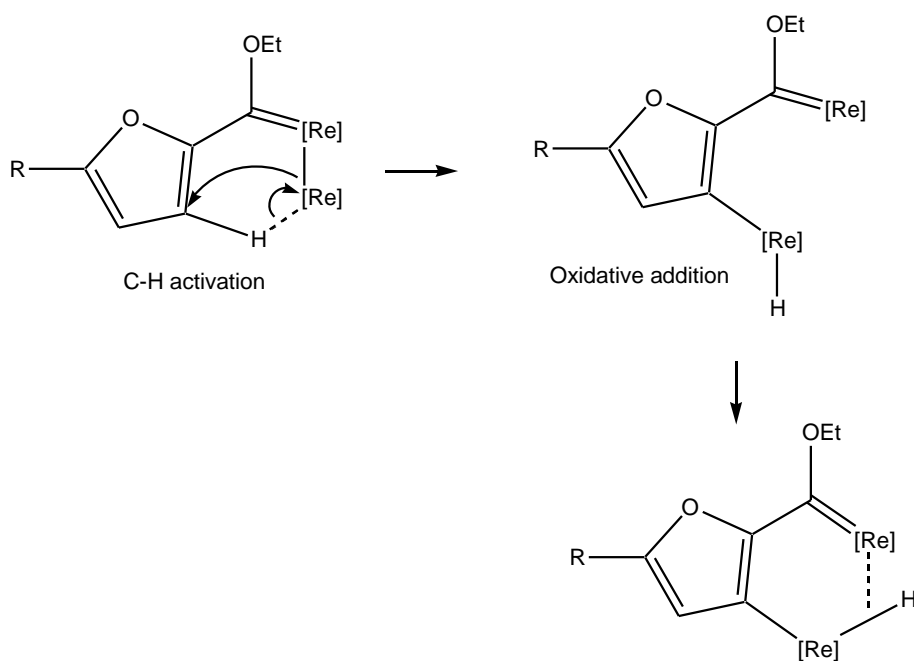


**Figure 4.34:** Hydride insertion and Re-Re bond dissociation

(19) Pretch, E.; Seibl, J.; Clerc, T.; Simon, W. *Tables of Spectral Data for Structure Determination of Organic Compounds*, 2<sup>nd</sup> Ed. Springer-Verlag, Berlin/Heidelberg **1989**.



The resulting complex now contains both a Re-C and Re-H bond. The Re atom from the Fischer carbene moiety is left with a vacant coordination site and is able to bridge to the newly formed hydride.

Ketenyl complexes of tungsten were previously reported by Kreissl<sup>20</sup> and in 2006 these types of complexes were also found for rhenium(VII)<sup>21</sup>. In Figure 4.35 it is shown how the insertion of a bridging CO leads to the ketene formation observed for complex **13**.

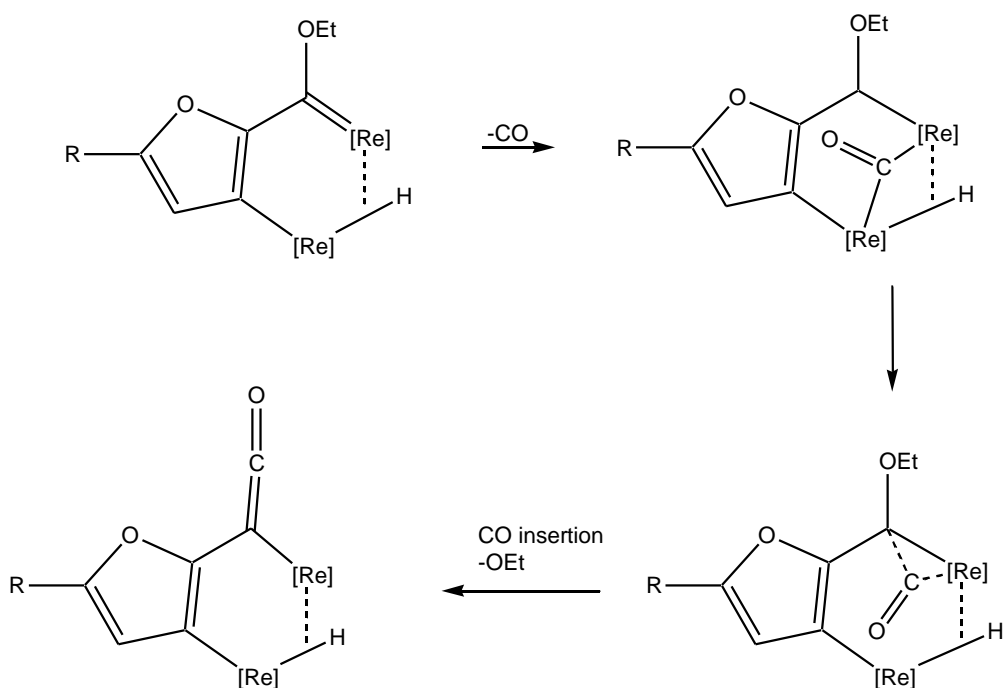


**Figure 4.35:** Ketene formation in complex **13**

(20) (a) Kreissl, F. R.; Frank, A.; Schubert, U.; Lindner, T. L.; Huttner, G. *Angew. Chem., Int. Ed. Engl.* **1976**, *15*, 632; (b) Kreissl, F. R.; Eberl, K.; Uedelhoven, W. *Chem. Ber.* **1977**, *110*, 3782.

(21) Li, X.; Schopf, M.; Stephan, J.; Kipke, J.; Harms, K.; Sundermeyer, J. *Organometallics* **2006**, *25*, 528.

## 4.5 Conclusion

Although a lot of research has been done on NHCs, to our knowledge, no dimetal NHC complexes (M=Re(I), Mn(I)) exhibiting a M-M bond have been reported. However, a cobalt carbonyl IMes dimer has been reported by van Rensburg *et al.*<sup>5</sup>, (Figure 4.3).

Different approaches towards synthesising the target complexes have been attempted since no precedents of its syntheses are documented. Variety in the use of base, reaction conditions, decarbonylation and substrate have been employed.

Fragmentation of products during formation and analyses occurred and this is reflected in the variety of side products obtained. Also, during rhenium Fischer carbene synthesis a novel biscarbene complex,  $[\text{Re}_2(\text{CO})_9\text{C}(\text{OEt})\text{C}_4\text{H}_2\text{O}(\text{OEt})\text{Re}_2(\text{CO})_9]$  **12**, (Figure 4.28) was isolated.

The synthetic route employing nBuLi as base (3c) was not only the most promising route but also lead to the isolation of one of the target complexes,  $[\text{Mn}_2(\text{CO})_9\text{IMes}]$ , (Figure 4.20).

## Chapter 5: Structural and Theoretical study

### 5.1 Molecular modelling

Molecular modelling is a useful tool in predicting experimental outcomes as well as confirming experimental results. Another objective is to qualitatively understand the structure and reactivities of molecules. Validation of the method used to describe the system of interest is important before theoretical data can be accepted as significant. The method should also reflect a correlation between the chemical behaviour of the molecule and related physical laws.

#### 5.1.1 Theoretical study

Molecular mechanics (MM) is one of the two methods used in molecular modelling and is based on the laws of classical physics<sup>1</sup>. The second method is based on quantum mechanics and is called the electronic structure method. This method can be subdivided into semi-empirical, *ab initio* and density functional theory (DFT)<sup>1</sup>. The latter is the most widely applied and except for the fact that it interacts with an average electron density it is very similar to the *ab initio* Hartree-Fock (HF) method<sup>1</sup>. The electronic energy in the DFT method consists of the kinetic energy of the electrons, the electron-electron repulsion energy, the potential energy of the nuclear electron interaction and an exchange correlation term that describes the remaining electron-electron interactions<sup>1</sup>.

The B3LYP functional is used in this study and it consists of an exchange functional, Becke (B), and a correlation functional, Lee-Yang-Parr (LYP)<sup>2</sup>. Although this is not the best orbital description available it is sufficient for the requirements of this study and allows for relatively short calculation times.

---

(1) Foresman, J. B.; Frisch, A. E. *Exploring Chemistry with Electronic structure methods*, 2<sup>nd</sup> Ed., Gaussian Inc., Pittsburgh, 1996.

(2) Becke, A. D. *Phys. Rev.* **1988**, A38, 3098.

### 5.1.2 Transition metal complexes

Recently a great amount of progress has been made regarding quantum chemical methods in the field of transition metal chemistry and much has been learned about the nature of the chemical bond in TM carbene complexes. A review article by Frenking and Frölich has given a comprehensive overview of and insight in the bonding in TM compounds<sup>3</sup>. Advances in modern methods allow for complex organometallic systems to be studied and include methods like atoms in molecules (AIM)<sup>4</sup>, charge decomposition analysis (CDA)<sup>5</sup>, energy decomposition analysis (EDA)<sup>6</sup> and natural bond orbital (NBO)<sup>7</sup> analysis.

### 5.1.3 Fischer Carbenes

DFT calculations have been used to study the reactivity and properties of Fischer carbenes<sup>8</sup> and this includes the theoretical study of the metal-carbon bond. For instance after CDA and EDA analyses of 16 and 18 valence electron (VE) complexes of Ru and Fe, it was found that the 16 VE complexes were more stabilised by the  $\sigma$  bond between the metal and carbon than compared to the 18 VE complexes, where a stronger  $\pi$ -contribution to the metal was found<sup>8c</sup>. Frenking *et al.*<sup>8</sup> also studied thermal

---

(3) Frenking, G.; Frölich, N. *Chem. Rev.* **2000**, *100*, 717.

(4) Bader, R. F. W. *Atoms in Molecules: A Quantum Theory*, Oxford University Press, **1990**.

(5) (a) Dapprich, S., Frenking, G. CDA 2.1, Marburg, **1994**; (b) Dapprich, S., Frenking, G. *J. Phys. Chem.* **1995**, *99*, 9352.

(6) (a) Ziegler, T., Rauk, A. *Inorg. Chem.* **1979**, *16*, 1755; (b) Bickelhaupt, F. M., Nibbering, N. M. M., van Wezenbeek, E. M., Baerend, E. J. *J. Phys. Chem.* **1992**, *96*, 4864; (c) Ziegler, T., Rauk, A. *Inorg. Chem.* **1979**, *18*, 1558; (d) Ziegler, T., Rauk, A. *Theor. Chim. Acta* **1977**, *46*, 1; (e) Kitaura, K., Morokuma, K. *Int. J. Quantum Chem.* **1976**, *10*, 325.

(7)(a) Foster, J.P.; Weinhold, F. *J. Am. Chem. Soc.* **1980**, *102*, 7211, (b) Reed, A.E.; Weinhold, F.J. *J. Chem. Phys.* **1985**, *83*, 1736, (c) Reed, A.E.; Weinstock, R.B.; Weinhold, F. *J. Chem. Phys.* **1985**, *83*, 735, (d) Reed, A.E.; Curtiss, L.A.; Weinhold, F. *Chem. Rev.* **1988**, *88*, 899.

(8)(a) Cases, M.; Frenking, G.; Duran, M.; Sol, M.; *Organometallics* **2002**, *21*, 4182, (b) Krapp, A.; Frenking, G.; *J. Am. Chem. Soc.* **2008**, *130*, 16646, (c) Krapp, A.; Pandey, K.K.; Frenking, G. *J. Am. Chem. Soc.* **2007**, *129*, 7596, (d) Frenking, G.; Sola, M.; Vyboishchikov, S.F. *J. Organomet. Chem.* **2005**, *690*, 6178, (e) Sierra, M.A.; Fernández, I.; Cossío, F.P. *Chem. Commun.* **2008**, 4761, (f) Lage, M.L.; Fernández, I.; Mancheño, M.J.; Sierra, M.A. *Inorg. Chem.* **2008**, *47*, 5253, (g) Andrada, D.M.; Zoloff Michoff, M.E.; Fernández, I. Granados, A.M.; Sierra, M.A. *Organometallics* **2007**, *26*, 5854.

and photochemical transformations (including reactivity and reaction mechanisms) of Fischer carbenes by employing molecular modelling.

#### 5.1.4 *N*-heterocyclic carbenes

Recently, the focus of theoretical studies of NHCs has been the nature of the metal-carbon bonding and in particular the contribution of  $\pi$ -bonding in typical NHC-complexes.

In a detailed study of the interaction of *N*-heterocyclic carbene ligands with  $[\text{Ni}(\text{CO})_4]$  to form saturated tricarbonyl complexes, it was found that, in comparison to their phosphine analogues, the NHC ligands are better  $\sigma$ -donors<sup>9</sup>.

The order of bond strength of a few NHC ligands complexed with Group IV, VI, VIII and X transition metals (TMs) have been studied by Frenking *et al.*<sup>10</sup>. DFT calculations were used to study the metal ligand bonding in complexes containing imidazole (IMID), imidazol-2-ylidene (nNHC) and imidazol-4-ylidene (aNHC) as ligands. It was found that the carbon  $\sigma$ -lone pair of the complex containing the aNHC has the highest energy level and decreases with complexes containing nNHC and IMID (Figure 5.1). Bond dissociation energy (BDE) analyses confirmed the trend observed for these complexes.

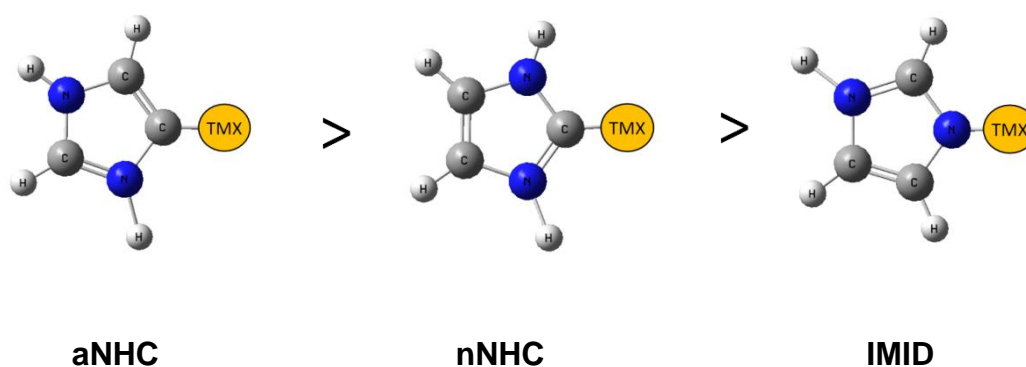


**Figure 5.1:** Trend in BDE for TM-CI NHC complexes

(9) Dorta, R., Stevens, E. D., Scott, N. M., Costabile, C., Cavallo, L., Hoff, C. D., Nolan, S. P. *J. Am. Chem. Soc.* **2005**, *127*, 2485.

(10) Tonner, R., Heydenrych, G., Frenking, G. *Chem. Asian J.* **2007**, *2*, 1555.

Experimental syntheses were aimed toward the bond formation between the transition metal and the carbene carbon atom of the NHC. Considering the results illustrated in Figure 5.1, two possible options were available and the type of carbene which indicates stronger attachment to the transition metal were preferred.

Boehme and Frenking<sup>11</sup> published a theoretical study, including CDA and NBO analyses, in which Group XI TM complexes of the type CI-TM-E, where E = nNHC, Si or Ge were investigated. Also, the strength of the metal-E bond decreases from nNHC to Ge as the dissociation energy of the bond is decreasing. For these complexes large BDE values of the carbene bond were observed and  $\pi$ -back donation could not be correlated with bond strengths. It is evident from the bond strength of the NHC to the transition metal compared to other isolobal atom bond strengths (Ge, Si), that the NHC still results in the stronger bond.

## 5.2 Computational details and validation of the theoretical method

The theoretical study (using Hartree Fock methods) described in this chapter was executed by using the GAUSSIAN 03 suite of programmes<sup>12</sup>. Together with restricted

---

(11) Boehme, C, Frenking, G. *Organometallics*. **1998**, *17*, 5801.

(12) Frisch, M.J.; Trucks, G.W.; Schlegel, H.B.; Scuseria, G.E.; Robb, M.A.; Cheeseman, J.R.; Montgomery Jr, J.A.; Vreven, T.; Kudin, K.N.; Burant, J.C.; Millam, J.M.; Iyengar, S.S.; Tomasi, J.; Barone, V.; Mennucci, B.; Cossi, M.; Scalmani, G.; Rega, N.; Petersson, G.A.; Nakatsuji, H.; Hada, M.; Ehara, M.; Toyota, K.; Fukuda, R.; Hasegawa, J.; Ishida, M.; Nakajima, T.; Honda, Y.; Kitao, O.; Nakai, H.; Klene, M.; Li, X.; Knox, J.E.; Hratchian, H.P.; Cross, J.B.; Bakken, V.; Adamo, C.; Jaramillo, J.; Gomperts, R.; Stratmann, R.E.; Yazyev, O.; Austin, A.J.; Cammi, R.; Pomelli, C.; Ochterski, J.W.; Ayala, P.Y.; Morokuma, K.; Voth, G.A.; Salvador, P.; Dannenberg, J.J.; Zakrzewski, V.; Dapprich, S.; Daniels, A.D.; Strain, M.C.; Farkas, O.; Malick, D.K.; Rabuck, A.D.; Raghavachari, K.; Foresman, J.B.; Ortiz, J.V.; Cui, Q.; Baboul, A.G.; Clifford, S.; Cioslowski, J.; Stefanov, B.B.; Liu, G.; Liashenko, A.; Piskorz, P.; Komaromi, I.; Martin, R.L.; Fox, D.J.; Keith, T.; Al-Laham, M.A.; Peng, C.Y.; Nanayakkara, A.; Challacombe, M.; Gill, P.M.W.; Johnson, B.; Chen, W.; Wong, M.W.; Gonzalez, C.; Pople, J.A. *Gaussian 03*, revision C.02; Gaussian, Inc.: Wallingford, CT, **2004**.

wavefunctions (RB3LYP)<sup>13</sup>, the basis set LANL2DZ was used. The former is chosen because of increased accuracy due to the inclusion of electron-electron interaction effects and the latter for its suitability in dealing with heavier transition metal atoms like Re in complexes. Symmetry constraints were not applied and geometric optimisations were employed with default convergence criteria. Modelling was done in the singlet spin state ( $S=1/2$ ) and minimum energy conformations were definite when no imaginary frequencies could be observed for the vibrational frequency analysis<sup>14</sup>.

Validation of this method is reflected in the RMSD (root-mean-square deviation) values obtained by comparing the optimised molecular structure with the crystal structure experimentally synthesised. These values were calculated by employing the 'molecular overlay' utility in Mercury Version 2.3<sup>15</sup>.

Excellent correlation between experimental and theoretically calculated structures was obtained (Figure 5.2) and this is also revealed by the RMSD values which range between 0.06 and 0.24Å.

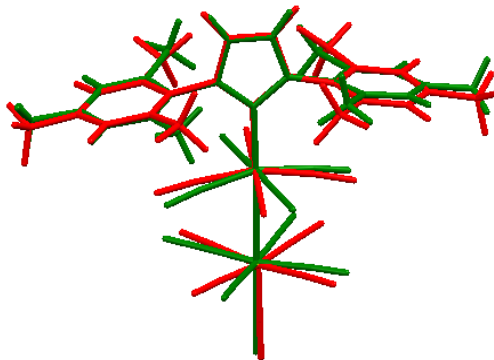


**Figure 5.2:** Representative overlay of the theoretically calculated structure and the crystal structure of complex **9**,  $[\text{Mn}_2(\text{CO})_9\text{IMes}]$

---

(13)(a) Becke, A.D. *J. Chem. Phys.* **1993**, *98*, 5648, (b) Lee, C.; Yang, W.; Parr, R.G. *Phys. Rev. B* **1998**, *37*, 785, (c) Vosko, S.H.; Wilk, L.; Nusair, M. *Can. J. Phys.* **1980**, *58*, 1200.

(14)McIver, J.W.; Komornicki, A.K. *J. Am. Chem. Soc.* **1972**, *94*, 2625.

(15) *Mercury*, Version 2.3 (build RC4), **2009**.

## 5.3 Structural analysis

### 5.3.1 Carbene position

#### Type [MBr(CO)<sub>4</sub>L]

It is well known that a ligand with strong  $\pi$ -acceptor ability would prefer to be situated across one with weak  $\pi$ -acceptor ability in a complex. This prevents the two ligands from competing for electron density from the metal, as illustrated in Figure 5.3.

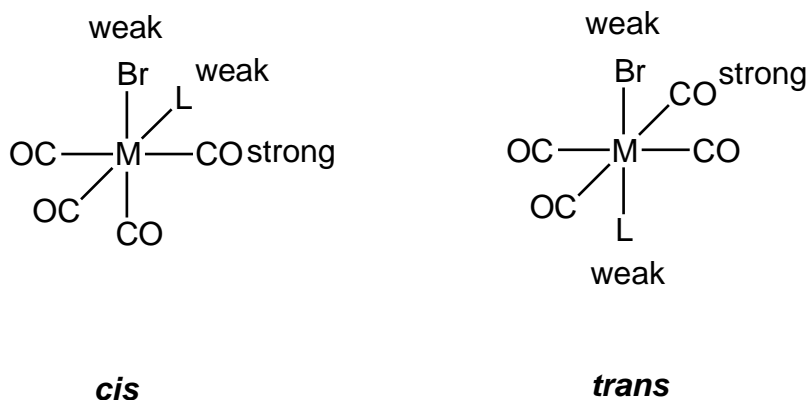
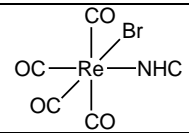
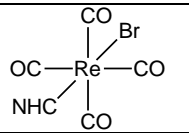


Figure 5.3: *cis* vs *trans* in [MBr(CO)<sub>4</sub>L] type complexes

In the *trans*-complex strong  $\pi$ -acceptor ligands (e.g. CO's) are situated across strong ones and weak  $\pi$ -acceptor ligands (e.g. Br and NHC) across weak ones. This is not favourable since four of the ligands in this complex compete for electron density from the metal. The *cis*-complex displays four ligands in a favourable position where a strong  $\pi$ -acceptor ligand is situated across from a weak  $\pi$ -acceptor and only two ligands are competing for electron density from the metal. The fact that the *cis*-complex is more favoured than the *trans* complex is also reflected by looking at the energy values associated with an example of this type of complex (Table 5.1).



**Table 5.1:** Energy values by Hartree-Fock method

Structure		
<b>Complex</b>	<b><i>cis</i> [ReBr(CO)<sub>4</sub>NHC]</b>	<b><i>trans</i> [ReBr(CO)<sub>4</sub>NHC]</b>
E <sub>SCF</sub> (Ha)	-1469.75	-1469.73
E <sub>SCF</sub> (kJ/mol)	-3858101.60	-3858054.40
ΔE = E <sub>SCF</sub> <i>trans</i> - E <sub>SCF</sub> <i>cis</i>	47.25 kJ/mol	

### Type [M<sub>2</sub>(CO)<sub>9</sub>L]

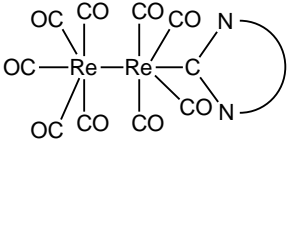
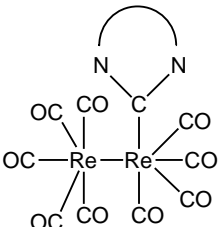
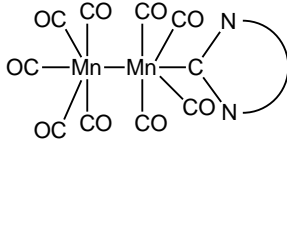
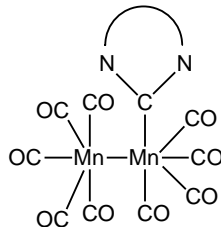
For dimetal carbonyl NHC complexes, the electronic favoured site of coordination of a carbene ligand is the *equatorial* position (see Chapter 4). Following this argument, it means that the carbene ligand is placed *trans* to a strong π-acceptor (carbonyl ligand) instead of the remaining M(CO)<sub>5</sub>-moiety<sup>16</sup>, which is a weak π-acceptor.

For [Re<sub>2</sub>(CO)<sub>9</sub>L] complexes the preferred position of the carbene substituent is the *equatorial* position due to steric reasons<sup>17</sup>. In [Mn<sub>2</sub>(CO)<sub>9</sub>L] complexes both the *equatorial* (electronic) and *axial* (steric) position of the carbene substituent are possible depending on the steric bulk of the carbene ligand. However, theoretically calculated energy values of examples of these complexes (Re and Mn) show that the *axial* position is the most favourable position of the carbene ligand (Table 5.2) for both the Re and Mn complexes. This theoretical result is confirmed by the crystal structure obtained for complex **9** and indicates that the steric effects in these complexes play a dominant role in determining the complex geometry.

(16) Bezuidenhout, D. I.; Liles, D. C.; van Rooyen, P. H.; Lotz, S. J. *J. Organomet. Chem.* **2007**, 692, 774.

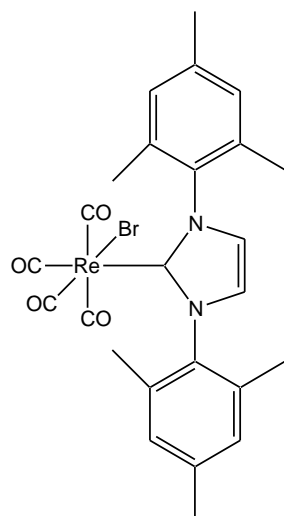
(17) Theses filed under the supervision of S. Lotz (University of Pretoria): (a) Bezuidenhout, D. I. MSc thesis, **2006**; Olivier, A. O. PhD thesis, **2009**.

Table 5.2: Energy values by Hartree-Fock method

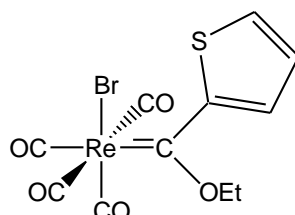
Structure				
<b>Complex</b>	<b>ax Re<sub>2</sub>(CO)<sub>9</sub>NHC</b>	<b>eq Re<sub>2</sub>(CO)<sub>9</sub>NHC</b>	<b>ax Mn<sub>2</sub>(CO)<sub>9</sub>NHC</b>	<b>eq Mn<sub>2</sub>(CO)<sub>9</sub>NHC</b>
E <sub>SCF</sub> (H)	-2102.32	-2102.31	-2151.81	-2151.80
E <sub>SCF</sub> (kJ/mol)	-5518590.78	-5518583.96	-5648515.42	-5648477.88
ΔE = E <sub>SCF</sub> <i>eq</i> - E <sub>SCF</sub> <i>ax</i>	6.82 kJ/mol		37.53 kJ/mol	

Although literature reports indicate a strong preference for [Re<sub>2</sub>(CO)<sub>9</sub>L] complexes having *equatorial* substitution, modelling shows that the *axial* position is energetically favoured. This might indicate that the bulk of the carbene ligand in this case also overrides the electronic effect and is reflected in the small energetic advantage of 6.8kJ/mol. The possibility of *axial* substitution could thus not be excluded. The large energetic advantage of 37.5kJ/mol signifies the preference for *axial* geometry for [Mn<sub>2</sub>(CO)<sub>9</sub>L] complexes.

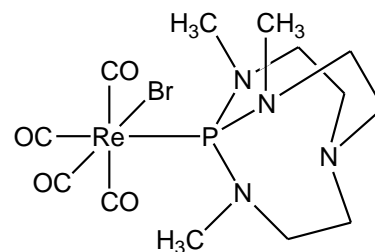
### 5.3.2 Complexes under discussion



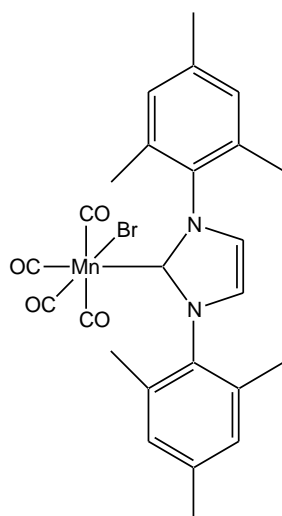
**I (2)**



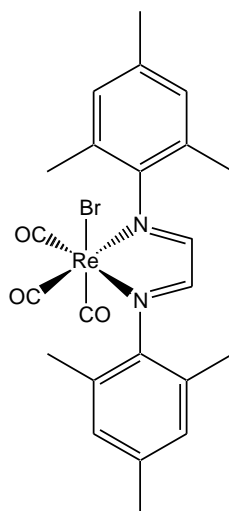
**II**



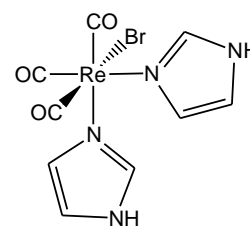
**III<sup>18</sup>**



**\*IV**



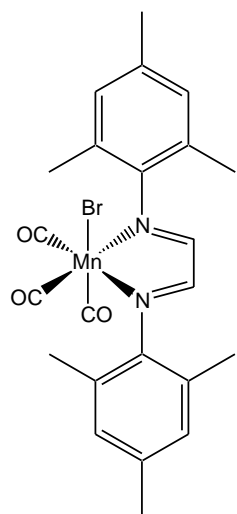
**V (1)**



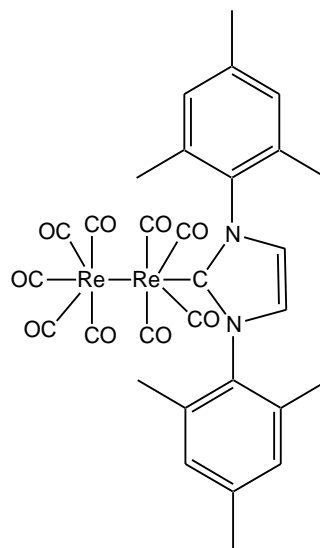
**\*VI<sup>19</sup>**

(18) Tang, J. S., Laramay, M. A. H., Young, V., Ringrose, S., Jacobson, R. A., Verkade, J. G. *J. Am. Chem. Soc.* **1992**, *114*, 3129.

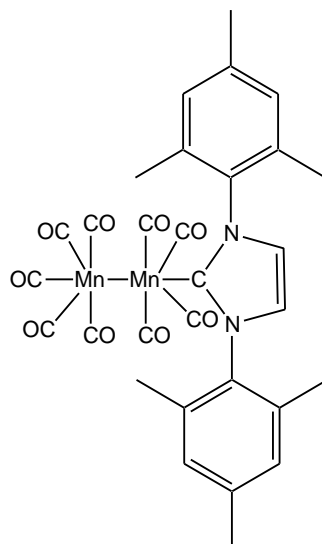
(19) Alberto, R., Schibli, R., Waibel, R., Abram, U., Schubiger, A. P., *Coord. Chem. Rev.* **1999**, *190*, 901.



**VII**



**VIII (5)**

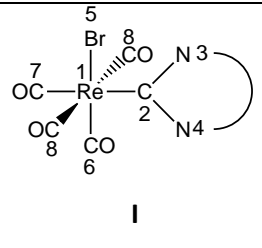
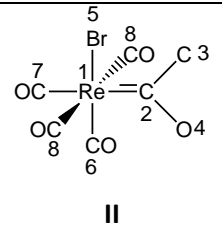
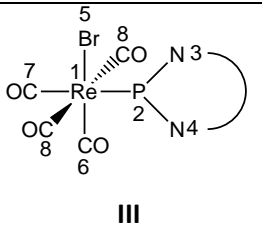
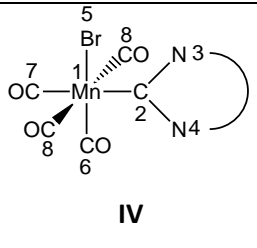


**IX (9)**

\*Experimental data available, not calculated as with other complexes

### 5.3.3 Monometal complexes

Table 5.3

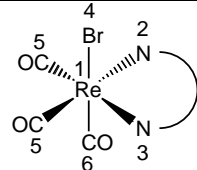
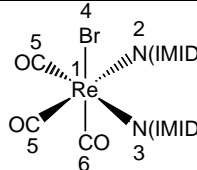
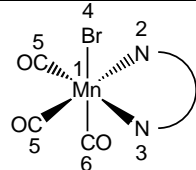
				
	I	II	III	IV
Bond	Bond Lengths (Å)			
1 – 2	2.20	2.15	2.64	2.09
2 – 3	1.39	1.45	1.75	1.39
2 – 4	1.39	1.36	1.76	1.39
1 – 5	2.74	2.72	2.73	2.62
1 – 6	1.90	1.92	1.99	1.78
1 – 7	1.96	1.98	1.95	1.83
1 – 8	1.99	1.99	1.99	1.86

In an article by Frenking *et al.*<sup>20</sup> it was found that the strength of the  $\sigma$ -bond from the carbene carbon atom to the transition metal determines the degree of electron deficiency of the carbene carbon. This in turn determines the degree of  $\pi$ -bonding from the nitrogen atoms for stabilisation of the carbene centre. The bond length of C-N decreases with strong  $\pi$ -interaction and this indicates the strength of the  $C_{\text{carbene}} \rightarrow M$   $\sigma$ -bond. Thus, the stronger the  $\sigma$ -donation, the shorter the N-C bond. This could also be observed with the phosphine containing complex **III**. The average calculated value for the P-N bond of the free ligand is 1.79Å and shortens to 1.76Å after complexation which indicates  $\sigma$ -donation to the metal.

(20) Frenking, G., Solà, M., Vyboishchikov, S. F.; *J. Organomet. Chem.* **2005**, 690, 6178.S

The different bond orders of the two carbene types **I** and **II** is supported by the shorter Re-C bond length in **II**, which indicates a more double bond character compared to a longer Re-C bond length in **I** which indicates less double bond character.

Table 5.4

			
<b>Bond</b>	<b>Bond Lengths (Å)</b>		
1 – 2	2.15	2.18	2.05
1 – 3	2.18	2.17	2.08
1 – 4	2.72	2.58	2.62
1 – 5	1.94	1.91	1.82
1 – 6	1.90	1.89	1.79

\* Experimental data available

By changing the substituent on the nitrogen atoms bound to the metal or even changing the metal from Re to Mn does not have a significant effect on the bond lengths as displayed in the table above. All the nitrogen atoms are trivalent and coordinated to the metal *via* its available lone pair.

No significant difference could be observed in Re-N bond length values between **V** (complex containing bidentate ligand) and **VI** (complex containing two monodentate ligands). However, there is a difference in the Re-Br bond lengths, and this can be attributed to the difference in steric bulk of the N ligands.

### 5.3.4 Dimetal complexes

Table 5.5

Bond	Bond Lengths (Å)	
1 – 2	2.14	2.04
2 – 3	1.39	1.39
2 – 4	1.39	1.39
1 – 5	1.97	1.83
1 – 7	3.16	3.03
7 – 6	1.99	1.84
7 – 8	1.93	1.78

Based on the same principle explained by Frenking, relative  $\sigma$ -donation from the carbene carbon to the metal can be determined by looking at C2-N3/4 bond lengths.

The C-N bond lengths in **VIII** and **IX** are very similar and thus similar backbonding can be expected for these two complexes.

### 5.4 Vibrational analysis

The stretching vibrational frequencies for terminal carbonyl ligands lie between 1850 and 2120 $\text{cm}^{-1}$ <sup>21</sup>. These frequencies are viewed as independent from the other frequencies in the complex. Correlation between the backbonding from the metal to the carbonyl ligand and the length (bond order) of the C-O bond. The stronger the backbonding from the metal to the ligand, the weaker the C-O bond which is then

(21) Braterman, P. S., *Metal Carbonyl Spectra*, Academic Press Inc., London. 1975.

reflected in a lower wavenumber. The number and type of ligands surrounding the metal influences the number and intensities of the stretching frequencies of these complexes.

The focus of this analysis is to compare the effect of the different ligands (NHC, Fischer carbene, phosphine) on the *trans* carbonyl of these complexes.

### 5.4.1 Monometal complexes

The *cis*-[M(CO)<sub>4</sub>L<sub>2</sub>] displays a four band pattern with the following order: A<sub>1</sub>(1)>A<sub>2</sub>(2)>B<sub>1</sub>>B<sub>2</sub><sup>22</sup>. This pattern corresponds to a C<sub>2v</sub> pattern.

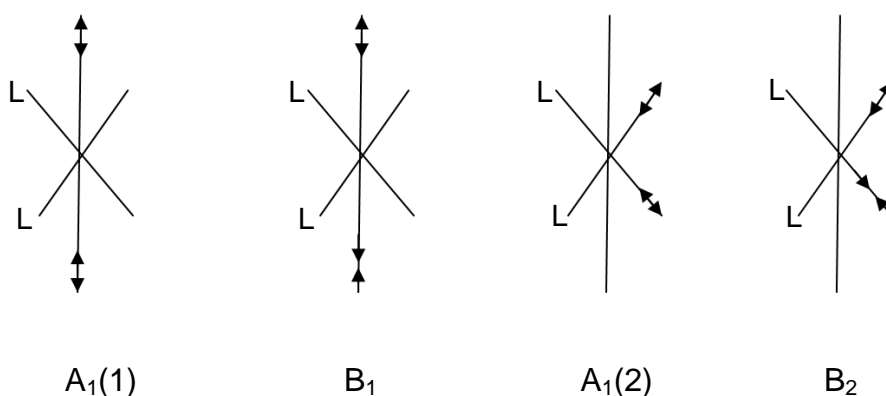


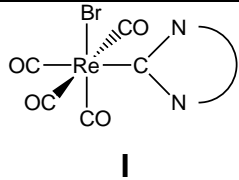
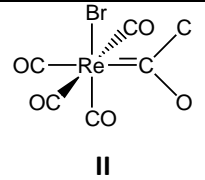
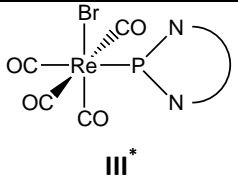
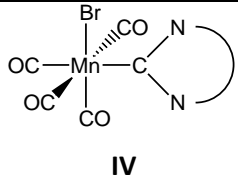
**Figure 5.4:** IR-active normal modes for *cis*-[M(CO)<sub>4</sub>L<sub>2</sub>]

It is important to note that numerical values obtained through experimental results and calculated values cannot be compared due to different mediums in which the data was collected. For the calculated data, the complexes were seen as being in gas phase and experimental data were recorded either in solid state or in solution. Moreover, even when the media are the same, a scale factor is needed to be able to numerically compare these values.

(22) Adams, D. M., *Metal-Ligand and Related Vibrations: A critical Survey of the Infrared and Raman Spectra of Metallic and Organometallic Compounds*, Edward Arnold Publishers Ltd, London. **1998**.



Table 5.6

				
Assignment	Vibrational (CO) frequencies (cm <sup>-1</sup> )			
B <sub>2</sub>	1888	1915	2216	1918
B <sub>1</sub>	1939	1946	2259	1919
A <sub>1</sub> (2)	1952	1970	2322	1966
A <sub>1</sub> (1)	2039	2046	2402	2035

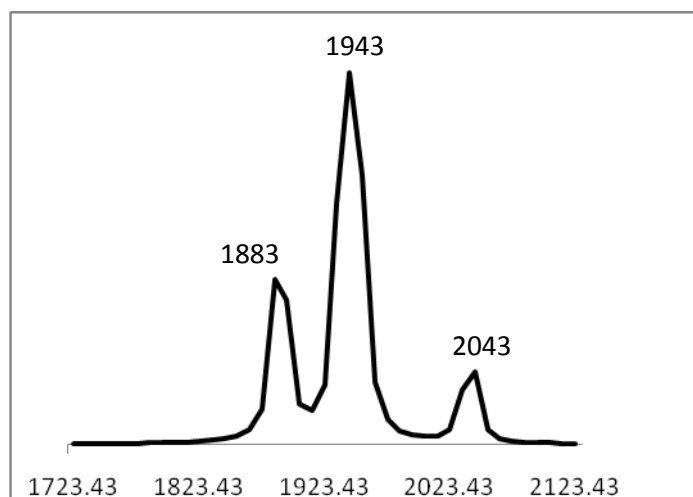


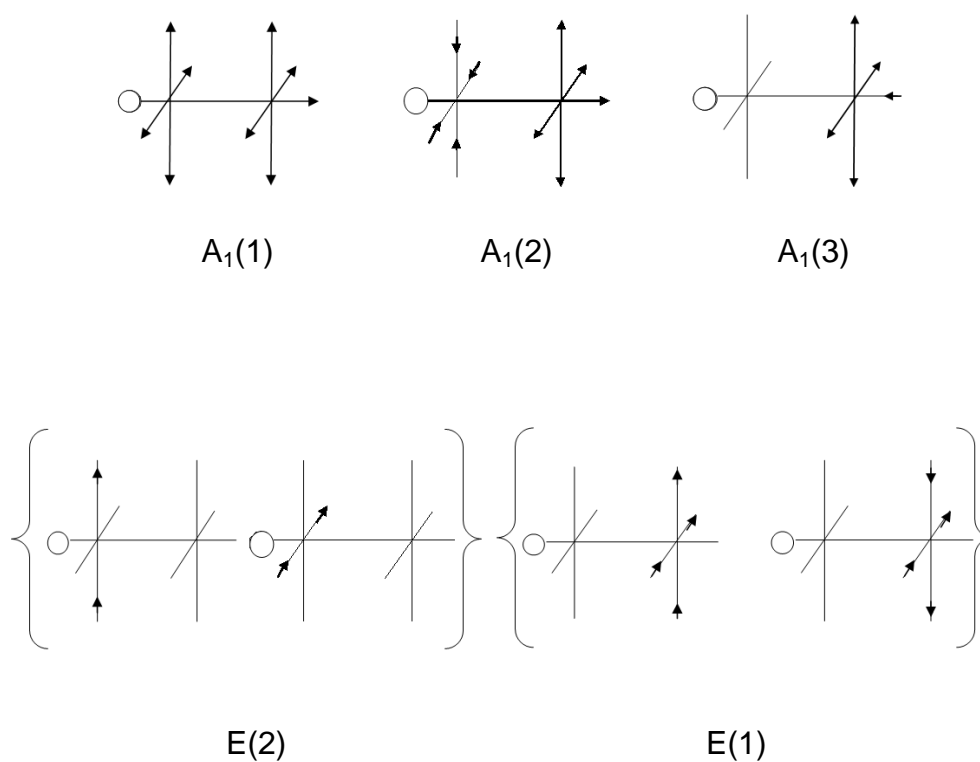
Figure 5.5: Calculated IR spectrum of complex I

The calculated IR spectrum pattern of [ReBr(CO)<sub>4</sub>IMes] (I) is illustrated in Figure 5.5. It can be seen that the A<sub>1</sub>(2) and B<sub>1</sub> vibration overlap to result the very strong band observed. This pattern compares well to the experimental patterns observed for the [MBr(CO)<sub>4</sub>IMes] complexes synthesised in Chapter 3.

### 5.4.2 Dimetal complexes

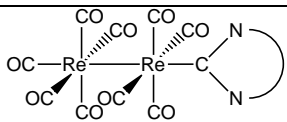
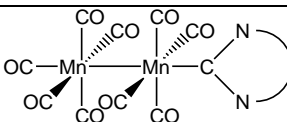
The  $ax-[M_2(CO)_9L]$  displays a five band pattern of which three are  $A'$  bands and the remaining two, E bands. (Figure 5.6). This corresponds to pseudo- $C_{4v}$  symmetry.

In Table 5.7, both  $A_1(1)$  and  $A_1(2)$  contribute to the stretching vibration frequency of the *trans* carbonyl ligand and trend is also seen in the C-O bond strength where  $\pi$  back donation is noticed.



**Figure 5.6:** IR active normal modes for  $ax-[M_2(CO)_9L]$

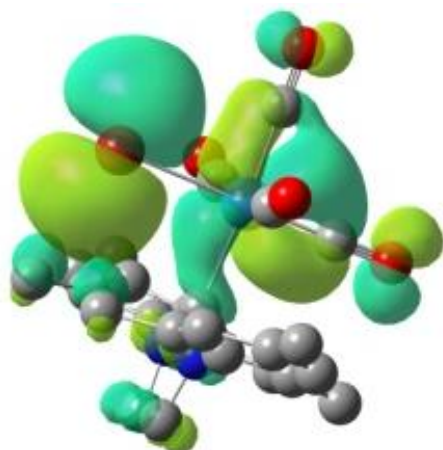
Table 5.7

	 <b>VIII</b>	 <b>IX(9)</b>
<b>Assignment</b>	<b>Vibrational (CO) frequencies (cm<sup>-1</sup>)</b>	
E(2)	1875	1897
A <sub>1</sub> (3)	1927	1925
E(1)	1946	1931
A <sub>1</sub> (2)	1969	1956
A <sub>1</sub> (1)	2052	2043

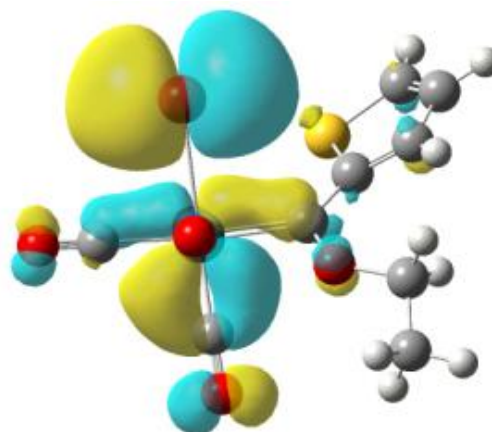
When the patterns experimentally obtained are compared to the calculated patterns more than the expected five bands are often observed. This is ascribed to distortion of the symmetry of these complexes caused by different ligands attached to the metal atoms.

## 5.5 Molecular orbital analysis

HOMO and LUMO calculations are important to consider since these frontier orbitals determine the susceptibility of a compound toward electrophilic or nucleophilic attack<sup>23</sup>.

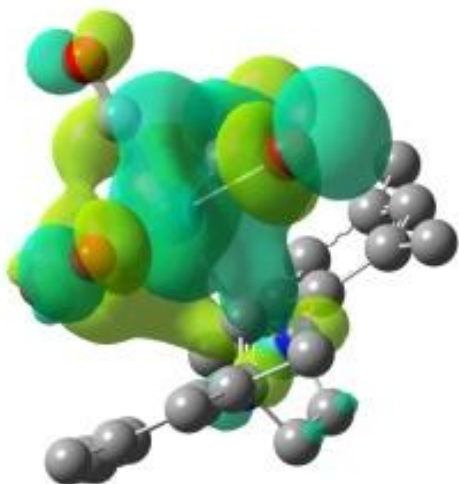


**Complex I:** Energy = -0.22 eV

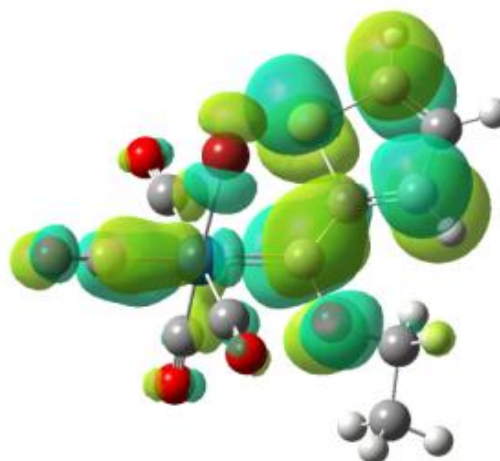


**Complex III:** Energy = -0.22 eV

Figure 5.7: HOMO presentations of I(2) and III with their associated energies



**Complex I:** Energy = -0.07 eV



**Complex III:** Energy = -0.12 eV

Figure 5.8: LUMO presentations of I(2) and III with their associated energies

(23)(a) Fukui, K.; Fujimoto, H. *Bull. Chem. Soc. Jpn.* **1969**, *42*, 3399, (b) Klopman, G.; Hudson, R.F. *Theor. Chim. Acta* **1967**, *8*, 165.

The spatial localisation of the HOMO (Highest Occupied Molecular Orbital) indicates the site where electrophilic attack is most likely to occur. The HOMO's of complex I and III are predominantly situated on the bromo ligand and not so much on the metal as is seen in the LUMOs of these complexes.

The localisation of the LUMO (Lowest Unoccupied Molecular Orbital) indicates the site where nucleophilic attack is most likely to occur. In complex I the LUMO is situated mostly on the metal and the carbene carbon atom. The site for nucleophilic attack in complex III, indicated by the LUMO's, are mainly on the carbene carbon, aromatic ring and the *trans*-carbonyl ligand.

Considering the specific values of the HOMO and LUMO energies it is evident from Table 5.8 that the energy difference between these two molecular orbitals are higher than the energy difference between the LUMO and the next LUMO (+1).

**Table 5.8:** Molecular orbital energy differences (eV)

<b>Complex</b>	<b>LUMO – HOMO</b>	<b>LUMO (+1) - LUMO</b>
<b>I</b>	0.15 eV	0.01 eV
<b>III</b>	0.10 eV	0.05 eV

## 5.6 Conclusion

Energy values of the metal complexes calculated by the Hartree Fock method revealed that the *cis* configuration is preferred over the *trans*-configuration in monometal complexes. Also, the *axial* position for dimetal complexes is the preferred site over the *equatorial* position. Although the observation for monometals were expected, the preferred positions of the carbene ligand across the  $M(CO)_5$ -moiety instead of a carbonyl ligand is quite surprising.

After molecular orbital analysis it was confirmed that the carbene carbon is the site most susceptible to nucleophilic attack.

## Chapter 6: Concluding remarks and Future work

### 6.1 Conclusion

In the preceding chapters it is evident that the syntheses of the target complexes of this study are not unproblematic. Although a variety of approaches have been explored the route which employs nBuLi as base appears to be the most promising in both the mono- and dimetal complexes. The potential of this route is reflected in the isolation of the target complex  $[\text{Mn}_2(\text{CO})_9\text{IMes}]$ .

Numerous challenges remain in the syntheses of these complexes and include the insolubility and air-moisture sensitivity which makes it difficult to perform spectroscopic analysis.

This brief chapter will include suggestions for future work regarding this study.

Much is learned of NHC complexes in this study but more still needs to be discovered of these reactive phosphine analogues.

### 6.2 Future work

#### 6.2.1 Relief of steric demand

Comparing the ligand size with the size of the substrate with which complexation should occur, one realises that steric demand is one of the factors requiring attention. There are two ways to bring about the relief of steric demand: by reducing the size of either the ligand or the substrate.

*Less sterically demanding metal substrate: eg. CpMn(CO)<sub>3</sub>*

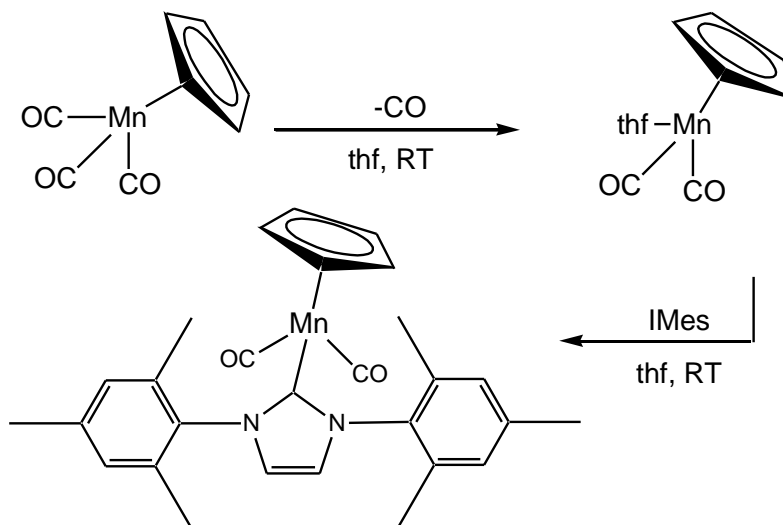


**Figure 6.1:** Synthetic approach in employing a less steric demanding substrate

The Cp-ring replaces three coordination sites of [MnCp(CO)<sub>3</sub>] which leaves more space for the IMes ligand to coordinate to the metal. It shows greater potential to accommodate the steric demand the IMes ligand comprise.

*Less sterically demanding ligand: dimethylimidazole*

In contrast to a large ligand, a smaller ligand would naturally be better accommodated by the metal than a sterically demanding ligand, especially if the metal substrate is itself very bulky. An example of such a ligand is N,N'-dimethylimidazol-2-ylidene.



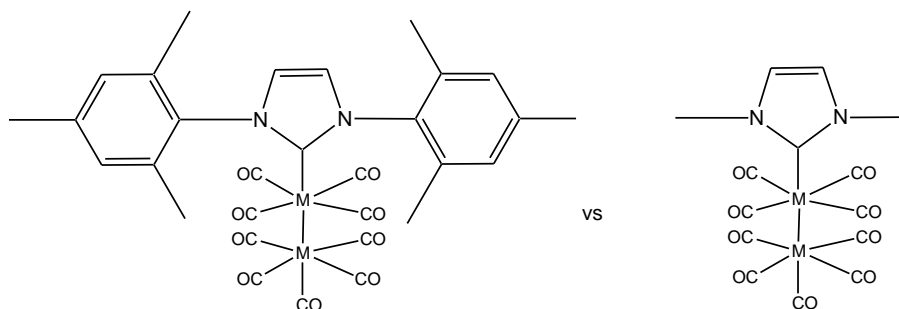


**Figure 6.2:** Illustration of the contrast between a smaller and a larger ligand.

### 6.2.2 Reaction conditions

The ideal conditions for these reactions would be to perform it in an inert (nitrogen or argon filled) glove box. This would limit side reactions of the ylidene and consequently optimise product formation. However, this is not always possible due to availability of apparatus.

Solvents can be made more oxygen and moisture free by employing the ‘thaw and freeze’ method<sup>1</sup> before use. Glassware could also be left in the oven overnight or flame dried prior to use.

### 6.2.3 Employing transfer reagents

The use of transmetalation to synthesise NHC complexes with a variety of metals have been reported<sup>2</sup> and recently Arnold<sup>3</sup> and Lin<sup>4</sup> have published papers regarding silver NHC complexes. Available reagents include organic molecules (eg. carboxylates) and Ag(I) reagents in which the NHC is complexed to silver prior to transmetalation. Both examples are illustrated in the reaction pathways below (Figures 6.3 and 6.4).

(1) “Procedure for Degassing of Liquids using Freeze-Pump-Thaw”. University of Houston.

(2) Garrison, J. C., Youngs, W. J.; *Chem. Rev.* **2005**, *105*, 3978.

(3) Arnold, P. L. *Heteroat. Chem.* **2002**, *13*, 534.

(4) Lin, I. J. B.; Vasam, C. S. *Comments Inorg. Chem.* **2004**, *25*, 75.

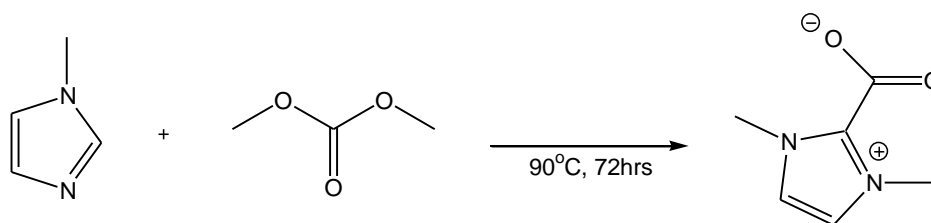


**Figure 6.3:** Synthesis of N,N'-dimethylimidazolium-2-carboxylate<sup>5</sup>

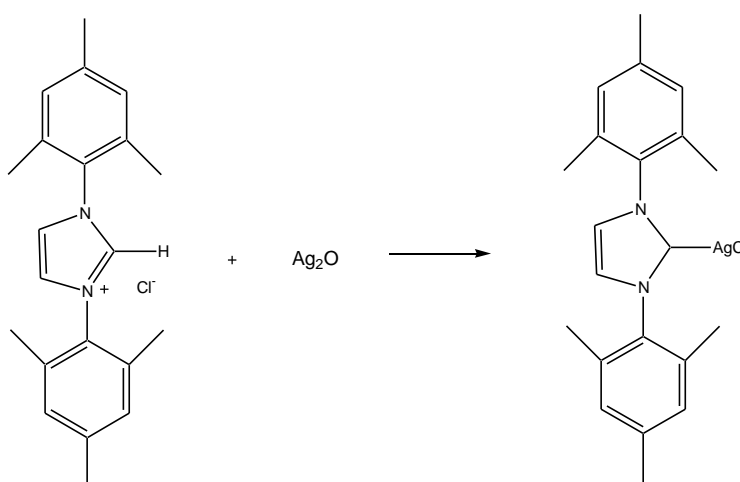


**Figure 6.4:** Synthesis of the silver transfer reagent, [IMesAgCl]<sup>6</sup>

After the formation of these reagents, it is complexed to the metal with the release of CO<sub>2</sub> and silver byproduct respectively. No decarbonylation step is needed for the metal carbonyl substrate.

(5) Voutchkova, A. M., Appelhans, L. N., Chianese, A. R., Crabtree, R. H.; *J. Am. Chem. Soc.* **2005**, *127*, 17624.

(6) Canal, J. P., Ramnial, T., Langlois, L. D., Abernethy, C. D., Clyburne, J. A. C.; *J. Chem. Ed.* **2008**, *85*, 416.

## Chapter 6: Concluding remarks and Future work

### 6.1 Conclusion

In the preceding chapters it is evident that the syntheses of the target complexes of this study are not unproblematic. Although a variety of approaches have been explored the route which employs nBuLi as base appears to be the most promising in both the mono- and dimetal complexes. The potential of this route is reflected in the isolation of the target complex  $[\text{Mn}_2(\text{CO})_9\text{IMes}]$ .

Numerous challenges remain in the syntheses of these complexes and include the insolubility and air-moisture sensitivity which makes it difficult to perform spectroscopic analysis.

This brief chapter will include suggestions for future work regarding this study.

Much is learned of NHC complexes in this study but more still needs to be discovered of these reactive phosphine analogues.

### 6.2 Future work

#### 6.2.1 Relief of steric demand

Comparing the ligand size with the size of the substrate with which complexation should occur, one realises that steric demand is one of the factors requiring attention. There are two ways to bring about the relief of steric demand: by reducing the size of either the ligand or the substrate.

*Less sterically demanding metal substrate: eg. CpMn(CO)<sub>3</sub>*

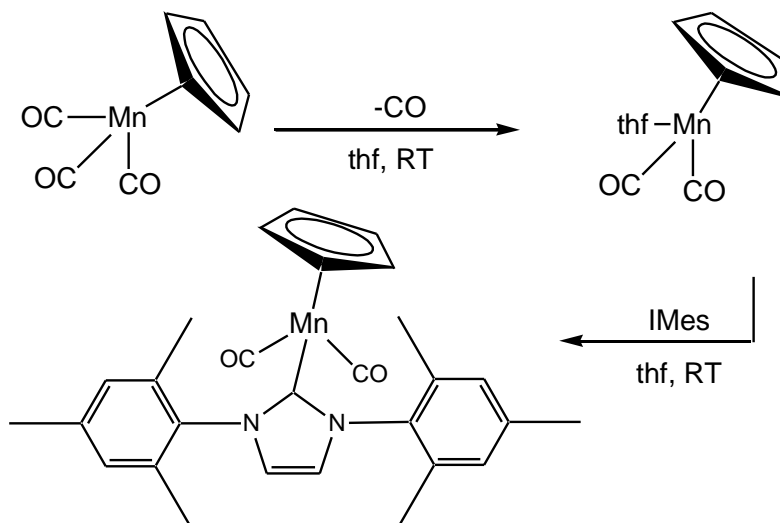


**Figure 6.1:** Synthetic approach in employing a less steric demanding substrate

The Cp-ring replaces three coordination sites of [MnCp(CO)<sub>3</sub>] which leaves more space for the IMes ligand to coordinate to the metal. It shows greater potential to accommodate the steric demand the IMes ligand comprise.

*Less sterically demanding ligand: dimethylimidazole*

In contrast to a large ligand, a smaller ligand would naturally be better accommodated by the metal than a sterically demanding ligand, especially if the metal substrate is itself very bulky. An example of such a ligand is N,N'-dimethylimidazol-2-ylidene.

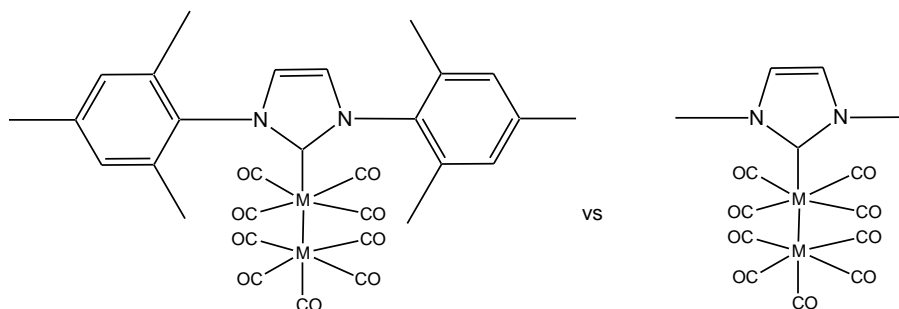


**Figure 6.2:** Illustration of the contrast between a smaller and a larger ligand.

## 6.2.2 Reaction conditions

The ideal conditions for these reactions would be to perform it in an inert (nitrogen or argon filled) glove box. This would limit side reactions of the ylidene and consequently optimise product formation. However, this is not always possible due to availability of apparatus.

Solvents can be made more oxygen and moisture free by employing the ‘thaw and freeze’ method<sup>1</sup> before use. Glassware could also be left in the oven overnight or flame dried prior to use.

## 6.2.3 Employing transfer reagents

The use of transmetalation to synthesise NHC complexes with a variety of metals have been reported<sup>2</sup> and recently Arnold<sup>3</sup> and Lin<sup>4</sup> have published papers regarding silver NHC complexes. Available reagents include organic molecules (eg. carboxylates) and Ag(I) reagents in which the NHC is complexed to silver prior to transmetalation. Both examples are illustrated in the reaction pathways below (Figures 6.3 and 6.4).

(1) “Procedure for Degassing of Liquids using Freeze-Pump-Thaw”. University of Houston.

(2) Garrison, J. C., Youngs, W. J.; *Chem. Rev.* **2005**, *105*, 3978.

(3) Arnold, P. L. *Heteroat. Chem.* **2002**, *13*, 534.

(4) Lin, I. J. B.; Vasam, C. S. *Comments Inorg. Chem.* **2004**, *25*, 75.

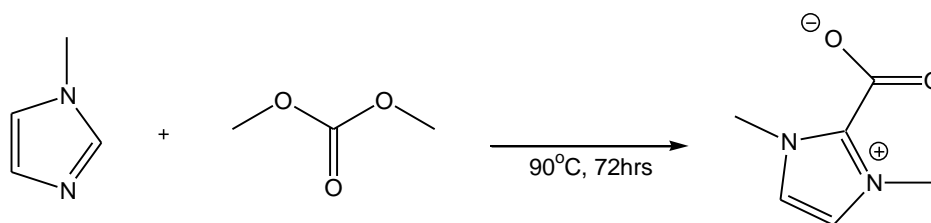


**Figure 6.3:** Synthesis of N,N'-dimethylimidazolium-2-carboxylate<sup>5</sup>

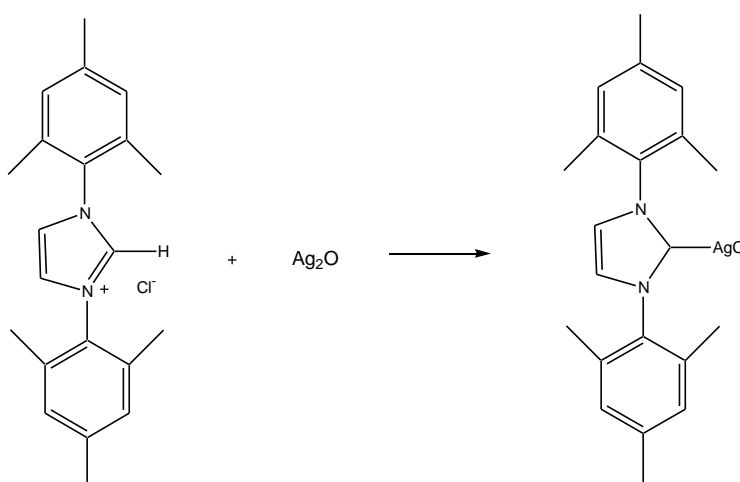


**Figure 6.4:** Synthesis of the silver transfer reagent, [IMesAgCl]<sup>6</sup>

After the formation of these reagents, it is complexed to the metal with the release of CO<sub>2</sub> and silver byproduct respectively. No decarbonylation step is needed for the metal carbonyl substrate.

(5) Voutchkova, A. M., Appelhans, L. N., Chianese, A. R., Crabtree, R. H.; *J. Am. Chem. Soc.* **2005**, *127*, 17624.

(6) Canal, J. P., Ramnial, T., Langlois, L. D., Abernethy, C. D., Clyburne, J. A. C.; *J. Chem. Ed.* **2008**, *85*, 416.

## Chapter 7: Experimental:

### Standard Operational Procedure and Specifications

#### 7.1 Standard Operational Procedure

All operations and reactions were performed in an inert atmosphere under nitrogen or argon gas and standard Schlenk techniques were employed. Solvents were dried and distilled as follows: Ether and thf were distilled from sodium with benzophenone as indicator; benzene, toluene, acetonitrile and hexane were distilled from sodium only; dcm was distilled from phosphorous pentoxide. Chemicals were used without prior purification unless stated otherwise. Column chromatography was performed at RT using the following resins: Kieselgel 60 (0.0063 – 0.200mm) or neutral aluminium oxide 90. Cold columns were also employed at -40°C and cooled with acetone in the column jacket. Resin used for cold column chromatography is florasil.

#### 7.2 Specifications

##### 7.2.1 Nuclear Magnetic Resonance Spectroscopy

The specifications of the spectrometers used for analysis are indicated in Table 7.1.

Table 7.1

<b>Spectrometer</b>	<b><sup>1</sup>H NMR (MHz)</b>	<b><sup>13</sup>C NMR (MHz)</b>
Bruker ARX-300	300.135	75.469
Bruker Ultrashield 400 Plus. Avance III.	400.21	100.63
AVANCE 500	500.139	125.75

The signals of the deuterated solvents<sup>1</sup> were used as references and are presented in Table 7.2

Table 7.2

Deuterated solvent	<sup>1</sup> H (ppm)	<sup>13</sup> C (ppm)
CDCl <sub>3</sub>	7.26	77.16
C <sub>6</sub> D <sub>6</sub>	7.16	128.06
thf- <i>d</i> <sub>8</sub>	1.72 3.58	67.21 25.31
CD <sub>3</sub> CN	1.94	1.32 118.26

Manual shimming and manipulation of the sweep width were used for resolution enhancement.

### 7.2.2 Infrared Spectroscopy

IR spectra were recorded on a Perkin-Elmer Spectrum RXI FT-IR spectrophotometer with an ATR device. Spectra were recorded in different solvents depending on solubility as well as solvent free. Solvents used were hexane, dcm, thf and acetonitrile. The vibrational stretching bands in the carbonyl region (ca. 1500 - 2200cm<sup>-1</sup>) were recorded for complexes.

### 7.2.3 Fast Atom Bombardment Mass Spectrometry

FAB-MS spectra were recorded on a VG 70SEQ Mass Spectrometer, with the resolution for FAB = 1000 in a field of 8kV. Nitrobenzyl alcohol was used as solvent and

---

(1) Fulmer, G. R., Miller, A. J. M., Sherden, N. H., Gottlieb, H. E., Nudelman, A., Stoltz, B. M., Bercaw, J. E., Goldberg, K. I. *Organometallics*. **2010**, 29, 2176.



internal standard. The spectra were recorded at the University of the Witwatersrand, Johannesburg, South Africa.

#### 7.2.4 X-Ray Crystallography

X-Ray crystal structure analyses were performed by Mr David C. Liles, University of Pretoria, South Africa. Data were collected at 20°C on a Siemens P4 Bruker 1K CCK diffractometer using graphite-monochromated, Mo-K $\alpha$  radiation. It was corrected for Lorenz polarisation effects and structures were solved by direct methods (SHELXS<sup>2</sup>) and refined by full-matrix least squares techniques.

Crystal data and structure refinement details are summarised in Tables 7.3 – 7.9.

---

(2) SMART (Version 5.054), SAINT (Version 6.45), SADABS (Version 2.10) and SHELXTS/SHELXTL (Version 6.12). Bruker AXS Inc., Madison, Wisconsin, USA, **2001**.

**Table 7.3: Crystallographic data of complex 1**

Identification code	bvdw20_pbca	
Empirical formula	C <sub>23</sub> H <sub>24</sub> Br N <sub>2</sub> O <sub>3</sub> Re	
Formula weight	642.55	
Temperature	293(2) K	
Wavelength	0.71073 Å	
Crystal system	Orthorhombic	
Space group	P b c a	
Unit cell dimensions	a = 14.1650(8) Å	a = 90°.
	b = 13.9713(7) Å	b = 90°.
	c = 23.5206(13) Å	g = 90°.
Volume	4654.8(4) Å <sup>3</sup>	
Z	8	
Density (calculated)	1.834 Mg/m <sup>3</sup>	
Absorption coefficient	6.963 mm <sup>-1</sup>	
F(000)	2480	
Crystal size	0.38 x 0.15 x 0.12 mm <sup>3</sup>	
Theta range for data collection	2.68 to 26.55°.	
Index ranges	-16<=h<=17, -17<=k<=6, -27<=l<=29	
Reflections collected	23519	
Independent reflections	4560 [R(int) = 0.0294]	
Completeness to $\theta = 25.00^\circ$	99.9 %	
Absorption correction	Semi-empirical from equivalents	
Max. and min. transmission	0.434 and 0.310	
Refinement method	Full-matrix least-squares on F <sup>2</sup>	
Data / restraints / parameters	4560 / 0 / 277	
Goodness-of-fit on F <sup>2</sup>	1.084	
Final R indices [ $I > 2\sigma(I)$ ]	R1 = 0.0299, wR2 = 0.0847	
R indices (all data)	R1 = 0.0359, wR2 = 0.0898	
Extinction coefficient	0	
Largest diff. peak and hole	0.981 and -1.661 e.Å <sup>-3</sup>	

**Table 7.4: Crystallographic data of complex 3**

Identification code	bvdw17_p21n	
Empirical formula	C <sub>10</sub> H <sub>13</sub> N O	
Formula weight	163.21	
Temperature	293(2) K	
Wavelength	0.71073 Å	
Crystal system	Monoclinic	
Space group	P 2 <sub>1</sub> /n	
Unit cell dimensions	a = 8.0659(7) Å	a = 90°.
	b = 15.9004(13) Å	b = 118.1640(10)°.
	c = 8.3329(7) Å	g = 90°.
Volume	942.17(14) Å <sup>3</sup>	
Z	4	
Density (calculated)	1.151 Mg/m <sup>3</sup>	
Absorption coefficient	0.074 mm <sup>-1</sup>	
F(000)	352	
Crystal size	0.44 x 0.38 x 0.28 mm <sup>3</sup>	
Theta range for data collection	2.56 to 26.42°.	
Index ranges	-10 ≤ h ≤ 9, -18 ≤ k ≤ 14, -10 ≤ l ≤ 7	
Reflections collected	4988	
Independent reflections	1778 [R(int) = 0.0255]	
Completeness to θ = 25.00°	99.5 %	
Absorption correction	Semi-empirical from equivalents	
Max. and min. transmission	0.978 and 0.961	
Refinement method	Full-matrix least-squares on F <sup>2</sup>	
Data / restraints / parameters	1778 / 0 / 161	
Goodness-of-fit on F <sup>2</sup>	1.095	
Final R indices [I > 2σ(I)]	R1 = 0.0477, wR2 = 0.1360	
R indices (all data)	R1 = 0.0508, wR2 = 0.1390	
Extinction coefficient	0	
Largest diff. peak and hole	0.204 and -0.204 e.Å <sup>-3</sup>	

**Table 7.5: Crystallographic data of complex 6**

Identification code	bvdw31_p21m	
Empirical formula	C <sub>21</sub> H <sub>25</sub> N <sub>2</sub> O <sub>4</sub> Re	
Formula weight	555.63	
Temperature	293(2) K	
Wavelength	0.71073 Å	
Crystal system	Monoclinic	
Space group	P 2 <sub>1</sub> /m	
Unit cell dimensions	a = 8.2989(12) Å	a = 90°.
	b = 16.373(2) Å	b = 111.948(2)°.
	c = 8.3168(12) Å	g = 90°.
Volume	1048.2(3) Å <sup>3</sup>	
Z	2	
Density (calculated)	1.760 Mg/m <sup>3</sup>	
Absorption coefficient	5.825 mm <sup>-1</sup>	
F(000)	544	
Crystal size	0.39 x 0.10 x 0.09 mm <sup>3</sup>	
Theta range for data collection	2.64 to 26.54°.	
Index ranges	-10 ≤ h ≤ 9, -19 ≤ k ≤ 20, -3 ≤ l ≤ 10	
Reflections collected	5654	
Independent reflections	2026 [R(int) = 0.0317]	
Completeness to θ = 25.00°	98.6 %	
Absorption correction	Semi-empirical from equivalents	
Max. and min. transmission	1.0 and 0.826	
Refinement method	Full-matrix least-squares on F <sup>2</sup>	
Data / restraints / parameters	2026 / 0 / 136	
Goodness-of-fit on F <sup>2</sup>	1.196	
Final R indices [I > 2σ(I)]	R1 = 0.0544, wR2 = 0.0853	
R indices (all data)	R1 = 0.0666, wR2 = 0.0873	
Extinction coefficient	0	
Largest diff. peak and hole	1.358 and -0.837 e.Å <sup>-3</sup>	

**Table 7.6: Crystallographic data of complex 9**

Identification code	bvdw30_p-1	
Empirical formula	C <sub>30</sub> H <sub>24</sub> Mn <sub>2</sub> N <sub>2</sub> O <sub>9</sub>	
Formula weight	666.39	
Temperature	293(2) K	
Wavelength	0.71073 Å	
Crystal system	Triclinic	
Space group	P1	
Unit cell dimensions	a = 11.2507(8) Å	a = 105.891(1)°.
	b = 11.5231(8) Å	b = 106.464(1)°.
	c = 12.9750(9) Å	g = 92.810(1)°.
Volume	1536.81(19) Å <sup>3</sup>	
Z	2	
Density (calculated)	1.440 Mg/m <sup>3</sup>	
Absorption coefficient	0.876 mm <sup>-1</sup>	
F(000)	680	
Crystal size	0.39 x 0.16 x 0.07 mm <sup>3</sup>	
Theta range for data collection	2.66 to 26.45°.	
Index ranges	-13<=h<=14, -14<=k<=14, -8<=l<=16	
Reflections collected	8282	
Independent reflections	5512 [R(int) = 0.0223]	
Completeness to $\theta = 25.00^\circ$	97.3 %	
Absorption correction	Semi-empirical from equivalents	
Max. and min. transmission	0.941 and 0.828	
Refinement method	Full-matrix least-squares on F <sup>2</sup>	
Data / restraints / parameters	5512 / 0 / 394	
Goodness-of-fit on F <sup>2</sup>	1.040	
Final R indices [ $I > 2\sigma(I)$ ]	R1 = 0.0408, wR2 = 0.1072	
R indices (all data)	R1 = 0.0499, wR2 = 0.1169	
Extinction coefficient	0	
Largest diff. peak and hole	0.384 and -0.244 e.Å <sup>-3</sup>	

**Table 7.7: Crystallographic data of complex 10**

Identification code	bvdw23b_p21n	
Empirical formula	C <sub>30</sub> H <sub>25</sub> Cl Mn <sub>2</sub> N <sub>2</sub> O <sub>9</sub>	
Formula weight	702.85	
Temperature	293(2) K	
Wavelength	0.71073 Å	
Crystal system	Monoclinic	
Space group	P 2 <sub>1</sub> /n	
Unit cell dimensions	a = 10.2211(19) Å	a = 90°.
	b = 16.374(3) Å	b = 94.463(3)°.
	c = 19.969(4) Å	g = 90°.
Volume	3331.9(11) Å <sup>3</sup>	
Z	4	
Density (calculated)	1.401 Mg/m <sup>3</sup>	
Absorption coefficient	0.890 mm <sup>-1</sup>	
F(000)	1432	
Crystal size	0.47 x 0.17 x 0.04 mm <sup>3</sup>	
Theta range for data collection	2.50 to 26.47°.	
Index ranges	-12<=h<=4, -20<=k<=19, -24<=l<=24	
Reflections collected	17307	
Independent reflections	6238 [R(int) = 0.0699]	
Completeness to $\theta = 25.00^\circ$	99.3 %	
Absorption correction	Semi-empirical from equivalents	
Max. and min. transmission	0.965 and 0.740	
Refinement method	Full-matrix least-squares on F <sup>2</sup>	
Data / restraints / parameters	6238 / 0 / 403	
Goodness-of-fit on F <sup>2</sup>	1.044	
Final R indices [I>2 $\sigma$ (I)]	R1 = 0.0849, wR2 = 0.2372	
R indices (all data)	R1 = 0.1852, wR2 = 0.2953	
Extinction coefficient	0	
Largest diff. peak and hole	0.662 and -0.455 e.Å <sup>-3</sup>	

**Table 7.8: Crystallographic data of complex 12**

Identification code	bvdw28as_p-1	
Empirical formula	C <sub>28</sub> H <sub>12</sub> O <sub>21</sub> Re <sub>4</sub>	
Formula weight	1429.18	
Temperature	293(2) K	
Wavelength	0.71073 Å	
Crystal system	Triclinic	
Space group	P -1	
Unit cell dimensions	a = 9.2999(7) Å	α = 113.4700(10)°.
	b = 13.9888(10) Å	β = 95.7180(10)°.
	c = 15.3766(12) Å	γ = 92.7970(10)°.
Volume	1817.2(2) Å <sup>3</sup>	
Z	2	
Density (calculated)	2.612 Mg/m <sup>3</sup>	
Absorption coefficient	13.363 mm <sup>-1</sup>	
F(000)	1296	
Crystal size	0.28 x 0.14 x 0.10 mm <sup>3</sup>	
Theta range for data collection	2.48 to 26.57°.	
Index ranges	-11 ≤ h ≤ 11, -15 ≤ k ≤ 16, -11 ≤ l ≤ 19	
Reflections collected	9954	
Independent reflections	6596 [R(int) = 0.0292]	
Completeness to θ = 25.00°	97.7 %	
Absorption correction	Semi-empirical from equivalents	
Max. and min. transmission	0.263 and 0.131	
Refinement method	Full-matrix least-squares on F <sup>2</sup>	
Data / restraints / parameters	6596 / 0 / 483	
Goodness-of-fit on F <sup>2</sup>	1.047	
Final R indices [I > 2σ(I)]	R1 = 0.0387, wR2 = 0.1005	
R indices (all data)	R1 = 0.0459, wR2 = 0.1077	
Extinction coefficient	0	
Largest diff. peak and hole	2.447 and -1.514 e.Å <sup>-3</sup>	

**Table 7.9: Crystallographic data of complex 13**

Identification code	bvdw24_p-1	
Empirical formula	C <sub>37</sub> H <sub>29</sub> N <sub>2</sub> O <sub>10.50</sub> Re <sub>2</sub>	
Formula weight	1042.02	
Temperature	293(2) K	
Wavelength	0.71073 Å	
Crystal system	Triclinic	
Space group	P 1	
Unit cell dimensions	a = 12.7058(7) Å	a = 60.7600(10)°.
	b = 13.8293(8) Å	b = 77.6800(10)°.
	c = 13.9679(8) Å	g = 89.5640(10)°.
Volume	2078.8(2) Å <sup>3</sup>	
Z	2	
Density (calculated)	1.665 Mg/m <sup>3</sup>	
Absorption coefficient	5.871 mm <sup>-1</sup>	
F(000)	998	
Crystal size	0.32 x 0.20 x 0.05 mm <sup>3</sup>	
Theta range for data collection	2.53 to 26.48°.	
Index ranges	-15<=h<=8, -14<=k<=16, -16<=l<=15	
Reflections collected	11288	
Independent reflections	7504 [R(int) = 0.0248]	
Completeness to $\theta = 25.00^\circ$	97.4 %	
Absorption correction	Semi-empirical from equivalents	
Max. and min. transmission	0.746 and 0.314	
Refinement method	Full-matrix least-squares on F <sup>2</sup>	
Data / restraints / parameters	7504 / 0 / 455	
Goodness-of-fit on F <sup>2</sup>	1.055	
Final R indices [I>2 $\sigma$ (I)]	R1 = 0.0404, wR2 = 0.1201	
R indices (all data)	R1 = 0.0504, wR2 = 0.1334	
Largest diff. peak and hole	2.144 and -0.820 e.Å <sup>-3</sup>	